Microalgae Growth and Lipid Production in a Vertical Flat-Plate Photobioreactor: Mechanistic Model Development

A Thesis

Presented to the

Graduate Faculty of the

University of Louisiana at Lafayette

In Partial Fulfillment of the

Requirements for the Degree

Master of Science

Qilin Bao

Fall 2013

Microalgae Growth and Lipid Production in a Vertical Flat-Plate Photobioreactor: Mechanistic Model Development

Qilin Bao

APPROVED:

Barbara C. Benson, Co-chair Assistant Professor of Environmental Science	Daniel D. Gang, Co-chair Professor of Civil Engineering
Emad Habib Professor of Civil Engineering	Stephen Dufreche Assistant Professor of Chemical Engineering
Carlos J. Fernandez Associate Professor of Agronomy Texas A&M AgriLife Research and Extension Center at Corpus Christi	Mary Farmer-Kaiser Interim Dean of the Graduate School

Acknowledgments

I would like to express my greatest and deepest gratitude to my research advisor Dr. Barbara C. Benson for her valuable guidance, encouragement, and dedication throughout the creation of this master's thesis. Dr. Benson not only taught me how to question thoughts and express ideas, but also helped me overcome many crisis situations and finish this thesis. Without Dr. Benson's constant guidance, support, patience, and tenacity over the last two years, this thesis would not have been completed.

I would like to express my profound gratitude to my thesis supervisor Dr. Daniel D. Gang for his invaluable assistance and support in every step of my thesis. His thoughtful guidance helped me with the research and the writing of the thesis. I am also thankful to him for encouraging the use of correct grammar and consistent notation in my writings and for carefully reading countless revisions of this manuscript.

I would like to thank my committee members, Dr. Emad Habib, Dr. Stephen Dufreche, and Dr. Carlos J. Fernandez for graciously serving on the committee. I am grateful to my thesis committee for their constructive criticisms and insightful comments.

I am also indebted to Dr. Carlos J. Fernandez and everyone in the Texas A&M AgriLife Research and Extension Center at Corpus Christi, Texas, for having provided me with the facilities, data, and valuable assistance which enable me to complete this research project. I am thankful to Dr. Joe M. Fox and his graduate research assistants at the Texas A&M University-Corpus Christi, for providing data from their lipid analysis. I would like to thank the Bioprocessing Research Laboratory at University of Louisiana at Lafayette for the

use of equipment and supplies. I would also like to acknowledge the financial support provided by the U.S. Department of Energy and U.S. Department of Agriculture SunGrant awarded to Dr. Benson.

Thank you to all faculty members and graduate students of the Department of Civil Engineering for providing extended assistance and moral support. Special thanks to Dr. Kenneth McMains, Dr. Xiaoduan Sun, Dr. Mohammad J. Khattak, Mr. Mark LeBlanc, Jing Nie, Ruwaida Bari, and Jacob Thompson who provided me with a good education and extended help during those two years' study.

Last, but not the least, I would like to express my gratitude to my family and my friends for their encouragement and for supporting me spiritually.

Table of Contents

List of Tables

List of Figures

List of Abbreviations

C	Carbohydrate Content
CAB	Controlled Automated Bioreactors
CO_2	Carbon Dioxide
D	Distance from the lamp
FACE 4	Four Fully Automated and Controlled Environment Photobioreactors
I_o	Surface PPFFR
I_a	Average Irradiance
I_z	The scalar PPFFR at z depth of penetration
K_a	Light Diffusion Coefficient
K_o	Overall Scalar Light Attenuation Coefficient
K_p	Wall Diffusion Coefficient
K_w	Water Attenuation Coefficient
K_b	Biomass Attenuation Coefficient
K_μ	Lipid Production Coefficient
L	Lipid Content

mg/L	Milligram per liter
P	Protein Content
PAR	Photosynthetic Active Radiation
PPFD	Photosynthetic Photo Flux Density
PPFFR	Photosynthetically Photon Flux Fluency Rate
TSS	Total Suspended Solids
Y	Biomass Yield
X	Biomass Concentration
μ	Specific Growth Rate
μ_{max}	Maximum Specific Growth Rate
Z	Culture Thickness

Chapter 1: Introduction

1.1 General

Biofuels and alternative energy from renewable sources are widely considered to be one of the most sustainable alternatives to fossil fuels and viable means to combat overcoming energy depletion crisis (Hill et al., 2006). Biofuels are obtained by processing different kinds of biomasses. They come in the forms of solids (bio-chair), liquid (bioethanol, bio-oil and biodiesel), and gases (biogas, biohydrogen and biosyngas). According to the Energy Information Administration (EIA), the world energy consumption will grow by 56% between 2010 and 2040 (IEO, 2013). In 2012, United States alone consumed 21% of the world's total energy with only 5% of world's population. Renewable energy has long been proposed as one solution of the most pressing issues in the U.S., including energy security, economic wellbeing, and the stability of global climate (U.S. DOE, 2010). Although fossil fuels continue to supply almost 80% of world energy use through 2040, renewable energy is the world's fastest-growing energy source, increasing by 2.5% per year (IEO, 2013). Due to the increasing combustion of fossil carbon worldwide, the amount of greenhouse gases have increased which lead to global warming and climate change. These concerns have given rise to the idea of investigating biofuels and have stimulated alternative energy development.

Lipid biofuels have been developed and optimized over the past several decades. First generation biofuels such as biodiesel and bioethanol from crop plants and oil seeds are currently on market. In 2012, about 969 million gallons of biodiesel were produced in the U.S. (IEO, 2013). However, first generation biofuels have some main problems, including (1)

they encroach on arable land, freshwater supplies or biodiverse natural landscapes; (2) they are limited in their ability to achieve targets for oil-product substitutes; (3) they are also in slow economic growth (Sims et al., 2008). The cumulative impact of these concerns has inspired searching for second-generation biofuels produced from non-food biomass or agricultural residues. Although use of second generation biofuels could help avoid many of the problems associated with first generation biofuels, it still faces major constraints to its technical and commercial development. Thus, it is necessary to make significant progress in the commercial and technology development of second generation biofuels.

Microalgal biofuels are alternatives to fossil fuel and use microalgae as a feedstock, which offer great promise in contributing to solutions for the rapidly growing energy demands and the climate change. Mircroalgae have the potential to produce biofuels to meet the world's growing energy demands. Their high actual photosynthetic yield compared to terrestrial plants (whose growth is limited by CO_2 availability) leads to large potential algal biomass productions in photobioreactors of several tens of tons per hectare, per year (Chisti, 2007). Microalgae appear to be the best choice of feed stock for biofuel production due to the fact that they grow 50 to 100 times faster than conventional food crops (Spolaore et al., 2006). Microalgae do not only have the capacity to produce high-value biomass, but also the ability to do so in an environmentally friendly and supportive way. This is because they use sunlight, carbon dioxide and water to grow without requiring freshwater resources or soil for growth. Microalgal biomass contains approximately 50% carbon by dry weight, and all of this carbon is typically derived from carbon dioxide fed continually during daylight hours (Sánchez et al.,

2003). Based on current and potential markets, microalgae have become a product valued at $1.25 billion a year globally, not including processed products (Becker, 2007).

The primary aspects of producing algal biofuels are the design of the growth system, optimization of biomass production, and economically efficient air extraction and processes. The cultivation systems of algae can be divided into two major categories, open ponds and photobioreactors. Open pond systems can be used for very fast growing strains or for strains that grow in extreme conditions, especially those strains with high oil content (Briggs, 2004; González Fernández et al., 2011). Photobioreactors are capable of achieving an ideal environment for high algae cultivation productivity (Mohan et al., 2007). The basic goal of designing a cultivation system is to maximize the growth rate and to obtain a high biomass production, eventually making the system economically practical. However, this goal may compare the main objective to produce more lipids because some scientist have reported an inverse relation between cell lipid content and cell growth rate in several algal species (Williams and Laurens, 2010).

Mechanistic simulation modeling is often used during the design of algae cultivation systems to assist management and improve the efficiency of microalgal oil productions. A mechanistic model based on mass balances and biological processes is a critical tool for predicting biomass and lipid production with respect to environmental conditions during optimization and the scale-up process. Complex mathematical expressions of the relationships of the various biological and physiological processes controlling microalgal production are needed to quantify, and then to be integrated into a mechanistic model aiming

at optimize the efficiency of microalgae production in the reactor (Benson et al., 2012).

1.2 Goals and Objectives of Research

In this study, a mechanistic model of a flat-plate microalgae photobioreactor has been developed using the approaches in the previous studies (Benson et al., 2007) in order to optimize biomass and lipid production and identify optimal operation conditions. This mechanistic model simulates the light dynamics, microalgae growth kinetics, biological and physiological responses, and production efficiency in microalgae culture. The main goal of the study is to improve the efficiency of the flat-plate photobioreactor through quantification and integration of various fundamental processes governing microalgae and lipid production. A complex network of numerical relationships within the photobioreactor systems was discussed and integrated in the mechanistic model to achieve simulations which can clarify the path to this goal.

The specific objectives had to be met to develop the model and accomplish the goal. They are as follows:

1. Determine the relationship between surface photosynthetic photo flux density (PPFD) (I_o) emitted by lamp and the distance of light source (D) from the culture surface;
2. Determine the relationship between average PPFFR at a given depth (I_a) as a function of I_o and bioimass concentration (X) in the photobioreator;
3. Determine the relationship between average PPFFR (I_a) and biomass concentration

(X) in the phtobioreactor;

4. Examine the effect of suspended biomass concentration (X) on light attenuation coefficient (k_r) expressed as biomass light attenuation coefficient (k_b);
5. Determine the microalgae growth kinetics, including maximum growth rate (μ_{max}) and optimum PPFD (I_{opt});
6. Develop of a mechanistic model that simulates biomass production, lipid production, and physiological responses.

Several lab experiments were done to meet these objectives. The model was developed using the parameters of light dynamics and growth kinetics within the flat-plate photobioreactors, and then used to gain a better understanding of various fundamental processes and to optimize the efficiency of microalgae-based lipid production systems.

Chapter 2: Literature Review

2.1 Microalgae Biofuels

Microalgae are considered as an alternative feedstock for next-generation biofuel production (Sakthivel et al., 2011). Mircroalgae are sunlight-driven cell factories that convert carbon dioxide to potential biofuels, foods, feeds and high-value bioactives (Christi and Gavrilescu, 2005). Recent increases in energy demand, environmental concerns, and oil prices have stimulated investment in second-generation biofuels research. The Energy Independence and Security Act of 2007 (EISA) established U.S. biofuel production targets requiring transportation fuel consumed in the U.S. to contain a minimum of 36 billion gallons of renewable fuels, including cellulosic biofuels and biomass-based diesel, by 2022 (U.S. DOE, 2010). Figure 2.1 shows the utilization of algae biomass as a resource for bioenergy.

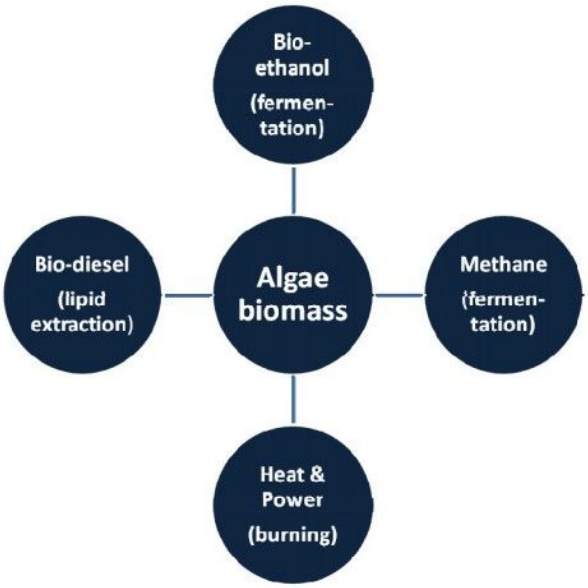

Figure 2.1: Utilization of algal biomass for bioenergy productions (Wegeberg and Felby, 2010).

Several advantages of microalgae biofuel productions over other energy crops have

attracted significant interest and investment. The diverse benefits of algae include: (1) a high potential yield per acre than terrestrial crops; (2) the ability to grow in non-arable land or non-potable water; (3) the potential for consumptions of CO_2 and other nutrients in waste streams during growth; (4) a high concentration of lipids; (5) a year-round daily harvest production; and (6) non-food based feedstock resources (Chisti, 2007; Gouveia and Oliveira, 2009; U.S. DOE, 2010). The high actual photosynthetic yield of algae compared to terrestrial plants (whose growth is limited by CO_2 availability) leads to large potential algal biomass productions in photobioreactors of several tens of tons per hectare, per year (Chisti, 2007).

The three major components which can be extracted from microalgal biomass are lipids, carbohydrates, and proteins (Chisti, 2007). Lipids and carbohydrates have roles as fuel precursors (gasoline, biodiesel and bioethanol), while proteins can be used as high value by-products such as aquaculture and livestock feeds (U.S. DOE, 2010). Although many previous researchers have focused on the lipid compositions from nutritional standpoint, there are currently have some critical technical barriers for the development of economical scale algal lipid production facilities. This is due to high energy needs associated with drying algal biomass and separating out desirable products, which results in a high cost to produce microalgae biofuels. As a result, new approaches are exploring cost optimization of the processes associated with the industrial scale up of algae biofuels productions.

Nannochloropsis has been identified as a promising source of lipid feedstock for biofuel production. It has a fairly high oil content at nearly 28% of dry weight, but more importantly it also contains enough unsaturated fatty acid for a quality biodiesel (Gouveia

and Oliveria, 2009). Compared with other microalgae species, *Nannochloropsis* is capable of generating ultra-high biomass densities, and it is rich in metabolites such as pigments (Lee et al., 2006). *Nannochloropsis* is also one of the most common types of microalgae, which has been exploited widely in aquaculture practices for food supplements (Lubian et al., 2000).

2.2 Microalgal Physiology and Biochemistry

2.2.1 Microalgal Photosynthesis

Microalgal photosynthesis is a biochemical process that transfers the energy from the incoming photons to electrons in the photosynthetic cells, subsequently converted into chemical energy in the form of carbohydrates (sugar). The efficiency of photosynthesis is directly proportional to the microalgal biomass production. An outline of photosynthesis can be seen in Figure 2.2.

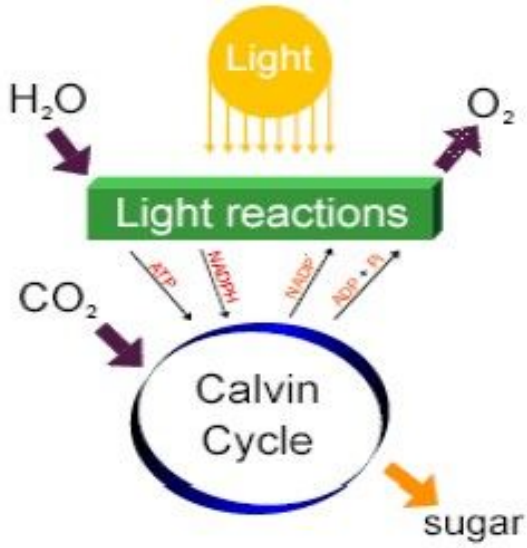

Figure 2.2: Reactions taking place during photosynthesis (Wegeberg and Felby, 2010).

The stoichiometry of photosynthesis can be simply written as (Karube et al., 1992):

$$6H_2O + 6CO_2 + light(photons) = C_6H_{12}O_6 + 6O_2 \quad (2.1)$$

where $C_6H_{12}O_6$ is a carbohydrate which is synthesized in photosynthesis. This equation is the net result of two processes: (1) a redox process that requires light, which is conventionally called as the "light reaction"; (2) a series of enzymatic reactions that require water to form Nicotinamide Adenine Dinucleotide Phosphate (NADP), and is often referred to as the "dark reaction." These two reactions can by written individually as (Karube et al., 1992):

$$\text{Light reaction: } 12H_2O + light \rightarrow 6O_2 + 24H^+ + 24e^- \quad (2.2)$$

$$\text{Dark reaction: } NADP^+ + H_2O \rightarrow NADPH + H^+ + O \quad (2.3)$$

The light energy that is captured by microalgal cells is stored in the form of chemical bonds of compounds such as NADPH; then the energy contained in NADPH is used to reduce CO_2 to glucose ($C_6H_{12}O_6$) (Chapra,1997).

Not all incoming wavelengths of light can be absorbed by the plant pigments. Photosynthetically available radiation (PAR) represents the useful regions 400-700 nm wavelengths that can be used for photosynthesis, which amounts to 45 -50% of total incoming radiation that reaches the earth's surface (Kirk, 1994).

2.2.2 Major Biochemical Composition of Microalgae

The three major components of microalgae biomass are lipids, carbohydrates, and proteins. They will greatly determine the economical value of biomass producers. Microalgal oil most accumulated as triglycerides can be transformed to biodiesel (Zhang et al., 2003). Maximizing microalgae photosynthesis productions with regards to lipids, carbohydrates and proteins will greatly increase their overall economic values.

Lipids are fatty acids and their derivatives serve both as energy reserves and structural membranes of the microalgae cell. Microalgae synthesize fatty acids principally for esterification into glycerol-based membrane lipids under optimal conditions of growth (Hu et al., 2008). The chemical structure of fatty acids generally consists of medium-chain (C10-14), long-chain (C16-18) and very-long-chain (≥C20) species and fatty acid derivatives (Thompson, 1996). The major membrane lipids are phospholipids and glycolipids, which individually reside in the chloroplast and in the plasma membrane (Wada and Murata, 1998). Microalgae have the ability of survival over a wide range of environmental conditions, due to the tremendous diversity of cellular lipids as well as the ability to modify lipid metabolism efficiently in responses to changes in temperature (Thompson, 1996). Thus, lipids are highly variable for various genera and are altered by environmental conditions. The typical lipid classes of microalgae consist of phospholipids, glycolipids, and triglycerides, which are important to biodiesel and biofuel production. It is known that the varieties of lipids determine the need for pretreatment before they are converted to biofuel properties (Christie, 2003). Phospholipids and glycolipids are major components of the cell's membrane, while triglycerides do not perform a structural role but instead serve as a storage form that are important energy reserves. The class distributions of lipids derived from published analyses on seven species including Nannochloropsis sp. are listed in Table 2.1 (Williams and Laurens, 2010). As the table shows, these constituents vary substantially depending on the species, the environmental conditions, and metabolism. The lipid class distribution also varies. High triglyceride proportion of the overall lipid fraction is often achieved as the metabolic rate

slows down (Lopez-Alonso et al., 2000).

Table 2.1: Mean lipid class content as a percent of total lipid of individual algal species (Williams and Laurens, 2010).

	Simple lipids	**Glycolipids**	**Phospholipids**
Chaetoceros species	37±16	36±8	25±8
Chlamydomonas species	48±10	44±13	6±3
Dunaliella tertiolecta	7±1	67±1	25±0
Dunalliella viridis	13±1	44±3	42±2
Isochrysis species	36±3	35±1	27±3
Nannochloropsis species	22±1	39±0	38±1
Phaeodactylum tricornutum	54±6	34±5	11±1

Carbohydrates are common single components that serve both structural and metabolic functions. Carbohydrates of microalgae are mainly represented by polysaccharides that include various soluble and physiologically active components (Maksimova et al., 2004). The structure of carbohydrates is often derived with acids or sulfate groups, indicating that biochemical conversion of microalgae is not a straightforward task. And different classes of microalgae produce specific types of polysaccharides as the early photosynthesis products. Studies have shown that carbohydrates such as starches and sugars can be processed into ethanol.

Proteins are biochemical compounds of different amino acids that serve both as structural and metabolic components (Maksimova et al., 2004). Microalgae proteins have important commodity value because of their high nutritional quality, so they are marketed as

health food, cosmetics, and animal feed (Adams et al., 2009). Due to their amino acid composition, proteins are considered as dietary essentials for mammals, yet they are unable to synthesize them. The nutritional quality of proteins is determined basically by the content and proportion of its amino acids.

Depending on the species and growth conditions, microalgae can yield a great variety of the major biochemical categories. Microalgae have varied lipid contents of 20 to 80% by dry weight (Chisti, 2007). Microalgae belonging to different species possess the ability to produce a large fraction of their dry mass as lipids, as shown in Table 2.2 (Chisti, 2007; Meng et al., 2009). A series of environmental stress factors give rise to the lipid content seen in the table, such as temperature and limitations of nitrogen, phosphorus, and salinity. Under optimal growth conditions, many microalgae have the ability to produce large amount of biomass but with relatively low lipid contents of 5-20% by dry weight (Sharma et al., 2012). Under photo-oxidative stress or other environmental stress conditions, many microalgae alter their lipid biosynthetic pathways toward the accumulation of neutral lipids as at amount of 20-50% dry weight (Hu et al., 2008). Lipids extracted from microalgae can be used to produce biodiesel, with leftover solids including mostly carbohydrates and proteins (Shen et al., 2009).

The relationship between lipid content and growth rate was investigated in previous studies. Shifrin and Chisholm (1981) found that there is a significant inverse relationship between growth rate and lipid content (Figure 2.3). A similar negative relationship is also reported by Thompson et al. (1990). From these relationships as plotted by Williams and

Laurens (2010), in Figure 2.3, the maximum lipid production for a given growth rate can be estimated.

Table 2.2: Oil content of microalgae (Chisti, 2007; Meng et al., 2009).

Microalgae	*Oil Content (% dry weight)*
Botryococcus braunii	25-75
Chlorella sp.	28-32
Crypthecodinium cohnii	20
Cylindrotheca sp.	16-37
Dunaliella primolecta	23
Isochrysis sp.	25-33
Monallanthus salina	＞20
Nannochloris sp.	20-35
Nannochloropsis sp.	31-68
Neochloris oleoabundans	35-54
Nitzschia sp.	45-47
Schizochytrium sp.	50-77

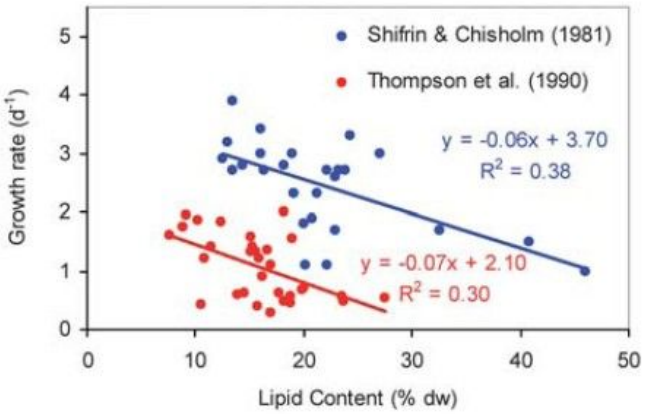

Figure 2.3: The variation of growth rate with lipid content (Williams and Laurens, 2010).

The conversion of microalgal photosynthesis products into the three major biochemical categories incurs a metabolic penalty in the form of loss of mass. Williams and Lauren (2010) developed a general equation that could predict the biomass yield during the biosynthesis of lipids, proteins, and carbohydrates:

$$Y=1/(1.11C + 1.7P+2.6L) \quad (2.4)$$

where

Y= biomass yield in mass per mass hexose synthesized

C= carbohydrate content (%)

P= protein content (%)

L= lipid content (%)

The assumptions for application of Equation 2.4 include C+P+L=1, and the protein to carbohydrate ratio is 3:2; there the above governing equation can be simplified to:

$$Y=1/(1.46+ 1.14L) \quad (2.5)$$

Based on this equation, the productions of biomass partitioning into lipid, protein, and

carbohydrate can be estimated:

$$L= \frac{\left(\frac{1}{Y}-1.46\right)}{1.14} \tag{2.6}$$

$$C=\frac{\left(\frac{1}{Y}-2.6\times\frac{1}{Y}-1.46\right)}{\frac{1.14}{3.66}} \tag{2.7}$$

$$P=\frac{\left(\frac{1}{Y}-2.6\times\frac{1}{Y}-1.46)\right)}{\frac{1.14}{3.66}}\times 1.5 \tag{2.8}$$

These three equations can be used to model and estimate lipid, protein, and carbohydrate productions during the biosythesis in microalgae culture systems.

2.2.3 Factors Affecting Lipid Productivities

Microalgal lipid yields rise obviously under stress conditions imposed by chemical or physical environmental stimulus (Sharma et al., 2012). Nutrient starvation, salinity, and growth-medium pH are identified as major chemical stimulus that would affect lipid accumulation; temperature, light, and turbulence are considered as major physical factors.

Nutrient availability has a major effect on microalgae growth and lipid content. When nutrients are limited, the cell division rate is steadily declining, resulting in active biosynthesis of lipids with enough light and CO_2 available for photosynthesis (Thompson, 1996). Based on previous studies, nitrogen limitation is the most critical nutrient affecting biofuel production in microalgae. Because nitrogen is the most growth-limiting factor for

microalgal metabolism and would be one of the first nutrients to be depleted during microalgae cultivation (Basova, 2005). Nitrogen starvation technique is widely studied in almost all the microalgae species, since it is also relatively easy to apply controlled nitrogen stress on microalgae by subtracting the nitrogen source in the microalgae cultivations (Merzlyak et al., 2007).

Study on the effects of salinity and pH have also been shown to effect lipid compositions of microalgae. Azachi et al. (2002) reported that an increase of NaCl concentration in cultivation of *Dunaliella salina* resulted in an increase in lipid content. Moreover, change of pH in the medium also alters the lipid composition of microalgae. Alkaline pH stress leads to neutral lipid accumulation in most green microalgae, and also leads to a decrease in membrane lipids (Guckert et al., 1990).

Temperature has been found to have a significant impact on the fatty acid composition of microalgae (Guschina, 2006). A general trend of increasing unsaturated fatty acids in response to decreasing temperature has been reported in numerous species of microalgae (Renaud et al., 2002). It is generally accepted that as membrane fluidity decreases at lower temperature, the unsaturation of fatty acid increases, thus providing an adaption to the changing environment. Temperature also affects the total lipid content in microalgae. For example, *Nannochloropsis salina* exhibits a very low grow rate and lipid production at temperature above 25 ℃, because this temperature lead to an abrupt interruption of microalgal growth and later the cell dead on further period of cultivation (Sayegh and Montagnes, 2010). *Nannochloropsis salina* have the optimal cultivation growth temperature

at temperature around 20 ℃ (Brown and Jeffrey, 1992).

Light is the most important factor for photosynthesis and lipid production. Different light intensities and wavelengths have been reported to change the lipid metabolism in microalgae altering the lipid profile (Harwood, 1998). A general trend towards increases in the amount of neutral storage lipids with decreasing membrane lipids have been observed on high light intensity condition, whereas low light intensity decreases the level of neutral lipids (Brown et al., 1996; Khotimchenko and Yakovleva, 2005). It is generally accepted that high light intensity increases fatty acid synthesis to produce more of the saturated fatty acids which in turn are stored as neutral lipids.

2.3 Microalgae Cultivation System

Algae cultivation can be achieved in either open ponds or photobioreactors, both varying in their advantages and challenges. To meet the increased demand for microalgal-based oil productions, it requires the development of highly efficient cultivation systems capable of low-cost production. While various cultivation systems have been widely investigated, there is a general consensus that the major barrier is the scale-up of these systems with economic feasibility. Based on numerous studies of this topic, open and closed systems are considered as the two most viable categories for large-scale commercial algae-based productions.

In February 2012, the Bioenergy Technologies Office announced a funding opportunity to support outdoor phototrophic algae R&D in two areas: (1) development of

integrated cultivation systems for algal production that demonstrate minimal nutrient and water inputs; (2) the development of algal technology testbed facilities (DOE/ASAP, 2012).

2.3.1 Open Pond Systems

Open ponds are the most common systems of algae cultivation. Of these raceway ponds have risen to be the predominant type studied because they are easy to operate (Richardson et al., 2012). In raceway ponds, algae, water and nutrients circulate around a race-shaped pond with paddlewheels providing the flow (Figure 2.4). Although open ponds have advantages of being low-cost and easy to operate, they are sensitive to contamination from unwanted organisms leading to the loss of algae biomass production. Another reason for low production and photosynthetic efficiency in open ponds is due to the long light path, which causes self-shadowing which also results in reduced utilization of CO_2 from gas streams. Other environmental factors such as temperature and microbial contaminants also reduce production. These disadvantages have led to the design and development of enclosed indoor photobioreactors (Watanabe et al., 2007).

Figure 2.4: Raceway-shape culture ponds in an outdoor algae farm (Seambiotic Co., 2010).

2.3.2 Photobioreactors

A photobioreactor is a closed device that provides a controlled environment and enables high productivity of algae. They have been successfully used for producing large quantities of microalgal biomass (Carvalho et al., 2006). As a closed system, photobioreactor offers better control the aspects of culture environment, such as light, carbon dioxide, pH, temperature, and water supply. The closed systems include the serial turbidostat, tubular, flat-plate, and column photobioreactors.

The serial turbidostat reactors were originally designed as a combination of enclosed photobioreactors and open systems to sustain low cost production (Rusch and Malone, 1998). As an example, a Hydraulically Integrated Serial Turbidostat Algal Reactor (HISTAR) system which was able to maintain high-quality monoculture of suspended microalgae by applying the hydraulically washout concept, has proven to be promising (Benson, 2003). This system was recently used to establish a mechanistic model to predict microalgal

productivity in order to establish practical feasibility for large-scale applications.

The critical design requirement of the photobioreactor is the illumination surface area per unit volume, which gives an efficient high surface area to volume ratio (S/V ratio) (Ogbonna and Tanaka, 1997). Flat-plate and tubular photobioreactors are the most widely used closed systems of photobioreactors due to their high S/V ratio (Ogbonna and Tanaka, 1997).

2.3.3 Types of Photobioreactor

The selection of the photobioreactor depends on its ability to maximize productivity and photosynthetic efficiency, which is the case for the flat-plate, serial turbidostat, and tubular reactors (Tredici and Zittelli, 1998).

The tubular photobioreactor consists of straight or coiled tubes arranged in various ways for maximizing the capture of sunlight (Figure 2.5). It has advantages of a larger illumination surface area, good biomass productivities, and better CO_2 transfer from the gas stream to the liquid culture medium. On the other hand, one of the major limitations of tubular photobioreactor is poor mass transfer. For instance, very high dissolved oxygen levels inhibitive to algal growth are easily reach in tubular photobioreactors (Molina et al., 2001). More limitations include: self or mutual shading by the algal cells which causes the light to be attenuated above the bottom of the culture, a decrease in light-saturated photosynthetic capacity (light and dark zones), and high cost of operation (Tredici and Zittelli, 1998). However, these limitations are even worse in open ponds or deeper reactor.

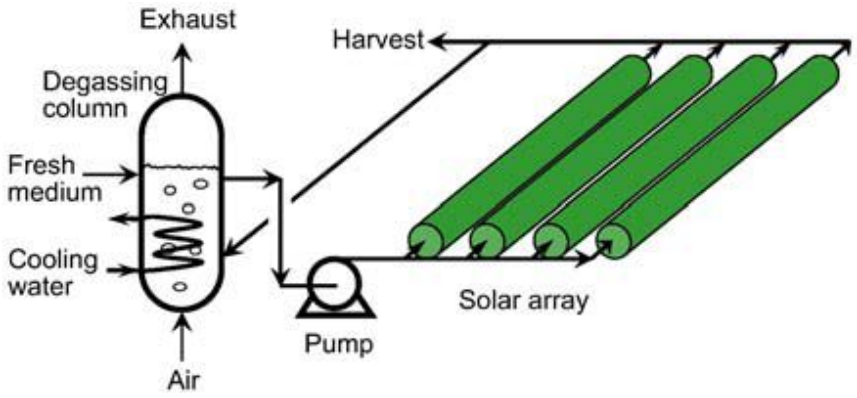

Figure 2.5: A tubular photobioreactor with parallel run horizontal tubes (Molina et al., 2001).

Flat-plate photobioreactors are comprised of transparent flat plates in which algae are cultivated (Figure 2.6). Flat-plate photobioreactors have received much research attention due to the large surface area exposed to illumination and high densities of photoautotrophic cells (Samson et al., 1985; Hu et al., 1998). Flat-plate photobioreactors are made of transparent materials for maximum solar energy capture, and a thin layer of dense culture flows across the flat plate, allowing radiation absorbance in the first few millimeters of thickness (Hu et al., 1998). When compared to tubular versions, flat-plate photobioreactors are more suitable for mass cultures of algae due to low accumulation of dissolved oxygen and the high photosynthetic efficiency achieved (Richmond et al., 2003). However, they also have some limitations, such as: scale-up requires many compartments and support materials, culture temperature is difficulty to control, any degree of wall growth blocks light, and there is an increased possibility of hydrodynamic stress to algal cells.

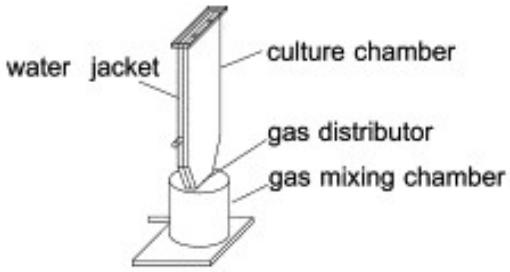

Figure 2.6: Experimental thin-layer flat-plate photobioreactor (Xu et al., 2011).

Hydraulically integrated serial turbidostat algal reactor (HISTAR) provides a robust system that superimposes suspended contaminant control on algal production, which takes advantage of the positive attributes of enclosed and open-tank reactors (Rusch et al., 2003). HISTAR consists of two sealed turbiodostats and a series of open, hydraulically connected, continuous flow stirred-tank reactors (CFSTRs) (Figure 2.7) (Benson et al., 2003). The sealed turbidostats produce a high quality monoalgal inoculum that is injected into the first CFSTR (Benson et al., 2003). This inoculation occurs at 10 minutes intervals and is automatically controlled to vary in duration in response to the turbidostat biomass density (Rusch and Christensen, 2007). HISTAR has advantages of providing reliable high quality monoculture of suspended microalgae through a series of linked turbidostats or chemostats (Benson et al., 2007).

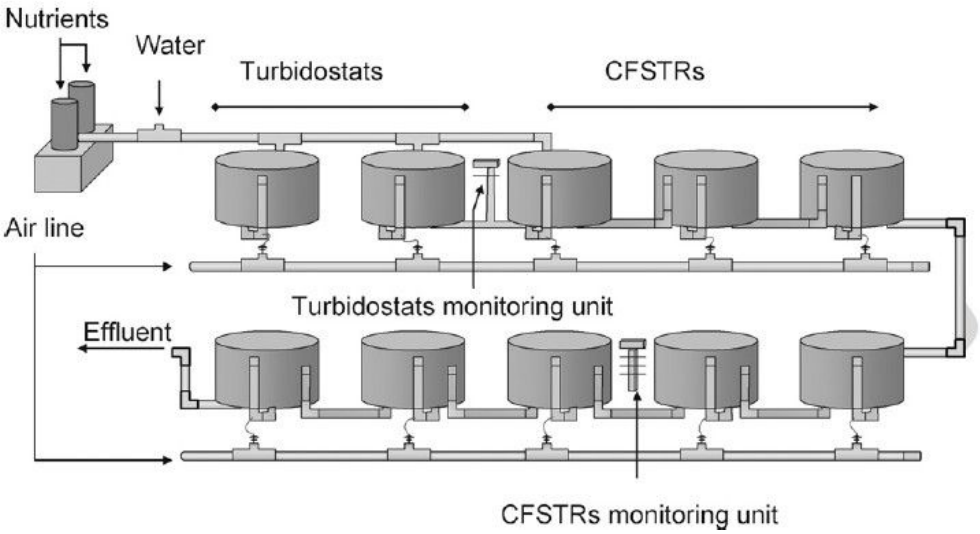

Figure 2.7: HISTAR system with two sealed turbidostats and the eight CFSTRs (Benson et al., 2003).

2.3.4 Flow Description

Culturing algae requires the input of light as an energy source for photosynthesis and a sufficient supply of nutrients in dissolved form in the culture medium. Biomass sedimentation in tubes is prevented by maintaining highly turbulent flow. Flow is produced using either a mechanical pump or a gentler airlift pump (Christi, 2007). First, the flow progresses to the diaphragm pump which moderates the flow of the algae into the actual tube from the feeder vessel. CO2 is dissolved into the cultivation systems from the CO2 inlet valve. Environmental parameters including light, pH, and temperatures are controlled in the photobioreactor in order to promote algal growth rates. A cleaning system inside the photobioreactor is beneficial to clean tubes without stopping the production. After the algae have completed the flow through the photobioreactor, it passes back to the feeder vessel. The

algae grow as the flow continues. When the algae are ready for harvesting, it passes through the connected filtering system.

Photosynthesis generates oxygen which cannot be removed within a photobioreactor tube, resulting in limitation of the maximum period length of a continuous run tube. The culture must periodically return to a degassing zone that is bubbled with air to strip out the accumulated oxygen (Christi, 2007). As the culture moves along a photobioreactor tube, the pH increases because of consumption of carbon dioxide (Molina Grima et al., 1999).So carbon dioxide is fed into the culture in the degassing zone in response to a pH controller. Additional carbon dioxide injection points may be necessary at intervals along the tubes to prevent carbon limitation and an excessive rise in pH (Molina Grima et al., 1999).

2.4 Light Dynamics and Growth Kinetics

2.4.1 PAR (Photosyntheticly Active Radiation)

Light availability is the most important factor in the growth and productivity of photosynthetic microalgal cultures (Kirk, 1994). When a beam of light reaches an aquatic layer, the number of photons are attenuated with depth in three ways: by particulate scattering, by absorption, or by transmittance (Benson, 2003). The sum of the absorption and the scatter represents the attenuation of the incident light (Kirk, 1994).

Photosynthetically Active Radiation (PAR) is the spectral range of solar light from 400 to 700 nm that is used by aquatic plants and algae in photosynthesis (Thimijan and Heins, 1983). The range of visible light (400-700 nm) represents the range of energy that is most

useful to the plant in photosynthesis, and other longer or shorter wavelengths are ignored (Thimijan and Heins, 1983). The PAR range of the spectrum contains 45% of the energy at the earth's surface (Kirk, 1994). It can be measured either as photon flux of incident or scalar light or as radiation energy. In the field of microalgae research, irradiance is usually taken as the total amount of PAR reaching a point from all directions (scalar irradiance), photon flux fluency rate (PPFFR).

The scalar PAR is the photon flux fluency rate at a given point available for photosynthesis and algae growth, and is considered to be the most representative of the light energy available to an algal cell within a photobioreactor since cells do not discriminate between photon directions for photosynthesis (Acien Fernandez et al., 1998; Benson and Rusch, 2006).

2.4.2 Surface Radiation

For a given point light source, the irradiance at the impacted surface can be determined using the inverse-square law, which states that the light intensity is inversely proportional to the square of the distance from the light source (Kimball, 1923; Beiser, 1973). This gives us the definition of the incident irradiance (I_o) at the surface of the microalgal cultures:

$$I_o = \frac{I_s}{D^2} \tag{2.1}$$

where: I_s = the PAR from the light source (μ mol s^{-1})

D = the distance of the light source (m).

However, most artificial light sources are fitted with collimating lenses or reflectors to redirect the light into parallel beams, which can drastically distort the relationship presented in Equation 2.1 (Benson and Rusch, 2005). Each type of light source can be empirically determined by a simple linear equation. The photosynthetic photon flux fluency rate (PPFFR) is used to quantity the scalar PAR quantum irradiance measured from all directions (Shibles, 1976). Therefore, the PPFFR at I_o as a function of light source distance (D) can be described by the following linear equation over the narrow range of elevation (Benson, 2003):

$$I_o = I_{D_o} - k_a D \tag{2.2}$$

Where: I_{D_o} = the theoretical I_o if D where equal to 0 (μ mol $s^{-1}m^{-2}$)

k_a = the change in I_o for each cm change in D (μ mol $s^{-1}m^{-2}cm^{-1}$).

2.4.3 Irradiance inside Culture

The Lambert-Beer Law represents a reasonable approach for the investigation of light attenuation within natural water bodies (Molina Grima et al., 1999). The assumption for application of this law includes low biomass density, monochromatic light, and unidirectional light path (Benson and Rusch, 2005; Dubinsky and Berman, 1979). In photobioreactors, the scalar PPFFR at a given distance of penetration is normally calculated following the exponential Lambert-Beer Law (Equation 2.3) where the light attenuation at a given distance of penetration (z). It derived from the total biomass (X_z) per volume contained in the layer penetrated (Huisman, 1999; Benson, 2003):

$$I_z = I_o e^{-k_o Z} \tag{2.3}$$

where: I_z = the scalar PPFFR (μmol $s^{-1}m^{-2}$) at z depth of penetration

I_o = the PPFFR surface intensity (μmol $s^{-1}m^{-2}$)

k_o = the culture attenuation coefficient ($Lmg^{-1}cm^{-1}$)

z = distance of penetration (cm)

Furthermore, the average irradiance (I_a) is the amount of light received by an average cell moving randomly inside the culture. I_a is impacted by the incident irradiance, biomass and the culture penetration and can be determined by the following equation over the penetration of the reactor (Ogbonna et al., 1995):

$$I_a = \frac{1}{d}\int_0^d I(z)dz = \frac{I_o(1-e^{-k_o Xd})}{(k_o Xd)} \tag{2.4}$$

where k_o = the culture attenuation coefficient ($Lmg^{-1}cm^{-1}$)

I_o = the PPFFR surface intensity (μmol $s^{-1}m^{-2}$)

z = the penetration of the reactor (cm)

d = the thickness of the reactor (m)

The relationship between I_a and X through experimentation at constant I_o and variable X can be determined using equation 2.4. This relationship is used in the study of the effects of I_a on growth rates.

2.5 Growth Kinetics

Different growth models have been proposed in the past several decades, but most of

them disregard the photoinhibition effect that may occur at the higher irradiance levels of artificial light and in natural light. To take photoinhibition into account, several microalgal growth kinetics models have been proposed (Table 2.3). Comparing the models shown in this table, researchers found that Steele (1977) and Molina Grima et al. (1993) model had the highest r^2 values, though all required parameter adjustments in response to extreme self-shading effects (Molina Grima et al., 1996).

In cultures where self-shading is high , a hyperbola is the better model to reflect the peak of the relationship between μ and I_a (Acien Fernandez et al., 1997). Steel's growth model acknowledges that growth is limited by low irradiance levels and inhibited by high light levels (Chapra, 1997). Steels's model is one of the simplest that acknowledge that growth is inhibited at high light levels and is adequate for modeling growth in shallow reactors (Steele, 1977):

$$\text{Steele's:} \quad \mu = \mu_{\max} \frac{I_a}{I_{opt}} e^{1-\frac{I_a}{I_{opt}}} \tag{2.5}$$

Where: I_{opt} = the optimum PPFFR that provides for ($\mu_{\max}$)

μ= growth rate (d^{-1})

I_a= average PPFFR.

Table 2.3: R^2 values for five different growth models as reported for three experimental series (Molina Grima et al., 1996).

Source	Experimental Series			Model
	A	B	C	
Molina Grima et al., 1993	0.995	0.997	0.995	$D = \frac{\mu_{\max} I_a}{I_{ki} + I_a} - m$
Tamiya et al., 1953	0.940	0.963	0.995	$\mu = \frac{\mu_{\max} I_a}{\mu_{\max} + I_a}$
Steele, 1977	0.990	0.971	0.996	$\mu = \mu_{\max} \frac{I_a}{I_{opt}} e^{\left(1 - \frac{I_a}{I_{opt}}\right)}$
Van Oorschot, 1955	0.944	0.989	0.988	$\mu = \mu_{\max}(1 - e^{(\frac{I_a}{I_{opy}})})$
Aiba, 1982	0.911	0.934	0.995	$\mu = \frac{\mu_{\max} I_a}{K_i + I_a + \frac{I_a^2}{k_i}}$

M = mortality rate; r = ration I_o/I_a; K_i is a fitting parameter

2.6 Previous Studies of Mechanistic Modeling

A mechanistic model which describes biomass growth and lipid productions is a crucial tool for predicting lipid production with respect to light dynamics and growth kinetics in the microalgae cultivation systems. It is necessary to develop a numerical model that takes environmental conditions, such as light and nutrient availability, into account for lipid production in order to gain insight into productivities and identify optimal process conditions.

Mechanistic modeling, using first-order microalgal growth kinetics combined with reactor kinetics, was used to simulate the light dynamics and microalgae growth kinetics on

system productivity (Rusch and Malone, 1998; Benson et al., 2007). This modeling approach used in prior studies. Benson et al. (2007) developed a mechanistic model to investigate the impacts of internal light dynamics on system productivity in HISTAR. They found that the average scalar irradiance within the cultures can be determined by integrating Lambert-Beer Law over the culture depth, and the growth rate can be estimated by using Steele's equation (Steele, 1965) in moderate density cultures and accounts for photoinhibition. They also showed that the biorhythms in the modeling of microalgal productivity can significantly enhance the accuracy of productivity forecasting (Benson et al., 2007).

Droop model (Droop, 1998) is a simplest model for describing microalgae growth under a nutrient (nitrogen or phosphorous) limitation. Drrop model considers that the biomass growth (x0 is related to the limited nutrient quota (q_n), while nutrient uptake depends on the external concentration of nutrient (s) :

$$\begin{cases} s = Ds_{in} - \rho(s)x - Ds \\ q_n = \rho(s) - \mu(q_n)q_n \\ x = \mu(q_n)x - Dx \end{cases} \tag{2.6}$$

where D is dilution rate, s_{in} is the influent nutrient concentration, $\rho(s)$ is the absorption rate which is generally taken as Michaelis-Menten, and $\mu(q_n)$ is the growth rate. In this model, $\mu(q_n)$ can be represented as follows:

$$\mu(q_n) = \mu_{\max}(1 - \frac{Q_o}{q_n}) \tag{2.7}$$

where Q_o and μ_{max} are the minimal cell quota and the maximum growth rate, respectively.

Various models have been proposed to predict lipid synthesis and microalgae growth

with respect to nutrients and light. Grognard et al. (2010) proposed a simple bioreactor model accounting for light attenuation in the reactor under the influence of day/night cycles due to biomass density to obtain the control law that optimizes productivity. They applied the Monod model (Monod, 1942) and Beer-Lambert Law to deal with substrate limitation, light attenuation, and light periodicity; then biomass productivity optimization was presented in a constant light environment. They found that because of the day-night constraint, the productivity rate is lower than without it; when the maximal growth rate is larger than the respiration rate, the maximal productivity rate can be achieved.

Packer et al. (2011) developed a mathematical model that describes neutral lipid production of green microalgae grown in batch cultures for nitrogen-limited conditions. In this model development, nitrogen-limited growth took the form of the well-established Droop model (Droop, 1998), and the model for chlorophyll synthesis coupling with nitrogen uptake was directly adopted from Geider et al (1998). They found that neutral lipid production can be simplified within the framework of ecological stoichiometry. They also deduced that the decoupling of photosynthesis from cellular growth is a possible explanation for excessive neural lipid production. Mairet et al. (2011) proposed a dynamical model of microalgae growth in photobioreactors in order to further optimize neutral lipids and carbohydrates productivities under light and nitrogen limitations:

$$q_l = (\beta q_n - q_l)\mu(q_n) - \gamma\rho(s) \tag{2.8}$$

where q_l is the neutral lipid quota, and γ is the parameter which can be computed from the pervious equations using measurements obtained at equilibrium. This model gathers two modeling

approaches based on Droop model (Droop, 1998) which was initially established to represent the effect of B_{12} vitamin internal quota on the growth rate of phytoplankton, and the experimental validation which was carried out under constant light. The light distribution inside the photobioreactor was computed using a Beer-Lambert Law. The model was assessed with experimental data under day/night cycles, and finally was used to predict carbohydrate and lipid productivities (Figure 2.8).

While there are existing models of microalgae growth and lipid production with respect to both light and nutrient limitation, it remains a significant research area with need for more mechanistic models of lipid production to help improve the production process (Klausmeier et al., 2008). These published models of microalgal lipid production can be used under both nutrient and light limitations, so no models for microalgal lipid synthesis with nutrient replete conditions have been developed to predict lipid production. Additional limiting factors of lipid production besides nutrients, such as temperature, CO_2 supply, and turbulence, are needed to consider in future model development. In future model development, it is necessary to combine existing models and frameworks in order to model lipid production and biological process in microalgae photobioreactors. The model to be formulated in this study can be used under nutrient replete condition, is largely based on stoichiometry, fundamental physiological processes, and environmental factor responses that governing lipid production. This model is designed to improve the biomass and lipid production process and gain a better understanding of biological processes in the flat-plate photobioreactor.

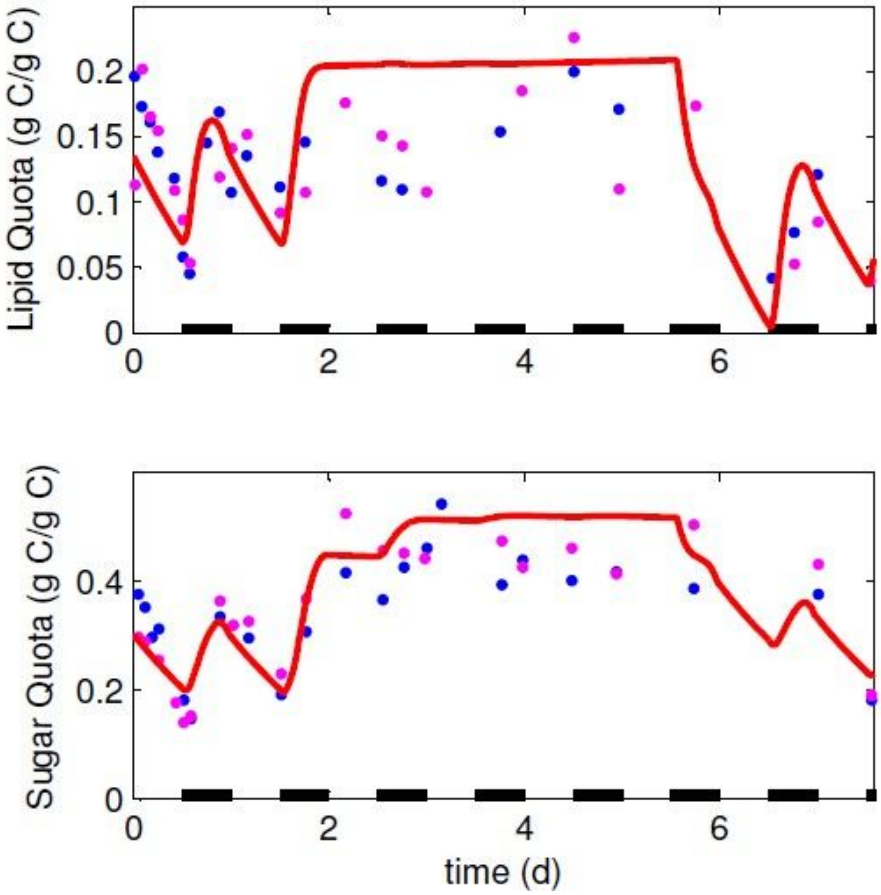

Figure 2.8: Neutral lipid and carbohydrate quotas during a continuous culture of *Isochrysis affinis galbana* under day/night cycles: comparison between model simulation (red lines) and experimental data (symbols) (Mairet et al., 2011).

Chapter 3: Materials and Methods

3.1 Organisms and Culture Method

The microalga used in this study was Nannochloropsis salina from the Texas AgriLife Research Center at Corpus Christi. Four fully automated and controlled environment photobioreactors (FACE 4) (111.76 cm x 51.12cm x 10.16 cm) were used to grow Nannochloropsis s. under various experimental conditions (Figure 3.1). Illumination was provided by two 400 watt metal halide lamps per reactor. The FACE 4 Photobioreactors where designed to optimize the exposure of the algal cell to light by minimizing the thickness of the culture (Z), controlling cell light/dark cycling frequency (ν), system dilution rate (Ds), the light spectrum for the subject species, culture density (X), and the lamp distance (D).

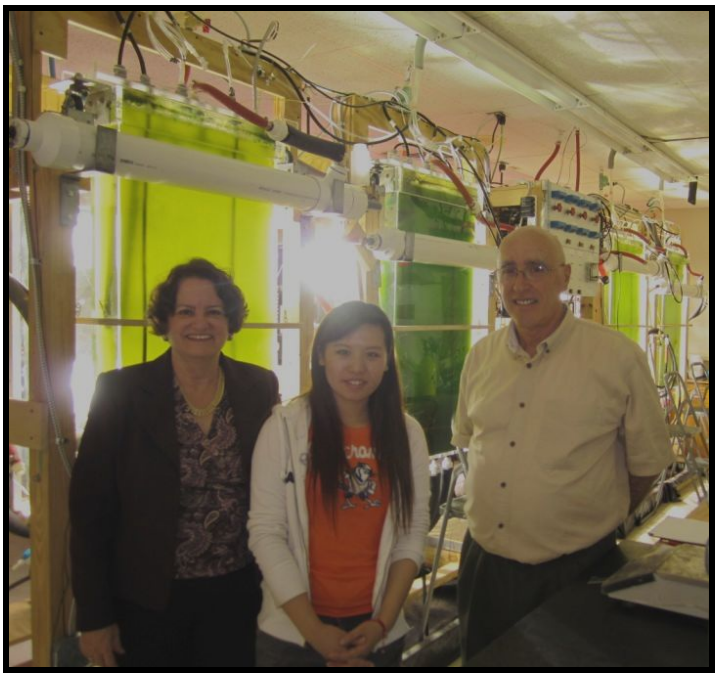

Figure 3.1: FACE 4 photobioreactor systems at the Microalgae Physiology Laboratory at the Texas AgriLife Research and Extension Center in Corpus Christi.

3.2 Experimental System and Operation

The FACE 4 is comprised of four individual flat-plate type controlled automated bioreactors (CAB). The experimental units in this study where operated as individual batch CABs with water, nutrients, air and CO_2 inflows and outflows (Figure 3.2). The CABs not only provided better experimental control, but also replication with the four reactors contained in FACE 4. The light intensity was measured via quantum sensors which were distributed in the reactor as shown in Figure 3.2. Scalar radiation was also monitored by using a bulb quantum sensor (Li-193 SA, Li-Cor Inc., U.S.A.) under different culture dilutions. Monitor systems were placed throughout the photobioreactor to measure the amount of CO_2 injection, temperature, pH, and nutrients injection.

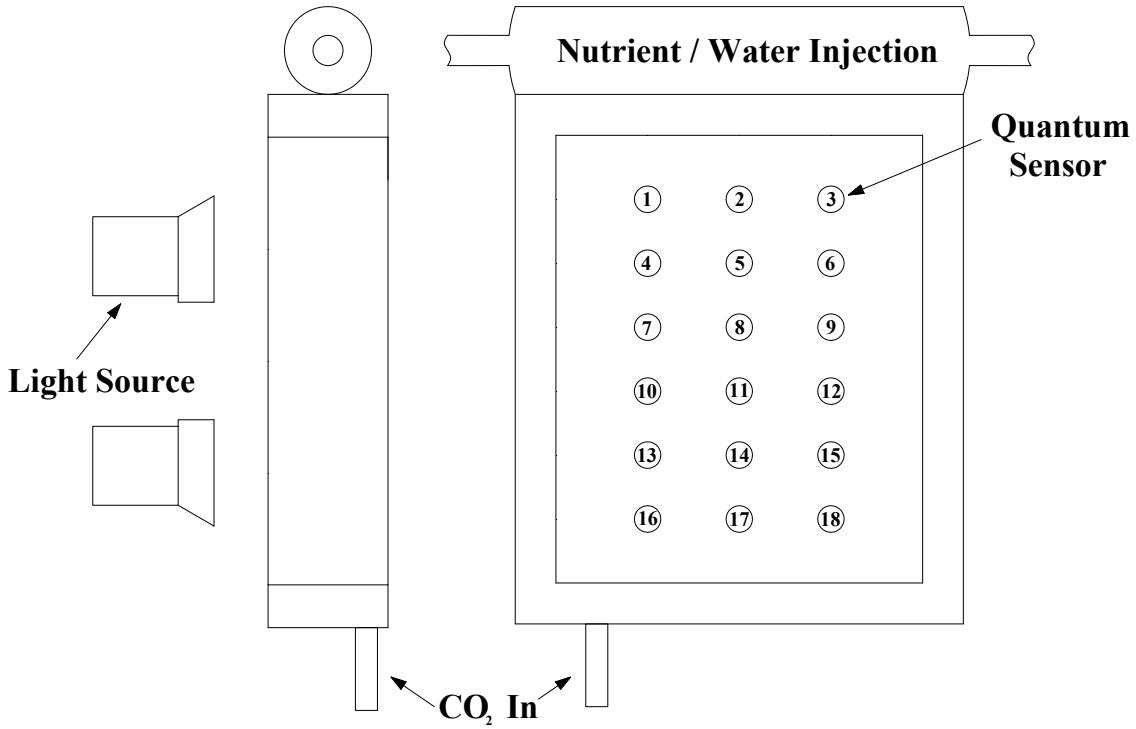

Figure 3.2: Front and side views of one CAB at FACE 4 systems.

3.3 Experiments

Three sets of experiments were conducted to determine the following relationships in the FACE 4 system: (1) The light distance study: surface PPFFR (I_o(PAR)) as a function of light source distance (D); (2)The light attenuation study: depth and biomass concentration dependent scalar irradiance (I_z(PAR)); (3) The growth kinetic study: specific growth rate (μ) as a function of average scalar irradiance (I_a(PAR)). Some basic methods were applied during each of these studies

Measurement of biomass by manual cell counting under a microscope was used to determine algal biomass density in the reactor daily. Measurement of alga biomass was also made on samples filtered through a pre-weight 0.45μm Durapore Membrane Filter (Millipore). The filter paper was dried well in an Isotemp Standard Lab Oven (Fischer Scientific, U.S.A.) at 80℃ for 24 hours before it was weighed again. The final dry weight of biomass concentration in the sample was assumed to be the difference between the final filter weight and the initial filter weight. Scalar radiation was monitored using a bulb quantum sensor as well as quantum sensors distributed on the surface of the reactor. Instantaneous PPFFR readings were recorded by data logger (LI-1400, Li-Cor Inc., U.S.A.) after the quantum sensor had stabilized.

3.3.1 Light Diffusion Study

The purpose of this study was to investigate the relationship between the distance of the light source from the surface of the CAB and diffusion of light through air. The diffusion

coefficient K_a describes the change in I_o with each cm change in D. Distance was considered to be the horizontal distance from the center of the metal halide lamp to the surface of the CAB. In the experiment, surface PPFFR was measured for each light source at three different distances (10.12-46.5 cm) in front of the CAB using quantum sensors on the surface of the experimental unit. Duplicate readings were taken for all four CABs. Quantum sensors at the surface of each CAB were distributed at incremental values from the center to the bottom and top at each horizontal level (center, 20.23 cm), and they were also distributed from center to the sidewall of the reactor at increment of 17.78 cm at vertical cross-section (Figure 3.2).

The two light sources were carefully centered to ensure symmetrical light distribution over the surface of the CAB. This symmetry divides the reactor into three concentric rings having radii 10.16 cm, 25 cm, and 40.886 cm (Figure 3.3). Data collected at three rings represented the surface irradiance within these rings. The PPFFR within each ring was weighted based on the proportion of the area within the corresponding concentric ring to the total surface area. The average surface PPFFR for the reactor was determined by the average PPFFR of three rings. A best-fit regression analysis of I_o versus D data was performed, and the relationship parameters were obtained.

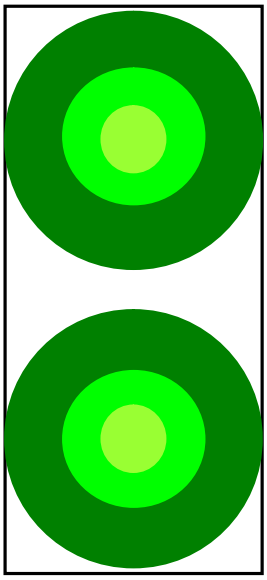

Figure 3.3: Diagram of symmetrical light distributed as three concentric rings for each lamp over the surface of the CAB.

3.3.2 Light Attenuation Study

In this study the relationship between scalar irradiance at a given depth of penetration in the culture and cell concentration was investigated. According to the Lambert-Beer Law the overall scalar attenuation coefficient (k_o) describes the decrease in scalar irradiance as the concentration of biomass and culture depth increases. K_o can be linearly partitioned between attenuation due to water and impacted by the biomass. So k_o can be described in the following equation:

$$k_o = k_b + k_w \qquad (3.1)$$

where: k_b = attenuation by *Nannochloropsis s*.

k_w = attenuation by water.

In the experiment, light attenuation studies were performed at five different values of biomass (X = 0 mg/L to X = 787.2 mg/L). Two lamps were centered horizontally in front of the reactor and the PPFFR was measured in suspensions of known biomass concentration at three different distances of penetration from the front side of the reactor to the back. At each distance of penetration, readings were taken at nine different locations in the same vertical plane by using the bulb quantum sensor (Figure 3.2). PPFFR was measured at 2.54 cm increments of penetration. At each increment of penetration, duplicate readings were taken from the center to the sidewall at 20.23 cm increments (center, 20.23cm), as well as taken from the center to the sidewall of the reactor at increment of 17.78 cm at vertical increments to the top and bottom of the reactor (Figure 3.2). So a total of nine light were recorded at each increment of penetration. Weighted means of I_z were calculated for each incremental of penetration by the same method used in the light diffusion study. An exponential regression of the I_z versus distance of penetration (z) was developed for each of the data sets, and the light attenuation coefficient (k_o) was estimated by regression analysis for each study.

3.3.3 Growth Kinetics Study

Growth studies were performed in a 1 L New Brunswick Scientific fermentor to determine the specific growth rate (μ_{max}) of *Nannochloropsis salina* collected from Texas AgriLife research at Corpus Christi. During the growth study, illumination was provided by a 120 W metal lamp (Philips Lighting Company) at a constant distance of 47 cm (Figure 3.4). Temperature in the fermentor was controlled at room temperature (25 ℃), and the speed of

mixings was kept at 200 rpm. A mini air pump was used to supply air in the fermentor. Temperature and pH of the media were monitored by automatic mini pH Control System Model pH-40 (New Brunswick Scientific Co., U.S.A.).

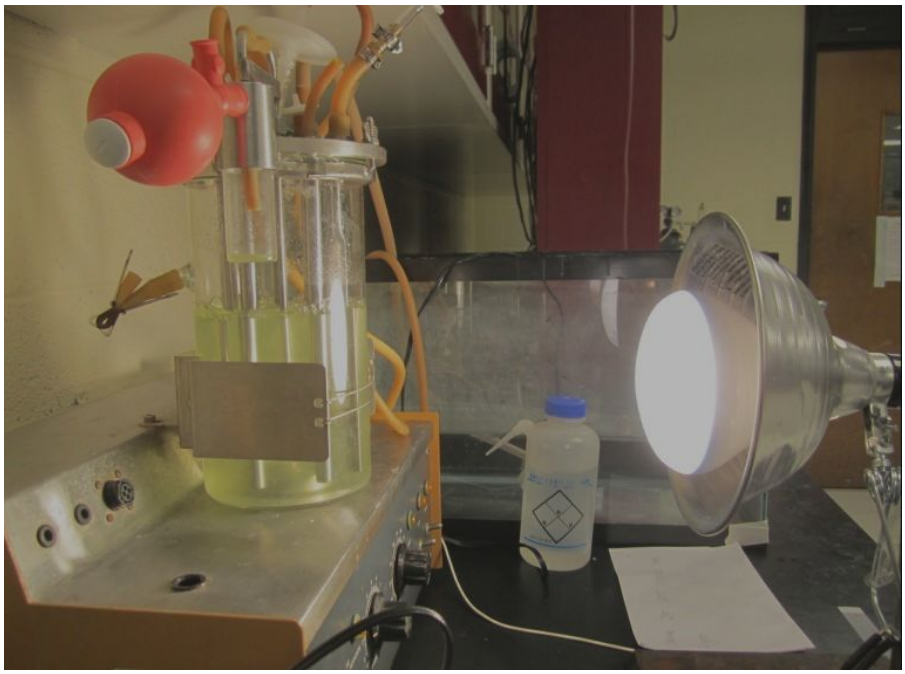

Figure 3.4: Experimental set-up for the growth kinetics study.

Samples were collected at six-hour intervals until the phase was stationary. OD was measured in the samples at 750 nm by using a DR 5000 UV-vis spectrophotometer (Hach Company, US). A growth curve was obtained from culture grown during the growth study. The maximum specific growth rate (μ_{max}) of algae is the maximum slop of the trend line in the plot of the natural log of dry cell weight concentration verse time.

The relationship between biomass and OD was determined at the end of the growth study by diluting the culture to five concentrations. At each dilution, biomass concentration

was measured by filtering the 10 ml sample through the pre-weight 0.45 μm acetate filter. The filter paper was dried in an Isotemp Standard Lab Oven (Fischer Scientific, USA) at 80 ℃ for 24 hours, and then was re-weighed after cooling down at room temperature. The dry weight of each dilution was the weight difference between the final weight and the initial filter weight. The values of OD and dry weight biomass collected at each dilution were used to determine a calibration curve of biomass concentration. Thus OD values collected at every 6 hour intervals were converted into cell dry weight concentration using this calibration curve.

3.3.4 Total Lipid Analysis

Microalgae lipid extraction was completed by the collaborators of this project in Department of Life Science at Texas A&M University-Corpus Christi. Lipid content of *Nannochloropsis salina* cultures generated from FACE 4 Photobioreactors were measured during various growth stages to determine lipid production. Lipid content was analyzed by using a procedure from the Folch method (1957). At the time of sample collection, TSS was measured to determine the biomass concentration in the sample. After spinning down and freeze drying samples of microalgae, 100 mg of dry sample was put into a 15ml falcon tube. The sample was homogenized by adding 2 ml of chloroform and 1 ml of methanol to the tube, and was orbited for 20 minutes at 50 rpm in an orbital shaker at room temperature. The sample was centrifuged at 2800 rpm for 10 minutes to recover the lipid phase. The lipids are soluble in the chloroform, which forms a dense layer at the bottom of the tube. In order to

separate the chloroform, methanol, and lipids from the rest of the cell materials, the top layer from the tube was poured off. The sample was then washed with 6 ml of 0.9% NaCl adding to the bottom layer left in the tube. After vortexing for some seconds, the sample was centrifuged again at 2800 rpm for 10 minutes to separate into two phases. The lipids and chloroform create the bottom layer, while the methanol and water form a top layer. To separate the NaCl and methanol from the lipids and chloroform, the bottom layer in the tube was removed using a transfer pipette, and then it was transferred into a pre-weighed scintillation vial. The scintillation vial was dried well on a hot plate at 80 ℃ for 24 hours in order to evaporate the chloroform and leave only lipids. The end product in the scintillation vial was weighed, and the final weight was subtracted from the scintillation vial weight. Then the final weight was divided by the weight of the original sample to gain the lipids content (C_{lipid}). The lipid production (P_l) was calculated by the following equation:

$$P_l = \frac{C_{lipid} \times X}{T} \tag{3.2}$$

where,
P_l = lipid production ($gl^{-1}d^{-1}$)
C_{lipid} = lipid content of cells (%)
X = dry cell weight (g/l)
T = the cultivation period (days)

Chapter 4: Results and Discussion

Studying light dynamics and growth kinetic in experimental units was essential to provide operational data for the FACE 4 photobioreactor. A series of experiments were performed to examine fundamental process relationships and determine the parameters, involving light attenuation, microalgae growth kinetics and suspended biomass concentrations.

4.1 Light Diffusion Study

Light diffuses as it passes through air, and then it is attenuated by walls, water and biomass as it continues to penetrate the culture. It is necessary to study the travel pathway of photons from the light source to the surface of the reactor, so that the PPFFR diffused by air (I_{oair}) was determined. I_{oair} is the surface PPFFR at each CAB, which was measured by quantum sensors.

The regressions relationship between surface PPFFR (I_{oair}) via air and distance (D) points from the light source for each of four CABs was investigated as shown in (Figure 4.1):

$$\text{Reactor 1:} \quad I_{oair} = 916.12e^{-0.0240D} \tag{4.1}$$

$$\text{Reactor 2:} \quad I_{oair} = 735.84e^{-0.0255D} \tag{4.2}$$

$$\text{Reactor 3:} \quad I_{oair} = 1067.3e^{-0.0292D} \tag{4.3}$$

$$\text{Reactor 4:} \quad I_{oair} = 894.38e^{-0.0241D} \tag{4.4}$$

In Figure 4.1, it shows negative exponential relationships over the distances studied within four CABs. Each set of data had an r^2 value of greater than 0.98. The relationship between

I_{oair} and D of FACE 4 photobioreactors used for model parameters is the average of data in these four equations, as shown in the following:

$$I_{oair} = 903.07e^{-0.0257D} \quad (4.5)$$

(for D = 10.12-46.5 cm; $R^2 = 0.9949$)

where 903.41 $\mu mols^{-1}m^{-2}$ is the hypothetical I_{oair} (PAR) at D=0, and 0.0257 cm^{-1} is the light energy dissipation coefficient constant (k_a) for FACE 4 systems using two 400 watt metal halide lamps. Thus, light is diffused through air according to an exponential relationship over the distances studied with a diffusion coefficient k_a of 0.0257 cm^{-1}.

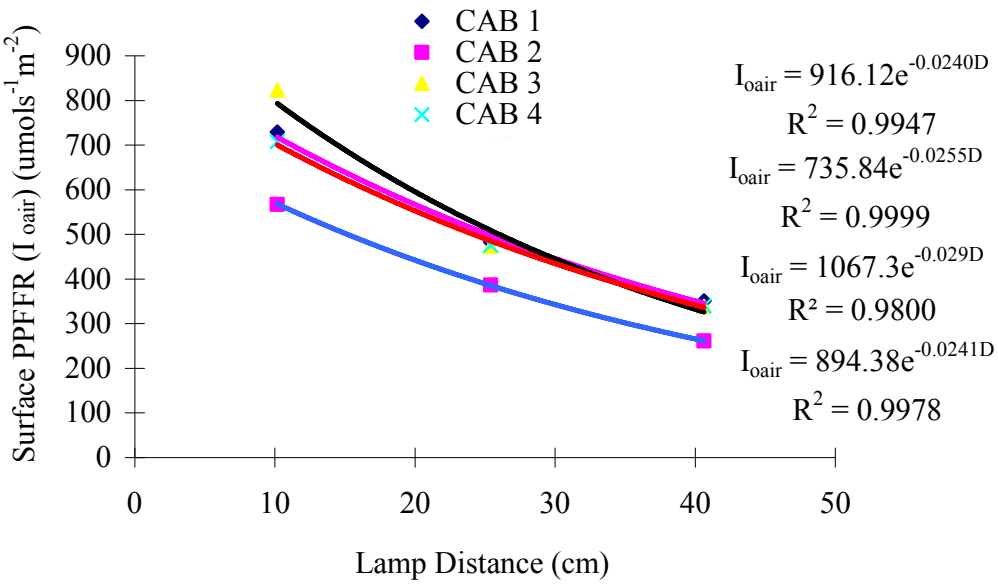

Figure 4.1: Relationship between surface PPFFR (I_{oair}) and lamp distance (D) at CAB surface.

The light attenuation coefficient (k_r) through the thickness of the reactor was determined by plotting the average PPFFR at both front and back sides of the CAB against the thickness under three different distance points of the light source (Figure 4.2). The thickness of the reactor included the 1.27 cm thick acrylic walls and clear saline within the

CAB. The results were averaged to yield a k_r value of 0.062 cm^{-1} for the three different cases.

(a)

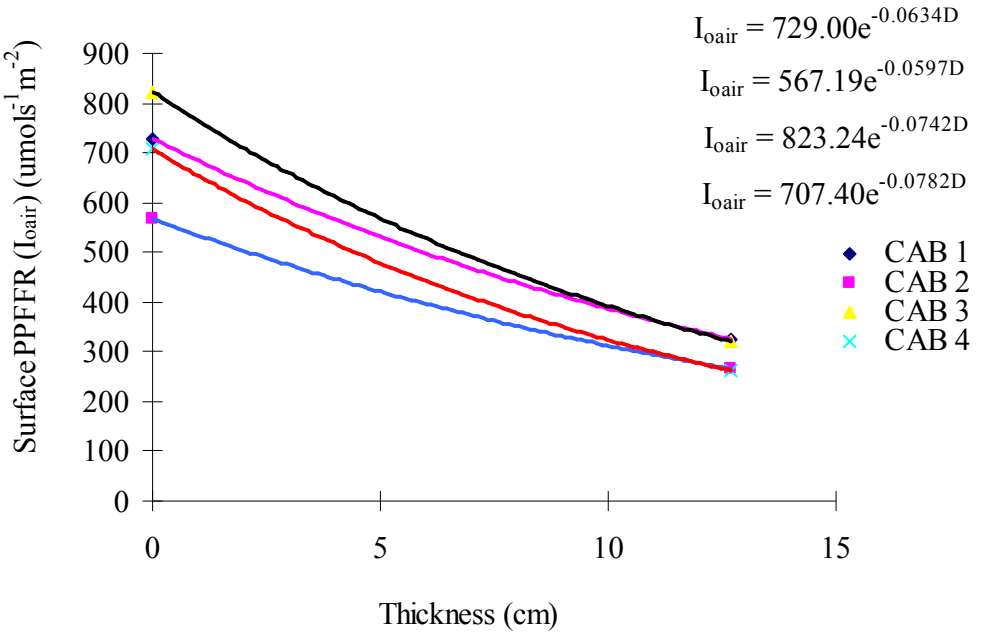

(b)

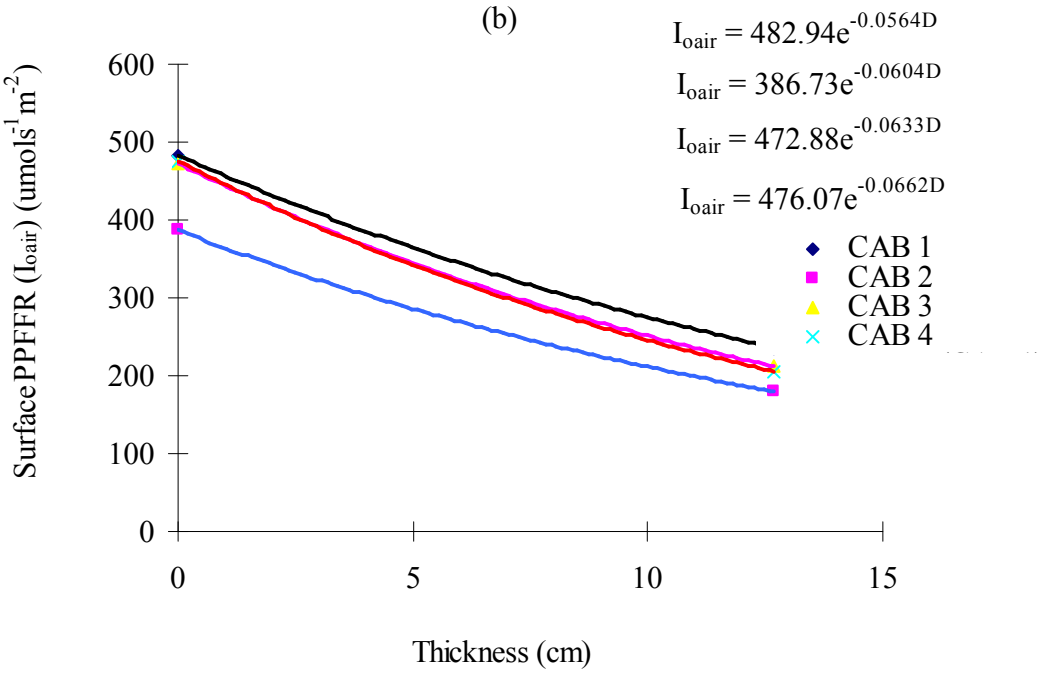

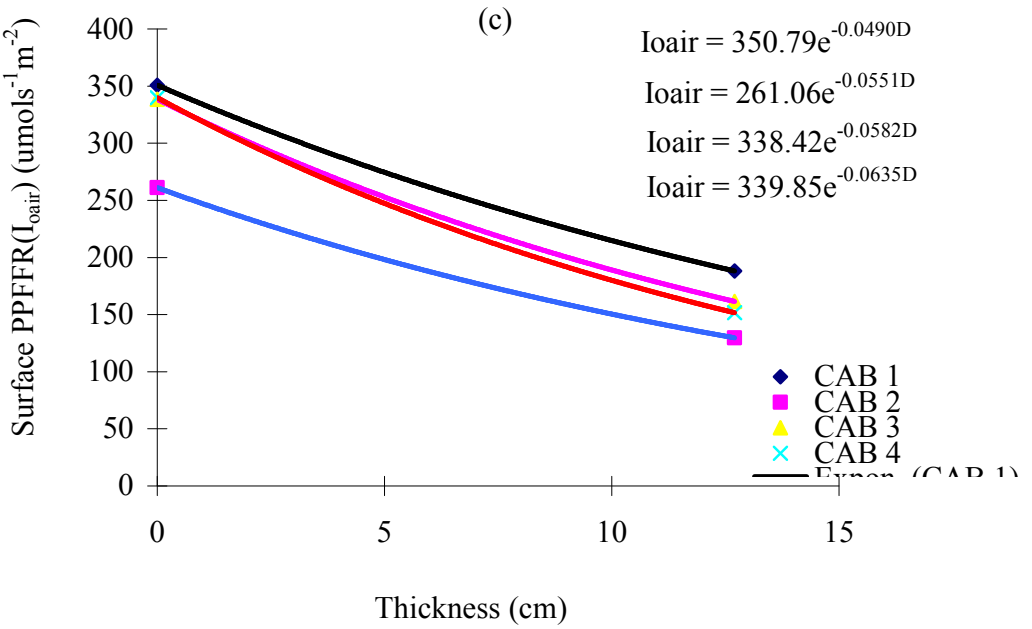

Figure 4.2: Relationships between surface PPFFR (I_{oair}) at both front and back sides of CABs and thickness at three selected distances from the light source. (a) distance =10.16 cm; (b) distance = 25.40 cm; (c) distance = 40.46 cm.

Using these light attenuation coefficients, I_o can be predicted over a range of D. The parameters obtained from the experiments will be used in modeling light dynamics in FACE 4 photobioreactors.

The surface PPFFR (I_o) is I_{oair} going through 1.27 cm thickness acrylic walls of the CAB. Light attenuation occurs when light passes through the walls, because the plastic walls absorb and reflect lights. Studying I_o will in turn determine the photon flux available at any thickness in the culture for a given light source. For the measurement of surface PPFFR, the bulb sensor was placed facing the light source in the culture such that the bulb was near the front wall of the CAB. I_o was measured for different locations in the CAB, corresponding with quantum sensors distributed at the front side of the CAB during the prior studies. In a

constant biomass concentration, the measured surface PPFFR within the culture has been plotted against I_{oair} in Figure 4.3. The slopes of the regressions give values of the diffusion coefficient (k_p) due to the acrylic walls. In 25%, 50%, 75%, and 100% biomass culture, the negative k_p indicates light was attenuated by the walls. In the clear water, there are seven positive k_p which indicate PPFFR was increased when light passed though the wall. It is probably due to light was reflected when it was incident on an interface between glass and water at these seven sensors. Errant data may also cause the positive k_p, because these sensors were located at the place closing to the fluorescent lights on the roof. The sensors are very sensitive, so they may caught photons from the fluorescent lights under these circumstances. When light goes through the CAB of clear water, the surface of wall is like a mirror reflecting light, leading to a positive k_p. Since k_p varied over the nine locations in the CAB, an average k_p was calculated under a given cell concentration. The averaged values of k_p were then plotted against different cell concentrations in Figure 4.4. The k_p was investigated for the different biomass concentration by the following equation:

$$k_p = 55.608 In(x) - 175.78 \qquad (4.6)$$

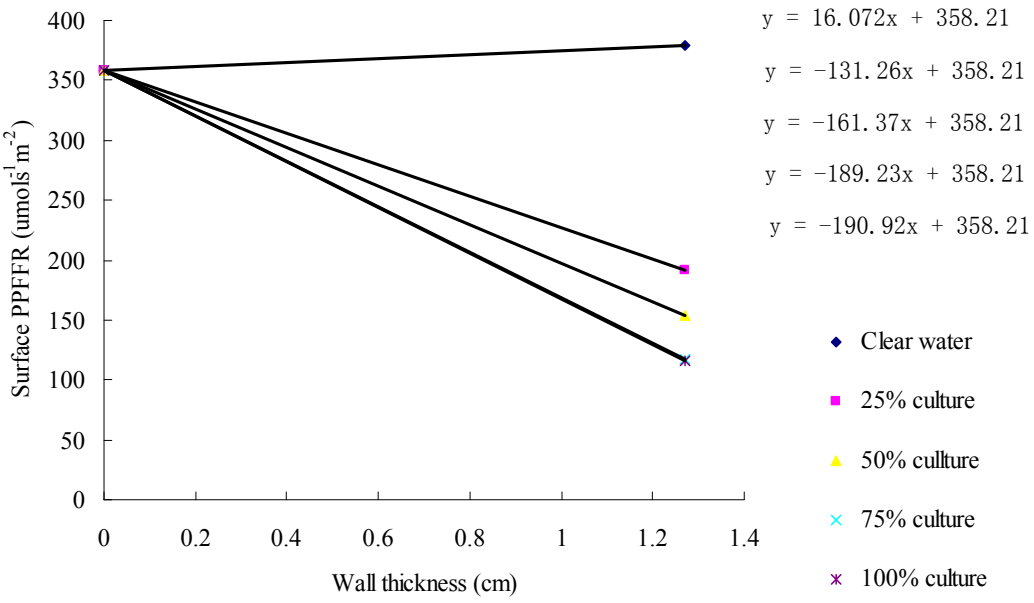

Figure 4.3: Relationships between I_o and I_{oair} under different biomass.

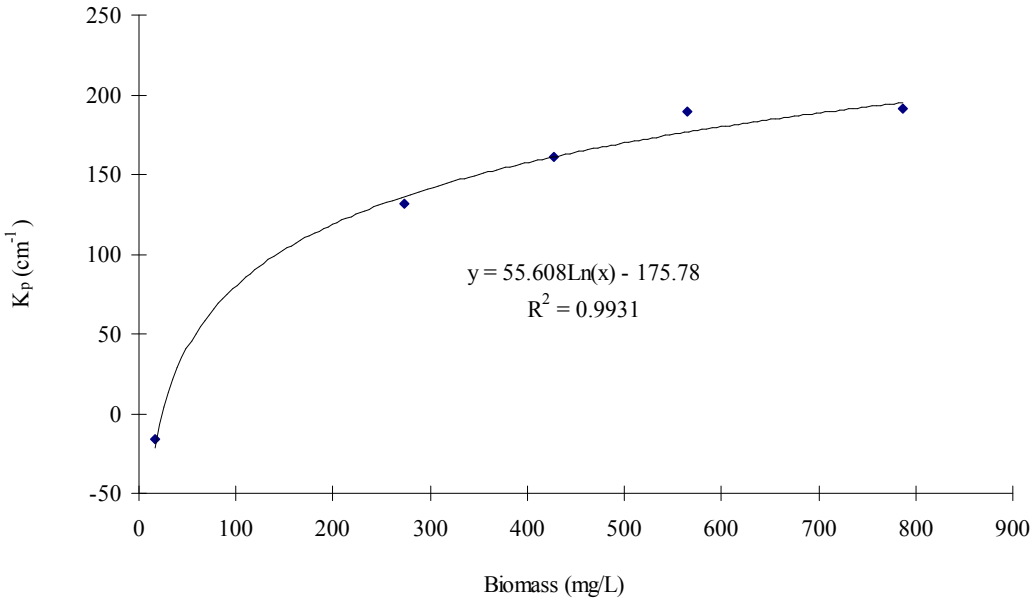

Figure 4.4: Light attenuation coefficient due to plastic walls (k_p) as a function of biomass concentration.

Equation 4.6 was used to determine k_p in model development. Based on Figure 4.3, the relationship between k_p and I_o can be best described by a linear equation (4.7) under different biomass. The 1.27 means the thickness of the acrylic wall.

$$I_o = k_p \times 1.27 + I_{oair} \qquad (4.7)$$

All the estimated parameters and relationships determined during this light study showed strong statistical correlation with experimental data having R^2 values greater than 0.97.

4.2 Light Attenuation Study

4.2.1 Effect of Biomass and Culture Penetration on Average PPFFR (I_z)

Understanding light dynamics within the culture is essential to study the behavior of algal growth activity in the reactor. At any distance of penetration into the culture, I_z is the mean of PPFFR taken at nine different locations in the same vertical plane. Culture penetration (z) was regressed against I_z for various cell concentrations to estimate light attenuation coefficient (k_o), and this plot has been presented in Figure 4.5. Fitting to Beer-Lambert Law, values of k_o and I_z were determined for each biomass study that is listed in Table 4.1. A similar study for k_o of green microalgae in the HISTAR was ranged between 0.1615 cm^{-1} to 0.9473 cm^{-1} (Benson and Rusch, 2005). The CAB is much thinner than the HISTAR, resulting in K_o value of 0.0098 cm^{-1} is much smaller than the value of 0.1615 cm^{-1} reported by Benson and Rusch (2005) under the clear water condition.

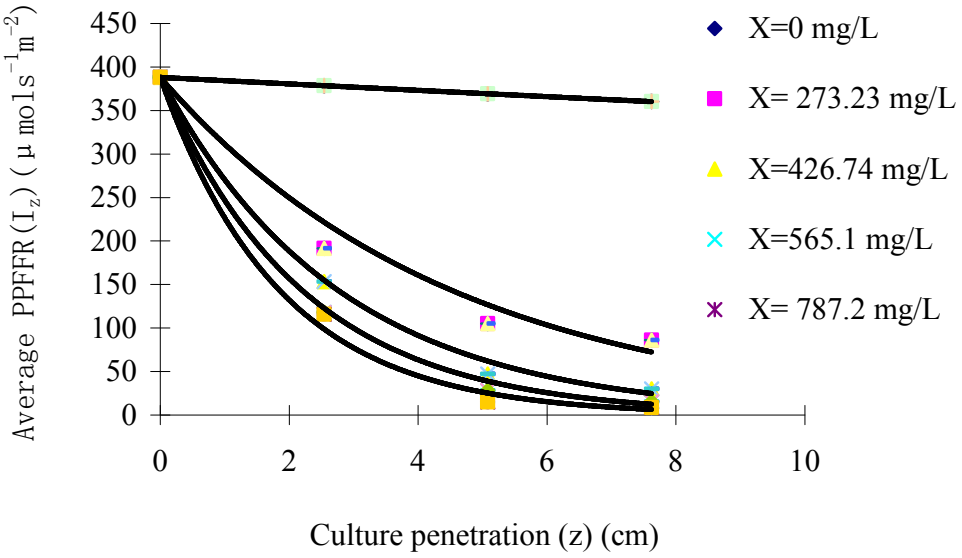

Figure 4.5: A plot of PPFFR at a given of penetration (distance from the front side of a CAB) with respect to the penetration for different biomass concentration (X, mg/L).

Generally, the average PPFFR decreased exponentially with increasing penetration. While in the clear water (X = 0 g/m^3), I_z fell in the linear range of the exponential attenuation curve. The attenuation by the microalgae presented the typical declining exponential fit. Microalgae cells absorb light through photosynthesis which results in decrease of light in the media.

Table 4.1: Results of k_o, I_z, and R^2 obtained from the light attenuation experiments.

Biomass concentrations, X (g/m^{-3})	I_z ($\mu mols^{-1}m^{-2}$)	R^2	Light attenuation coefficient, $k_o(cm^{-1})$
0	$388.09e^{-0.0098z}$	0.9999	0.0098
273.23	$388.09e^{-0.2203z}$	0.9367	0.2203
426.74	$388.09e^{-0.3611z}$	0.9729	0.3611
565.10	$388.09e^{-0.4526z}$	0.9753	0.4526
787.20	$388.09e^{-0.5383z}$	0.9581	0.5383

4.2.2 Effect of Biomass on the Determination of K_o, K_w and K_b

K_o for each study was regressed against the respective biomass concentration in Figure 4.6, yielding a linear partition:

$$k_o = 0.0326 + 0.0007X \quad (4.8)$$

It can be observed from equation 4.8 that light attenuation coefficient (k_o) can be linearly partitioned into water (k_w) and biomass (k_b), where $k_b = 0.0007 cm^{-1}$ and $k_w = 0.0326\ cm^{-1}$. In other words, average irradiance in the culture decreased by the sum of Equation 4.8 per g dry wt/m^3. Light attenuation linearly increases as biomass concentration increases. The attenuation due to the biomass (k_b) is comparable to the k_b value of 0.00064 cm^{-1} obtained by Kirk (1994) for outdoor algae cultures. Benson and Rusch (2005) reported that artificial

illumination produces similar attenuation patterns to those obtained for nature light. The attenuation due to water (k_w) estimated in this study is high compared to the k_w value of 0.0016 cm^{-1} for seawater reported by Gallegos (1994). This is due to a shallow depth of the CAB compared to the depth of nature water. With an increase of water depth, k_w is decreased due to wavelengths of less energy are absorbed in deep water (Kirk, 1994).

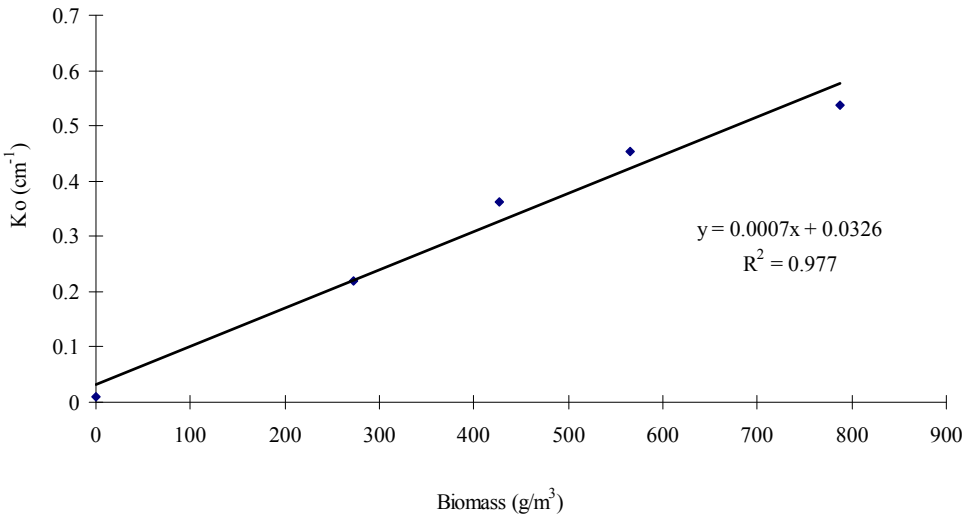

Figure 4.6: Linear regression between k_o and biomass.

4.2.3 Effect of Biomass on the Average PPFFR (I_a) within the Culture

The relationship between average light in the reactor and biomass concentration was obtained by plotting PPFFR as dependent on X in the experimental unit (Figure 4.7). This relationship can be used to estimate the average PPFFR during transitional growth rate. An exponential trend curve fit the data, so average PPFFR can be generally predicted in equation 4.9:

$$I_a = 296.69e^{-0.0027x} \quad (4.9)$$

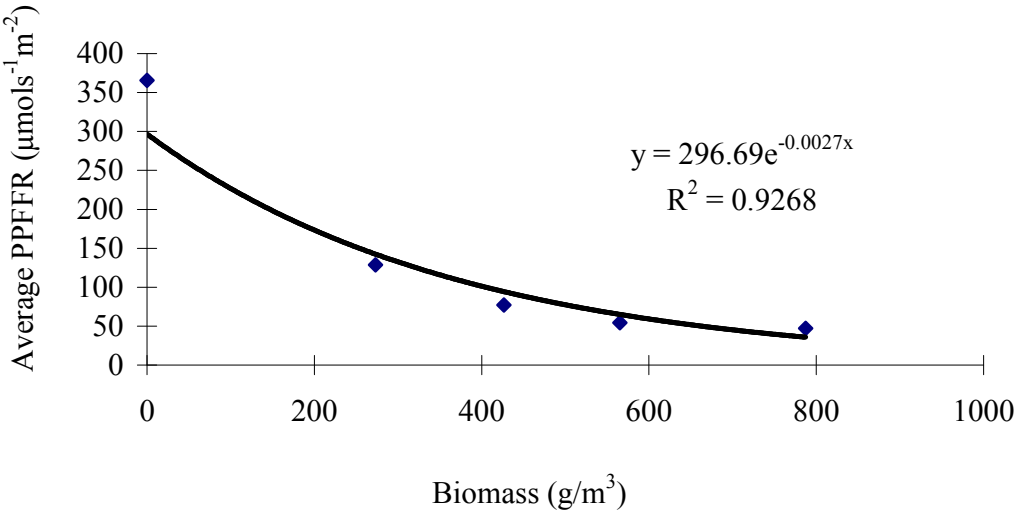

Figure 4.7: Average light irradiance as a function of biomass concentration in the FACE 4 biophotoreactor.

4.3 Growth Study

A growth study was performed to investigate the impact of average scalar irradiance on the net specific growth rate of *Nannochloropsis salina.* Optical density (OD) values were measured in samples at every six hours. The data for the growth studies are given in Appendix C. OD values were converted into dry biomass densities using a calibration curve. The calibration curve (Figure 4.8) was generated using algae cells from the end of the growth study. The growth behavior of algae has been shown in Figure 4.9. The maximum specific growth rate (μ_{max}) of algal cells was the maximum slope of trend line in the plot of the natural log of (biomass concentration) vs. time. It was obtained by fitting a best possible linear fit to the growth curve (Figure 4.9). As shown in Figure 4.10, the μ_{max} for *Nannochloropsis s.* was 0.0521 h^{-1} or 1.25 d^{-1} as observed between 42 to 54 hours after

inoculation. The maximum growth rate was reported to be 1.3 d^{-1} in a previous study (Jon et al., 2012). In Jon's growth study, the maximum growth rate was achieved by using high intensity fluorescent bulbs (250 $\mu molm^{-2}s^{-1}$) at 23 ℃, while a 120 W metal lamp was used as illumination in this study. Thus, the μ_{max} in this study is lower than other studies, probably because the thicker reactor and the different light source were used.

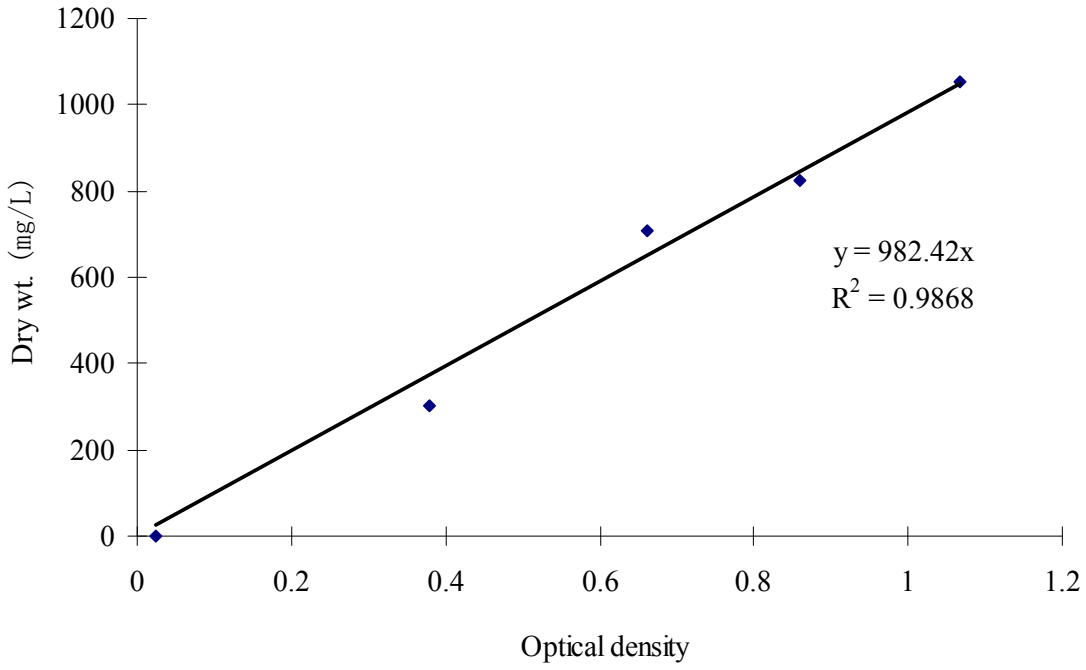

Figure 4.8: Calibration curve for cell dry weight concentration.

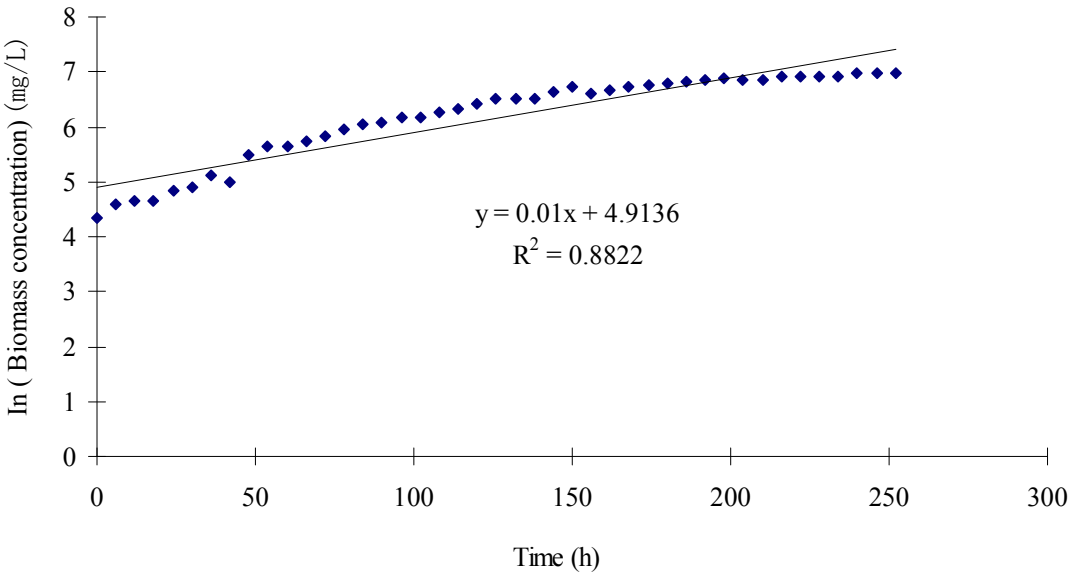

Figure 4.9: Natural log of biomass concentration during the growth study.

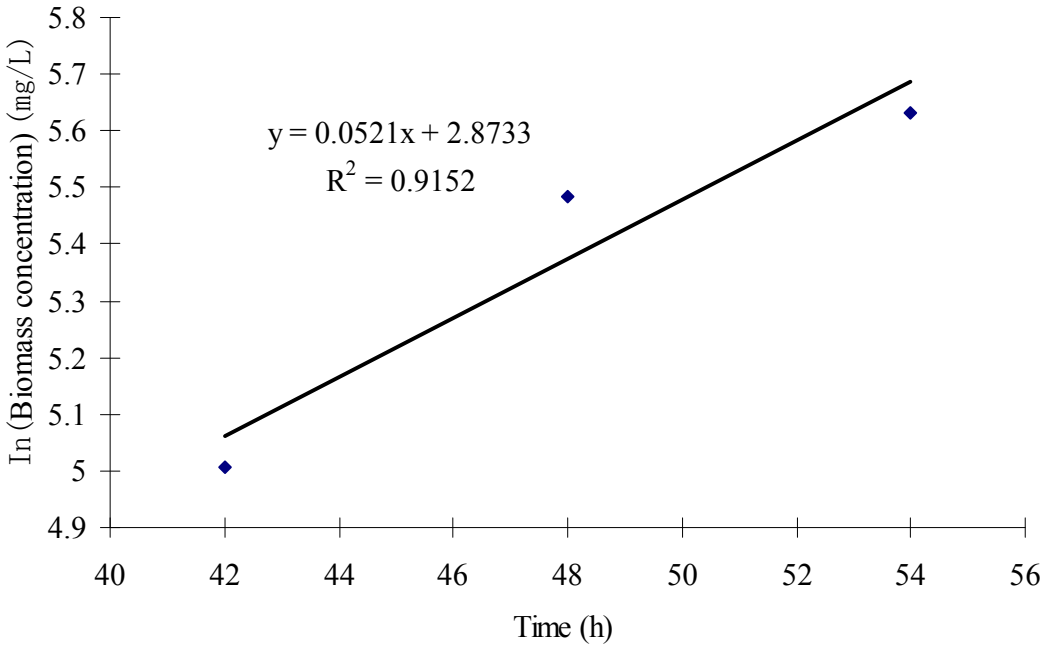

Figure 4.10: Maximum specific growth rate in this growth study.

Also, the photon flux densities were regressed against biomass concentration (Figure 4.11) to study the relationship between PPFFR and biomass concentration. At the end of the growth study, the culture medium was diluted four times to obtain the specified cell concentration. The average irradiance for the final culture medium and the four dilutions were measured from bulb quantum sensor at proximal, central, and distal from the light source to the fermenter. Biomass concentrations for the four dilutions of the culture medium were calculated using the calibration curve in Figure 4.8 to convert corresponding OD values. Using the non-linear regression relationship that was found in Figure 4.11, the PPFFR in the fermenter was estimated for every 6-hour intervals by converting biomass concentration at each interval during the growth studies. Based on the regression illustrated in Figure 4.11 and measured biomass concentrations at 6-hour intervals, the relationship between the I_a (PPFFR) and biomass concentration was estimated for each time interval within the experimental range (Figure 4.12). The change in light and biomass throughout the growth study is plotted in Figure 4.12. The change in the average PPFFR over time during the growth study were inversely related to the biomass concentration.

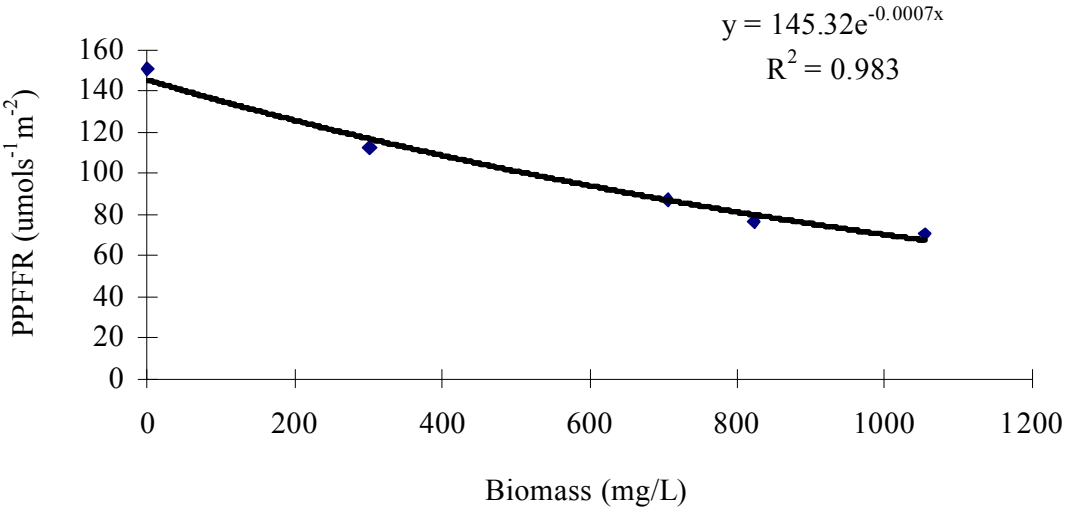

Figure 4.11: Calibration of photon flux vs. cell dry biomass concentration in the fermenter.

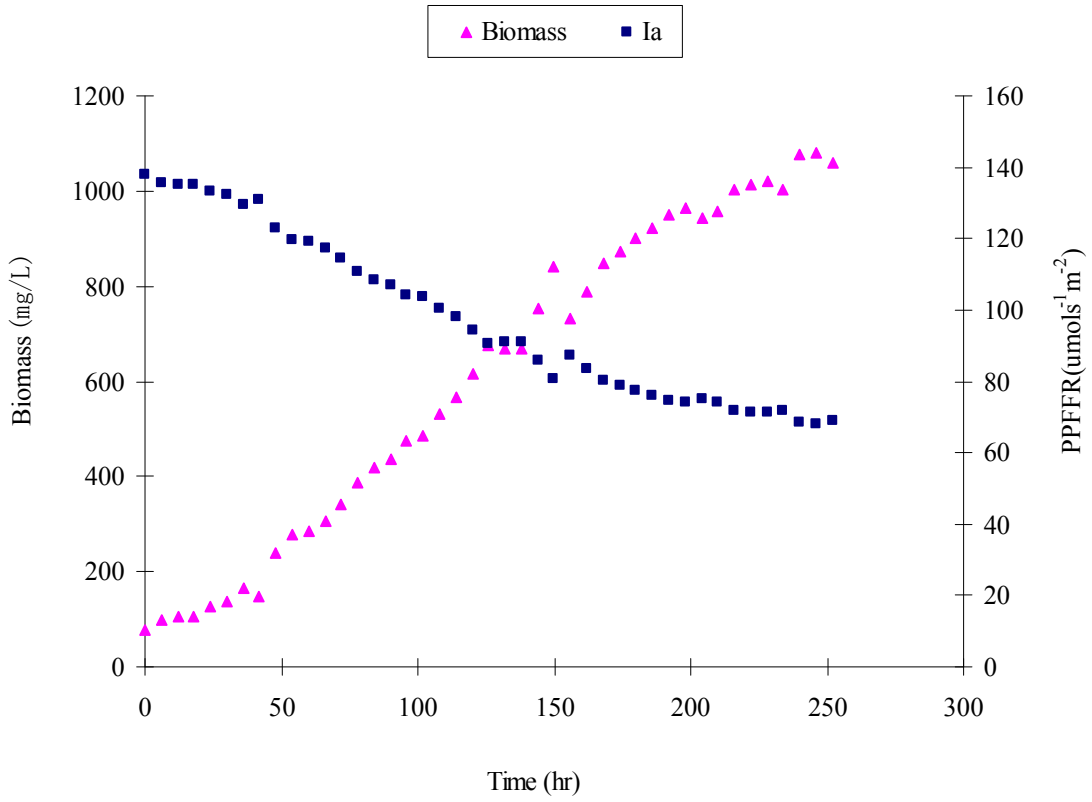

Figure 4.12: The change in the biomass concentration and light (average PPFFR) in the fermenter during growth study.

4.4 Lipid Analysis

4.4.1 Total Lipid Productivity

The percent lipid concentrations of dry weight biomass produced in each CAB of the FACE 4 photobioreactors at various growth rates was assessed by colleagues at the Texas A&M University-Corpus Christi. The total lipid content of biomass ranged from the 14% to 19.5 % in the four CABs. From Figure 4.13, the highest lipids content was typically observed in the stationary phase and decay phase of the growth curve when growth rate was low (CAB 1, 2, and3), while the lowest lipids content was exhibited toward the end of the exponential growth phase while growth rate was high (CAB 1, 2, and 3). The trends of lipid production and biomass concentration over cultivation period are similar to those in the literature (Williams and Laurens, 2010). As the growth rate increased the protein content of the biomass increased, the lipid content and lipid productivity decreased. As shown in (a) and (b) of Figure 4.13, *Nannochloropsis salina* had accumulated significant amounts of lipids by day 4 of cultivation and reached maximum lipid content in the stationary growth phase. The lipid content of *Nannochloropsis salina* grown in this experiment was comparably to values reported in the literature (Mohammady, 2011). The lipid content was reported as high as 40 % for *Nannochloropsis salina* under the nutrient limitation condition by Mohammady (2011). Although this experiment was unable to achieve such high lipid percentages, gaining the average lipid content of 17% was reasonable without optimization operating conditions. Previous study by Thompson et al (1990) found that the lipid content of biomass concentration was around 10% to 20% when the growth rate below 2 d^{-1}. The lipid

production results in this study supported by previous study (Thompson et al., 1990) at the low growth rate range. The results also suggest that higher lipid production could be achieved in FACE 4 photobioreactors with nutrient limitation or optimization of operating conditions.

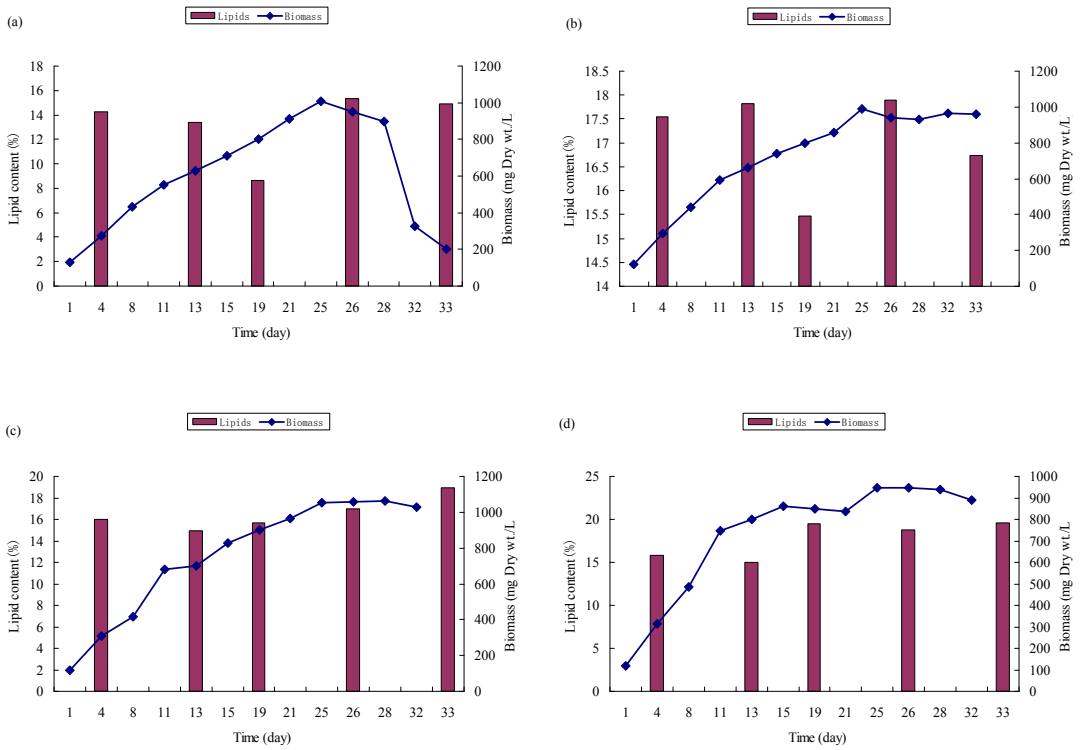

Figure 4.13: Lipid content and biomass growth during batch run in FACE 4 photobioreactors. (a) CAB 1; (b) CAB 2; (c) CAB 3; (4) CAB 4.

4.4.2 Lipid Content as a Function of Growth Rate

The relationship between lipid content and growth rate was determined using data from the lipid analysis study. The specific growth rate at the each time period prior to lipid analysis can be calculated using change in dry cell biomass concentrations over each time period. The net specific growth rate (μ) for each lipid collection period was calculated using

the Two-Point method (Levasseur et al., 1993). In Two-Point method, the growth rate was estimated by selecting two points in the log phase of each time period prior to lipid collection. Thus, μ was calculated using the formula:

$$\mu(d^{-1}) = \frac{InX_2 - InX_1}{(t_2 - t_1)} \tag{4.10}$$

where X_1 and X_2 are the biomass dry weight (mg/L) at the first day (t_1) and final day (t_2) respectively in each time period prior to lipid analysis.

Though not the correct approach, the relationship between lipid content and growth rate with lipid as the independent variable was investigated using the similar approach in prior studies (Shifrin and Chisholm, 1981; Thompson et al., 1990). Growth rate should actually be the independent variable which determines lipid content. When studying the overall relationship between lipid content and growth rate in the FACE 4 photobioreactors, CAB 1 and 2 data were used later for model calibration, while data from CAB 3 and 4 were used for model development. Based on the results of the lipid production and growth rate for each lipid collection period, an inverse relationship between lipid content and growth rate was found for each CAB. As shown in Figure 4.14, an inverse correlation between lipid content and growth rate were found in both CAB 3 and CAB 4 due to the relative high lipid production at low growth rate in these two CABs. The R^2 value of this figure is 0.7534, 0.4714, and 0.5132 for CAB 3, CAB 4, and CAB 3 & 4, respectively. This indicates a good exponential relationship between lipid content and growth rate. Shifrin and Chisholm(1981) and Thompson et al. (1990) reported a linear regression with R^2 of 0.38 and 0.30 respectively

for this type of relationship. Thus the relationship between lipid content and growth rate was best modeled by an exponential relationship rather than a linear relationship due to a higher R^2 was gained in the exponential function. For model development purposes, the relationship between μ and % lipid content was regressed with growth rate as the independent variable. Figure 4.15 containing data from CAB 3 and CAB 4 shows a significant non-linear regression relationship between lipid content and growth rate with growth rate as the independent variable. The R^2 of the exponential equation in Figure 4.15 is better than an R^2 0.38 of liner relationship reported by Shifrin & Chisholm (1981). Again an R^2 of 0.30 was reported by Thompson et al. (1990) for a similar study with liner relationship. Thus, it suggests that the exponential fit for all the data yielded good results compared to the linear regression found in other studies to model the relationship between lipid production and growth rate. Using Equation 4.11 given from Figure 4.15, the lipid production in FACE 4 photobioreactors can be estimated by the model. Thus, the lipid production can be predicted using the following equation:

$$y = 18.543e^{-0.5125x} \quad (4.11)$$

where 18.543 is the intercept and -0.5125 is the lipid production coefficient (k_μ). The constant k_μ of -0.5125 d^{-1} represents the declining effect that growth rate has an exponential relationship with % lipid of biomass content.

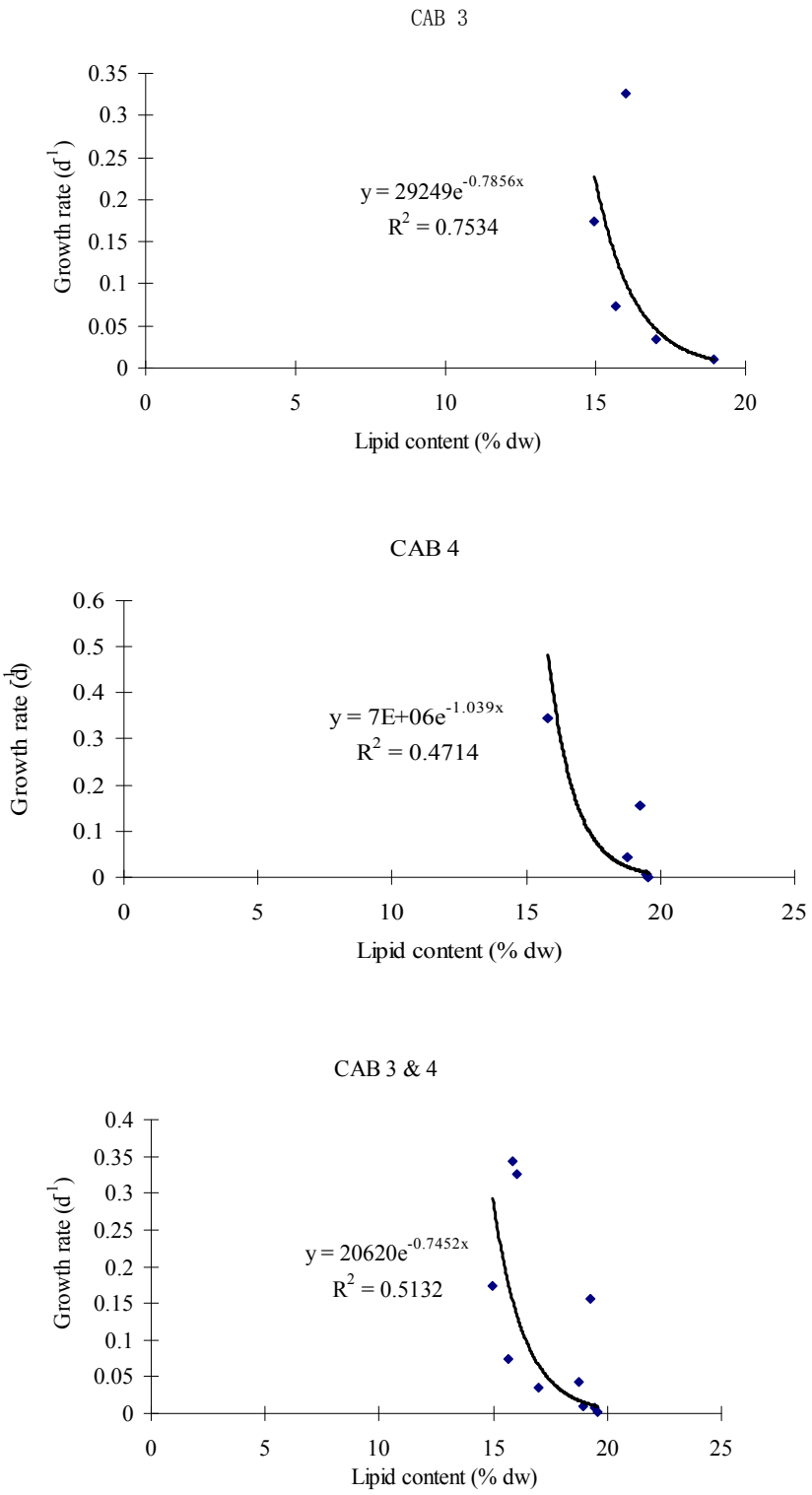

Figure 4.14: Lipid content vs. growth rate in CAB 3, CAB 4, and CAB 3 & CAB 4.

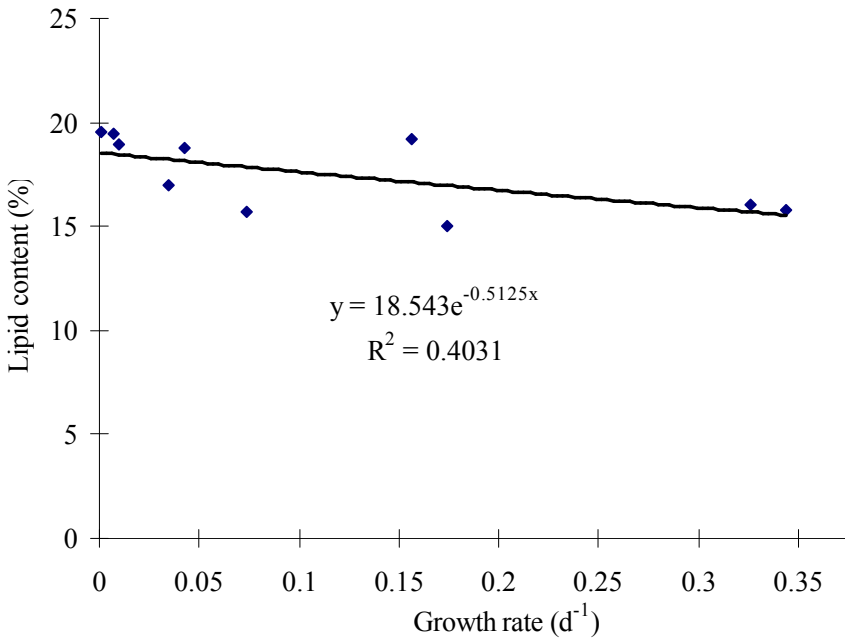

Figure 4.15: Exponential regression relationship between lipid content and growth rate.

Chapter 5: Model Development

A mechanic model that integrates the mass balance analyses within the FACE 4 photobioreactors with light dynamics (Lambert-Beer Law), biological Processes, and lipid production relative to growth rate was developed using Stella^{TM} software. The mechanistic model was developed to represent the fundamental biological and physiological processes gaining lipid production by microalgae in the FACE 4 photobioreactors, such as mass balance, light effects on growth rate, nutrient stoichiometry on biomass production, and the partitioning of accumulated biomass into primary organic fractions.

5.1 Introduction

The mechanistic light and lipid production model follows the law of thermodynamics, light dynamics, stiochiometry and basic hydrology and mass balance. It is able to estimate the cellular partitioning of microalgae into lipid, proteins and carbohydrates as the environment of the photobioreactor changes. Biomass flows through the series of modules which governs biological and physiological responses. The important driving forces for microalgae productions, such as light, nutrient level, and temperature, were developed in the model. Among them, light is the most dynamic and complex optimization parameter. The production model was designed to understand the complex relationships between all of these optimization parameters and microalgal productivity in the FACE 4 photobioreactor.

5.2 Data Acquisition

Data acquisition for the model development has been discussed in Chapter 3 and 4.

The data used for the estimation of irradiance parameters were collected from a series of experiments in Chapter 3. These data were conducted in the model to estimate (1) surface irradiance (I_o) as a function of lamp distance; (2) depth of penetration and biomass concentration dependent scalar irradiance (I_z); (3) average scalar irradiance (I_a); (4) specific growth rate (μ) and optimum irradiance (I_{opt}) as a function of Ia. The optimization parameters collected during all the parameters estimation experiments were determined by regression analyses and are summarized in Table 5.1.

Table 5.1: The summary of regression analyses statistics for experimental estimated parameters.

Parameters	Experimental Estimation	R^2	Process of Estimation
Light parameters			
I_{Do} ($\mu mols^{-1}m^{-2}$)	903.41	0.9931	Experimental data
k_a (cm^{-1})	0.0256	0.9931	Experimental data
k_r ($\mu mols^{-1}m^{-2}cm^{-1}$)	0.062	1	Experimental data
k_b (cm^{-1})	0.0007	0.977	Experimental data
Growth parameters			
μ_{max} (day^{-1})	1.262	0.904	Experimental data
I_{opt} ($\mu mols^{-1}m^{-2}$)	158		Experimental data
Lipid parameters			
k_μ (day^{-1})	-0.5125 *	0.4031	Experimental data

*calibrated parameter

5.3 Model Development

A mechanistic production model that estimates lipid production and biomass generated within the FACE 4 Photobioreactor was developed using the STELLA modeling platform (Figure 5.1). It will enhance our understanding of fundamental biological and physiological processes governing lipid production by microalgae in a flat-plate

photobioreactors. The complete conceptual mechanistic model is given in Appendix A.

The conceptual mechanistic model includes incidence of PPFD, the average irradiance and its effect on microalgael broth, mass balance, CO_2 uptake through photosynthesis, biomass production and the effect of growth rate on lipid production and its partitioning into major organic fractions. Biomass inflows and outflows through the continuous-flow stirred-tank reactors (CFSTR) are calculated reflecting mass balance, microalgal growth kinetics, lipid production, nitrogen, phosphates, and carbon consumptions at a unique specific growth rate. In the phosphate cycle, it is converted to biomass stoichiometrically. To figure out the balance as phosphate is transformed to phosphorous tired up as a mass balance equation was included in the model. The carbon cycle and nitrogen cycle are similar to the phosphate cycle using stoichiometry and mass balance to calculate how much is transformed into biomass. The carbon dioxide is also coupled to a pH cycle in the system. The dynamic specific growth rate (μ) is influenced by a sum of the average scalar irradiance (I_a), nutrient consumptions, temperature factor, maximum growth rate (μ_{max}) and optimum light attenuation (I_{opt}).

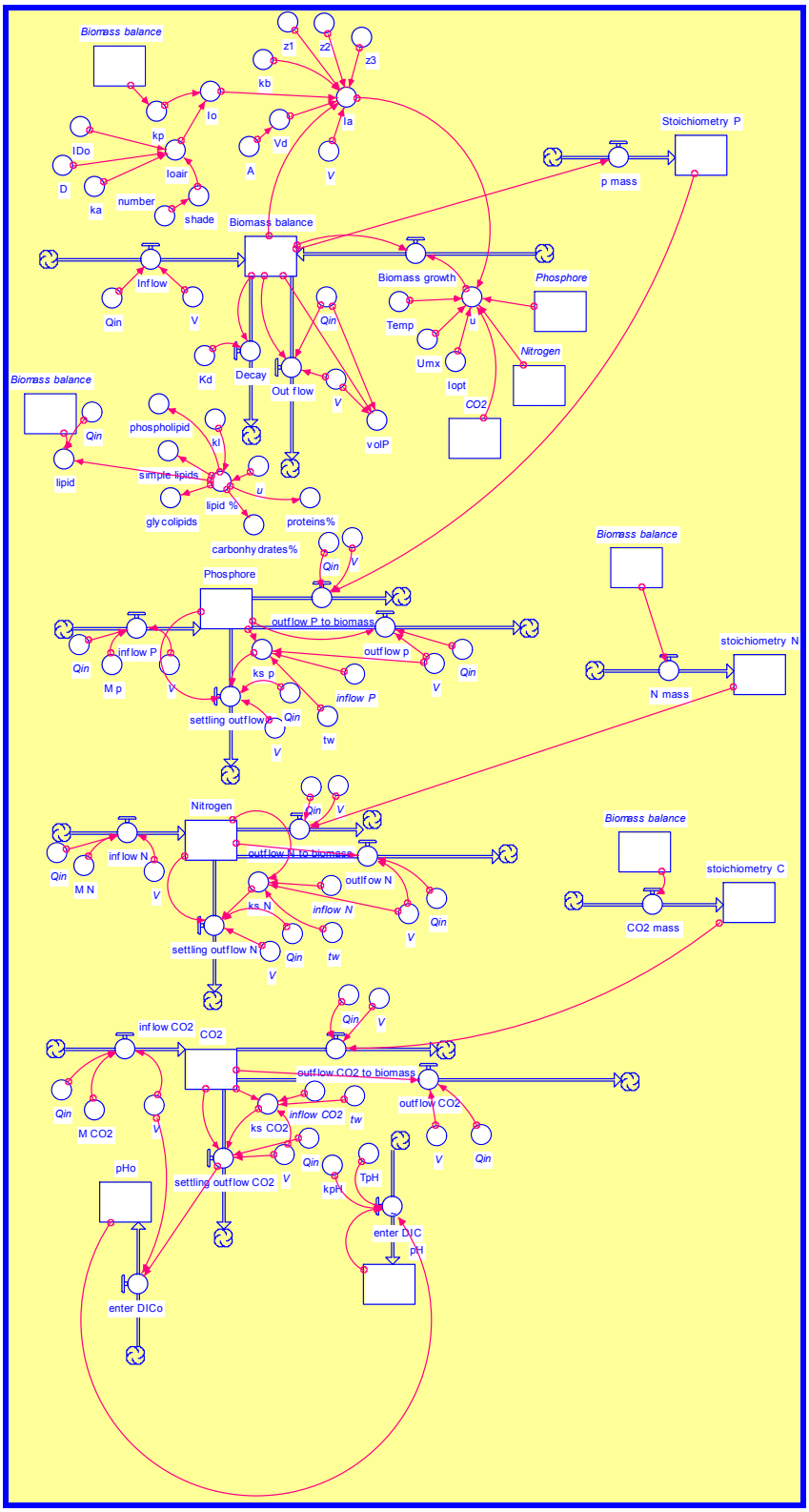

Figure 5.1: The stella diagram of the FACE 4 Photobioreactor model

5.4 Governing Equations

The behavior of one of four CABs of the FACE 4 photobioreactors was modeled in this study as a CFSTR. In the FACE 4 systems, it assumes that the composition is uniform at all points in the CAB. The mass balance in the CAB is dependent on the combination of influent flow rate (Q_{in}) and biomass concentration (X_{in}), as well as effluent flow rate (Q_{out}), net specific growth rate (μ), and biomass concentration (X_{out}). The governing equation for the CAB can be written as:

$$V\frac{dx}{dt} = Q_{in}X_{in} - Q_{out}X_{out} + \mu XV - k_d XV \qquad (5.1)$$

where,

V = the volume of a CAB

μ= net specific growth rate in the CAB

Q_{in} = influent flow rate

Q_{out} = effluent flow rate

X_{in} = biomass concentration injected into the CAB

X_{out} = biomass concentration harvested from the the CAB

k_d = the decay rate

k_d is increased by average cell age, which has been reported to be 0.1 d^{-1} for fresh water phytoplankton (Jorgensen, 1979). The term $\frac{dx}{dt}$ of equation 5.1 represents the change in biomass concentration over time in the CAB providing for dynamic modeling. The net growth occurring in the CAB is a function of the maximum growth rate (μ_{max}), effects of lighting dynamics, temperature, and nutrient parameters. These parameters impacting the

biomass densities in the CAB photobioreactor were gained from previous research (Benson et al., 2007) or estimated through experiments (Table 5.1).

5.4.1 Growth Kinetics

Algae grow as a function of temperature, nutrients, and light radiation. The governing equation (Chapra, 1997) for growth kinetics model can be developed as

$$\mu = \mu_{\max}\left(1.066^{T-25}\right)\cdot\left(\frac{I_a}{I_{opt}}e^{\frac{-I_a}{I_{opt}}+1}\right)\cdot D_s F\cdot\min\left(\frac{n}{n+k_{sn}},\frac{p}{p+k_{sp}},\frac{CO_2}{CO_2+k_{sco_2}}\right) \qquad (5.2)$$

where n, p, and CO_2 are concentrations of available nitrogen, phosphorus, and carbon dioxide, respectively. K_s is the half saturation constant, which was calculated by prior studies (Chapra, 1997). For green microalgae, $k_{sn} = 0.02\ mgL^{-1}$, $k_{sp} = 0.005\ mgL^{-1}$ $k_{sco_2} = 0.02\ mgL^{-1}$. D_sF is the dilution factor which incorporates effects of change in self-shading effect, degassing and metabolite, and nutrient flushing (Benson et al., 2007).

The first term ($\mu_{\max}\cdot(1.066^{T-25})$) on the right-hand side of Equation 5.2 represents the effect of temperature on microalgae growth. Eppley (1972) proposed a coefficient value of 1.066 based on a number of studies, and this value can be used in temporization formulation. μmax was determined in specific growth experiments conducted at 25℃ environmental temperature. Temperature effect can be formulated mathematically by using the coefficient.

The second term ($\frac{I_a}{I_{opt}}e^{\frac{-I_a}{I_{opt}}+1}$) represents the effect of the light on microalgae growth. Several factors have to be integrated to come up with the total light effect, including surface

light diffusion, light attenuation with distance of penetration and dependence of the growth rate on light. Steel's (1965) equation was used for this term which accurately models growth in moderate density cultures and accounts for photoinhibition.

The last term ($\min\left(\frac{n}{n+k_{sn}}, \frac{p}{p+k_{sp}}, \frac{CO_2}{CO_2+k_{sco_2}}\right)$) represents how multiple nutrients effect the growth and are factored into estimation of growth rate. The approach was based on Liebig's Law of the minimum, which means the nutrient in shortest supply controls growth. Each of the parameters impacting the specific growth kinetics is discussed further in the following subsections.

5.4.2 Light Dynamics

To estimate μ in the CAB, the average scalar irradiance I_a(PAR) must be calculated (Molina Grima et al., 1994). The second term ($\frac{I_a}{I_{opt}} e^{\frac{-I_a}{I_{opt}}+1}$) on the right side of Equation 5.2 represents the effect that the average PPFFR (I_a) in the reactor has on growth rate μ. When the second term is multiplied by μmax, it converts to Steele's equation (Steele, 1965). Steele's equation can be used to model algae production in moderate density cultures and accounts for photoinhibition, which was experimentally determined to occur at I_a greater than 360 $\mu mols^{-1}m^{-2}$ for metal halide light sources (Benson, 2006).

To estimate the instantaneous average I_a, the model integrates the Lambert-Beer's Law over the distance of penetration through the CAB at the instantaneous biomass concentration for each time step using Equation 2.4 ($I_a = \frac{1}{d}\int_0^d I(z)dz = \frac{I_o(1-e^{-k_o Xd})}{(k_o Xd)}$). The

light averaging component vertically slices the FACE 4 into three distances (z) of penetration intervals (Figure 5.2). The average scalar irradiance within each interval (I_z) can be determined by integrating the Lambert-Beer Law (Equation 2.3 of $I_z = I_{os}e^{-k_oZ}$). The average scalar irradiance within each interval was determined by experiments discussed in Chapter 4. All three intervals are averaged to calculate the average PPFFR (I_a), which can be used in Equation 5.2 to represent the effect of I_a on μ.

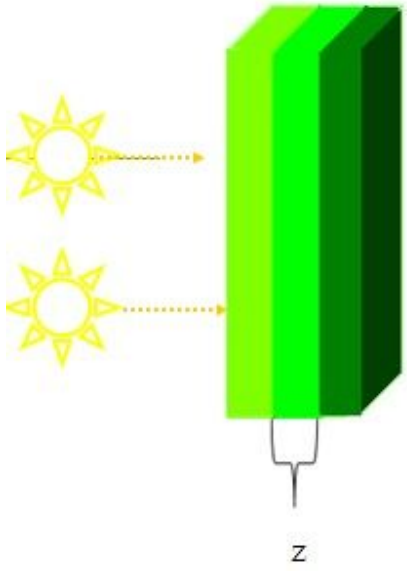

Figure 5.2: Diagram of intervals in the FACE 4 as used in a light averaging component.

The forcing function of the I_a is the surface irradiance (I_o), which was estimated experimentally from light diffusion studies, as described in Equation 2.2 ($I_o = I_{E_o} - k_a D$). I_o was estimated as discussed in Chapter 4, then it was utilized along with X and D in Lambert-Beer Law to compute I_z in the reactor. The I_z for each interval is averaged by the model to estimate I_a in the model.

5.4.3 Nutrients and Stoichiometry

The governing equations for nutrient concentrations were based on biomass balance flow and stoichiomertric composition of organic matter. An adequate supply of nitrogen, phosphorus, and CO_2 is imperative to ensure high lipid production in microalgal cultures. Inorganic nutrients are required in large quantities for microalgae cell development and hence are called macronutrients. The model development has focused on three macronutrients: phosphorus, nitrogen, and carbon. All these three macronutrients are important factors for microalgae growth. For example, phosphorus has a critical role in storage and transfer of cell energy; nitrogen not only acts as a fertilizer in algae growth, but also decomposes to form nitrite and nitrate which can be utilized by certain algae and bacteria; carbon plays a role as a nutrient and is a main component of biomass.

As microalgae grow, they take up inorganic nutrients from the water in proportion to their stoichiometry. The stoichiometric composition of organic matter is an important factor in the process where production converts inorganic nutrients into organic biomass. The dry-weight composition can be idealized as the following representation of the photosynthesis/respiration process (Stumm and Morgan 1981):

$$106CO_2 + 16NH_4^+ + HPO_4^{2-} + 108H_2O \Leftrightarrow C_{106}H_{263}O_{110}N_{16}P_1 + 107O_2 + 14H^+ \quad (5.3)$$

In this formula, $C_{106}H_{263}O_{110}N_{16}P_1$ represents algae, so the mass ratio of carbon to nitrogen to phosphorus can be determined as percentages of dry weight (Chapra, 1997):

$$C: N: P = 106\times12 : 16\times14 : 1\times31 = \ 40\%: 7.2\%: 1\% \quad (5.4)$$

Thus, the production of a gram of dry weight of algae utilizes approximately 10 mg of

phosphorus, 72 mg of nitrogen, and 400 mg of carbon.

Dynamics for the nutrient concentration was obtained by applying mass conservation laws. Based on the governing equation of the CAB (equation 5.1), the nutrient loading equation based on mass balance can be expressed as (Chapra, 1997):

$$V\frac{dX_n}{dt} = W - Q_{out}X_n - ks_nVX_n \tag{5.5}$$

where V = the volume of a CAB (m^3)

X_n = total nutrient concentration of a CAB (n = phosphorus, nitrogen, or CO_2) (g/m^3)

W = total nutrient loading rate (g/d)

t = time (d)

Q_{out} = effluent flow rate (m^3/d)

k_s = a first-order settling loss rate (d^{-1})

In the equation, the loss rate (k_s) can be determined as $k_s = \frac{W}{VX_n} - \frac{1}{t_w}$, where t_w is the residence time. The nutrient loading approach was included in the model to investigate the effect of phosphorus, nitrogen, and CO_2 concentrations on microalgae growth and lipid production.

In the presence of light, microalgae consume carbon from dissolved CO_2, while releasing O_2. Based on Equation 5.4, microalgae biomass is 40% carbon by dry weight. Since a mole of CO_2 has a mass of 44 grams and 12 of these grams come from carbon, the amount of CO_2 consumed to grow one gram of microalgae was calculated as following (Buehner, al et.2009):

$$m_{CO2\,(g)} = \frac{44 gCO_2 / mol}{12 gC / mol} \times \frac{40\% gC}{ga\lg ae} = 1.47 \frac{gCO_2}{ga\lg ae} = 1.47 m_{algae\,(g)} \quad (5.6)$$

In general, 1 gram of microalgae consumes 1.47 grams of CO_2 to produce energy and biomass. Using the cell stoichiometry, the amount of the three nutrients consumed for biomass production can be calculated and simulated dynamically by the model.

5.4.4 Lipid, Proteins, and Carbohydrates Partitioning

Microalgae biomass break down into the basic products: lipids, proteins, and carbohydrates. A major challenge in algal production is maximizing the biomass with regards to lipids, carbohydrates, and proteins. The following equation used to calculate the lipid production in the FACE 4 photobioreactors was developed from the exponential regression equation of lipid production and growth rate (Figure 4.15), as shown in the following:

$$L = 18.543e^{-0.5125\mu} \quad (5.7)$$

where L = lipid content (% dw). This equation is used in the model to demonstrate the outcome and potential of lipid content. As nutrient limitation affects growth rate, this provides an explanation for the negative relationship between growth rate and lipid content. Overall production of lipid is more complex than this lipid content analysis, as there are many other considerations. In order to calculate protein and carbohydrates fractions, it is assumed that the overall fractions of the three major biochemical classes are equal to one, which means C+P+L=100; and the protein to carbohydrate ratio is 3:2. Thus, the conversion of biomass productions into protein and carbohydrate fractions can be simply calculated:

$$C = (100-18.543e^{-0.5125\mu})*0.4 \quad (5.8)$$

$$P = (100\text{-}18.543e^{-0.5125\mu})*0.6 \quad (5.9)$$

where,

C = carbohydrate content (% dw)

P = protein content (% dw)

Based on the three equations above, the productivities of lipids, proteins, and carbohydrates during the biosythesis in the reactor can be predicted in the model.

The overall algae lipids have major class compositions of phospholipids, glycolipids, and triglycerides. For *Nannochloropsis*, the lipid class distribution derived from published analyses was as following (Williams and Laurens, 2010) :

$$\text{Phospholipids} = \text{lipids} \times 0.38 \quad (5.10)$$

$$\text{Glycolipids} = \text{lipids} \times 0.39 \quad (5.11)$$

$$\text{Triglycerides} = \text{lipids} \times 0.22 \quad (5.12)$$

These three types of lipids compose 99% of total lipids for *Nannochloropsis,* while the rest of 1 % of lipids consists of fat-soluble vitamins and waxes. Using these equations in the model, the mean lipid class contents can be estimated. It is known that many factors lead to the variations in lipid class distribution. For example, triglycerides, which are important energy reserves, may increase proportional to total lipid fraction as the metabolic rate goes down.

5.4.5 pH Modeling

The dynamic model for pH is based on carbonate ions system to obtain a relationship between pH and the dissolved CO_2 concentration. CO_2 input is the main factor affecting pH

in the bioreactor. The pH is dominated by the carbonate buffering system, which includes carbon dioxide (CO_2), bicarbonate ion (HCO_3^-), and carbonate ion (CO_3^{2-}). When CO_2 is introduced into the culture, it dissolves in water and converts to carbonic acid,

$$CO_2 + H_2O \Leftrightarrow H_2CO_3 \tag{5.13}$$

The carbonic acid is diprotic, which in turn dissociates into ionic form, as in

$$H_2CO_3 \Leftrightarrow HCO_3^- + H^+ \tag{5.14}$$

The combination of all of these carbonate species make up the total dissolved inorganic carbon (DIC). The total amount of carbonic acid, bicarbonate, and carbonate species determines the pH value. It usually takes 2-3 seconds for CO_2 to completely dissolve and only a fraction of the input CO_2 dissolves before leaving the vent. A pH model was developed based on DIC dynamics in the media. This pH model is linearized about a pH of 7.3 (Buehner, al et.2009).

$$pH(t) = \frac{1}{\tau_{pH}}(K_{pH} m_{DIC}(t) - pH(t)) \tag{5.15}$$

where τ_{pH} = the lag time associated with the DIC settling (days)

K_{pH} = the conversion factor from DIC to pH units.

m_{DIC} = DIC concentration ($g/m^3/d$)

As microalgae grow, CO_2 is removed from the media, resulting in a rise in pH. As CO_2 is continually input into the media, the addition of dissolved CO_2 decreases the pH. By controlling and measuring CO_2 variables, pH can be calculated via the model. In turn, adjusting CO_2 inputs is significant to maintaining pH in a constant range during microalgae

growth.

5.5 Model Calibration

In the model, the relationship between biomass growth and lipid production was included to simulate dynamic change in lipid production as biomass growth rate change in the CAB. The related parameters were initially estimated experimentally from data taken in CAB 3 and 4. These parameters as well as relationships measured during the experiments of the light study and growth study are summarized in Table 5.1.

The production model was calibrated on actual lipid data sets collected from the CAB 1 and 2 of the FACE 4 Photobioreactors under various biomass concentrations. Since experiments were carried out with low growth rates, the assumption for application in the model was that Equation 4.11 can be applied in high growth rate ranges as well. As shown in Figure 5.3, the model simulated data was compared with the actual experimental data (symbols) in order to explain the complex dynamics of lipid production. The standard error of the prediction is a measure of the accuracy of predictions. To calibrate the lipid production parameter in Equation 4.11, a general equation based on the weighted standard error of prediction was used (Equation 5.16).

$$\text{Standard error of prediction} = \sqrt{\frac{\sum_{1}^{n}(X_{pi} - X_{pa})^{2}}{n-1}} \qquad (5.16)$$

where:

X_{pi} = predicted lipid content in the model

X_{pa} = actual lipid content in the FACE 4 photobioreactors.

n = the total number of samples included in the data set.

The result of the standard error of prediction for the data set used in the validation process was 21%, which is greater than the 20% acceptability level. Thus, an adjustment was made on the main calibration parameters in order to validate the model. Taking an average of the data in the experimental equation and model equation and drawing an exponential treadline, a calibrated equation (Equation 5.17) for the trend line of the data was achieved for improved fitting of simulation to experimental data.

$$L = 17.6e^{-0.5323\mu} \quad (5.17)$$

where L = lipid content (%), μ= growth rate (d^{-1}), and -0.5323 = lipid production coefficient (k_μ). The standard error of prediction for the calibrated model resulted in an improved acceptable values of 14.5% for the prediction for the data set. Biological models typically have a high (sometimes as high as 60 %) standard error of prediction because of their stochastic nature (Acien Fernandez et al., 1998). So a low value of 14.6% standard error of prediction for the specific data set is good for a biological system. The calibrated model fitted the experimental data well because of the calibrated k_μ minimized the standard error between the model and the measurements. The results of the calibration are presented in Table 5.2.

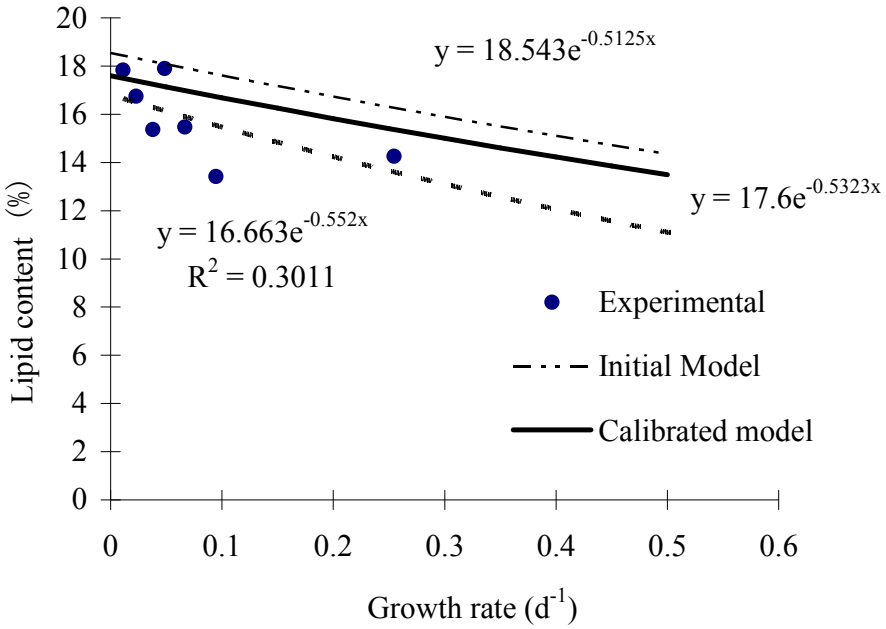

Figure 5.3: Comparison of initial model simulation, experimental data (symbols), trend line of experimental data, and calibrated model simulation.

Table 5.2: The summary of estimated parameters for the production model.

Parameters	Experimental estimation	Final Calibrated parameters
k_μ	-0.5125	-0.5323

5.6 Model Simulations

Once the model was calibrated, simulations were run for a 7-day period to estimate the optimum dilution rate for the CABs. For each model simulation, Q_{in} was set to obtain the operational D_s of the simulated culture. Q_{in} is the operational inflow rate of the culture media, which can be adjusted to determine the operational system dilution rate (D_s), as follows:

$$D_s = Q/V \quad (5.18)$$

D_s is the most sensitive factor that affects the cell retention time or the average cell age in the culture. A low D_s allows the culture to increase in biomass density, while a high D_s sustains culture health and keeps the culture less concentrated allowing better light penetration by washing out inadvertent contaminants and metabolites in the reactor. Sensitivity analysis was used to indicate the importance of calibrated parameters as a whole to a single parameter, compared with the accuracy on the observation. A Sensitivity analysis of the parameter D_s was performed to obtain the maximum value of lipid production. Based on the analysis, the optimal D_s that can get the maximum lipid production is 0.709 d^{-1}. The maximum lipid production observed in the simulations was 3.27gd^{-1} per CAB or 50.42 $gm^{-3}d^{-1}$. Mairet et al. (2011) reported an optimal 0.5 d^{-1} dilution rate to obtain a 25 $gm^{-3}d^{-1}$ lipid production for a dynamic model of microalgae growth in a raceway pond. Compared with Mairet et al.'s model, the model in this study simulated a higher lipid production due to higher optimum D_s and higher production in the closed photobioreactor system. The values of D_s, $Q_{in,}$ and lipid production (P_l) used to represent the three different data sets are summarized in Table 5.3.

Table 5.3: The operational parameters and results for each simulation.

Parameter	**Ds = 0.0107 d^{-1}**	**Ds = 0.478 d^{-1}**	**Ds = 0.709 d^{-1}**	**Ds = 0.925 d^{-1}**
Qin (m^3/d)	0.0007	0.031	0.046	0.06
P_l (gd^{-1}) per CAB	1.9189	3.1178	3.2724	3.0640
P_l ($gm^{-3}d^{-1}$)	29.57	48.05	50.42	47.21

The simulations mimic the general oscillating trends in the actual data under actual dilution rates (Figure 5.4). Many lipid production runs were performed at various D_s until the maximum lipid production was approached the four final runs had D_s = 0.0107, 0.478, 0.709, and 0.925 day^{-1} as shown in Figure 5.4. The actual lipid production in the CAB was simulated with D_s = 0.0107 and Q_{in} = 0.0007 m^3/d, which was compared with lipid production under higher dilution rates in Figure 5.4. As expected, at the beginning of each simulation (lag phase) lipid production increase slowly due to low biomass concentration, while lipid production increase greatly at the steady-state phase, and then lipid production goes down again at the end of each simulation during the stationary phase. When D_s is below the optimal D_s, the lipid production increases in the reactor as D_s increases; when D_s is above the optimal D_s, the lipid production decreases in the reactor as D_s increases. This is due to the washing out of the culture at a faster rate than the accumulation of lipids at high D_s.

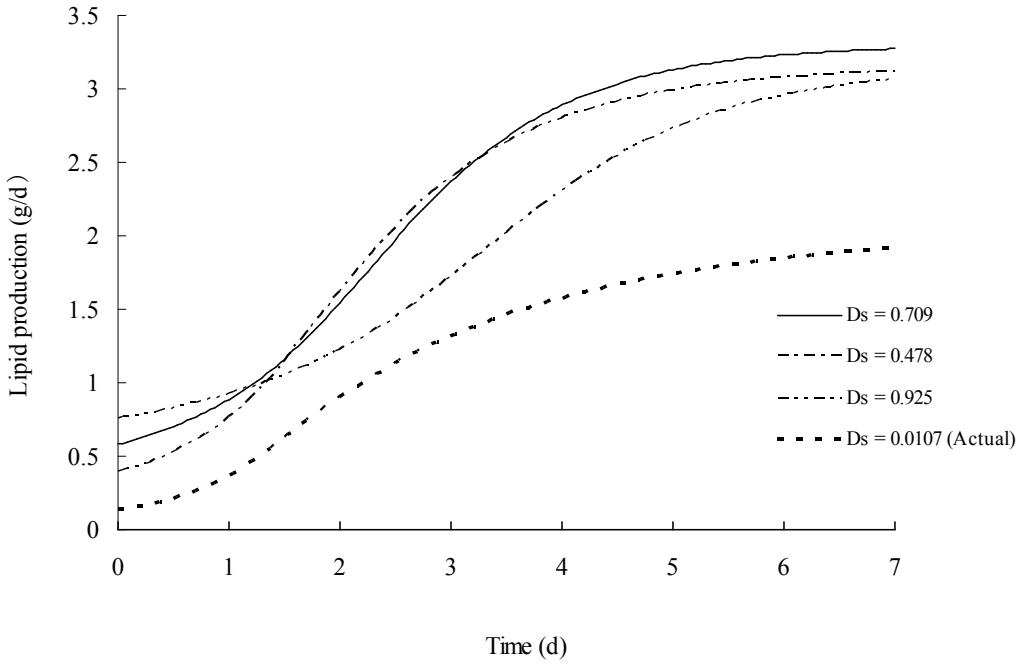

Figure 5.4: The calibrated model simulations of the change over time of lipid production.

Simulations (D_s = 0.709 d^{-1}, Q_{in} = 0.046 m^3/d) were run to investigate the effect of biomass fluctuation on PPFFR (Figure 5.5). Biomass and average PPFFR in the reactor change with respect to time were expected. During the transition phase, the biomass concentration was low along with high I_a. As steady-state was reached, the highest biomass concentration and lowest I_a were observed. Because I_a in the reactor is inversely proportional to the biomass concentration. Biomass concentration and lipid production were also simulated at optimum D_s over time in Figure 5.6. As expected, lipids production increased exponential as biomass growth and the maximum lipid production reached 3.27 g/d. The amount of lipids increased greatly and reached 3.13 g/d during the first 4 days, and then almost kept constant, suggesting that cells were much more active for lipid synthesis rather than cell propagation in the exponential growth phase. In the Figure 5.7, growth rate and

carbohydrates, proteins, and lipids partitioning were simulated in the model. As expected, the growth rate increased at beginning of the simulation, and then kept going down greatly until it reached the stationary phase; while the curves of lipids, carbohydrates, and proteins productions followed the trend of the biomass curve. These simulations indicated the model is capable of predicting the basic trends of light dynamics, growth kinetics, and lipid production in the FACE 4 photobioreacors.

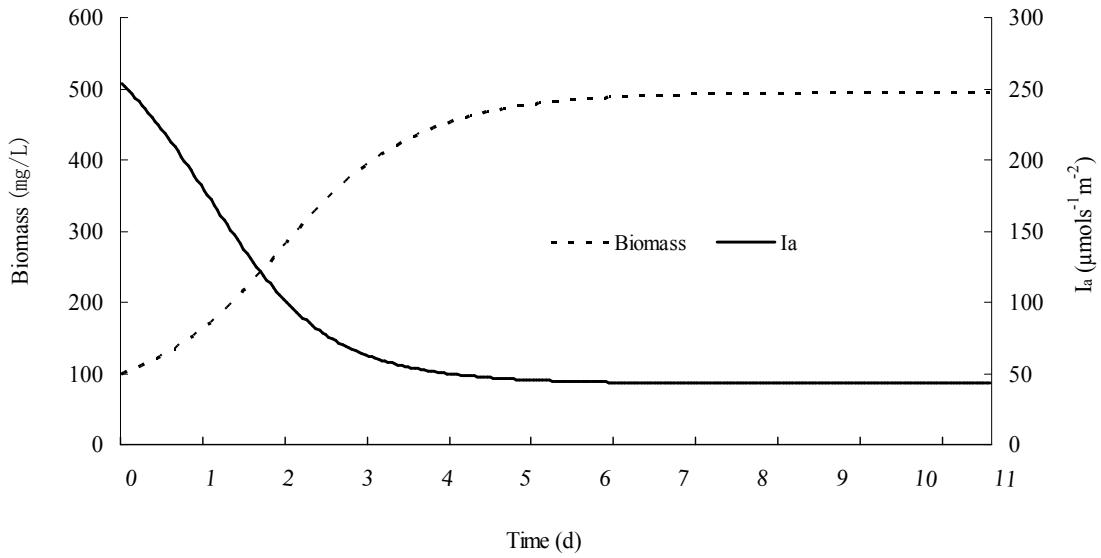

Figure 5.5: A model simulation of the change in biomass concentration and concurrent changes in average PPFFR over time in the CAB.

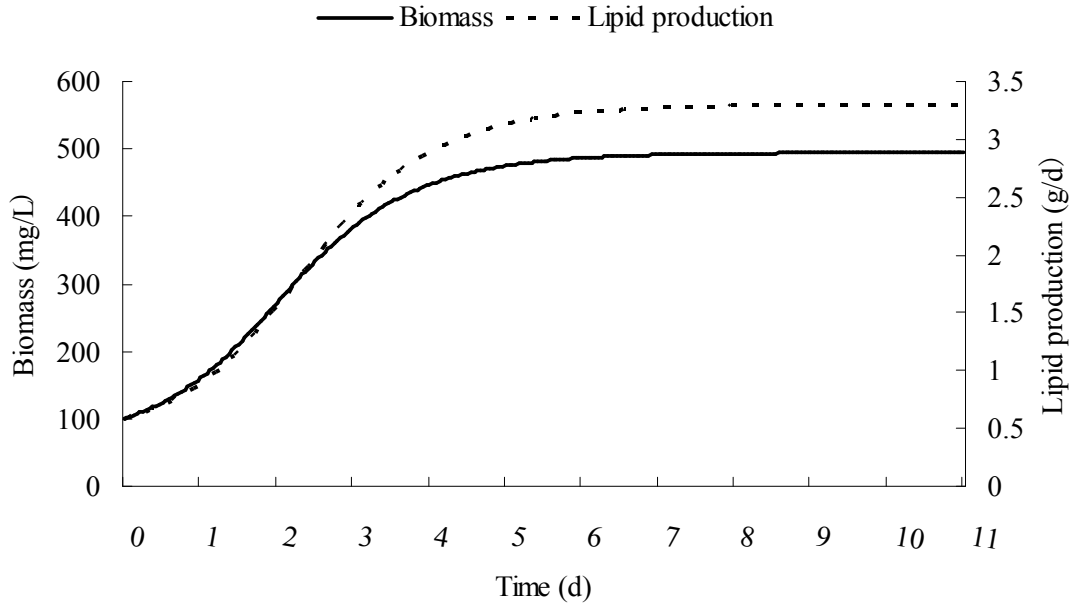

Figure 5.6: A model simulation of the change in biomass concentration and concurrent changes in lipid production over time in the CAB.

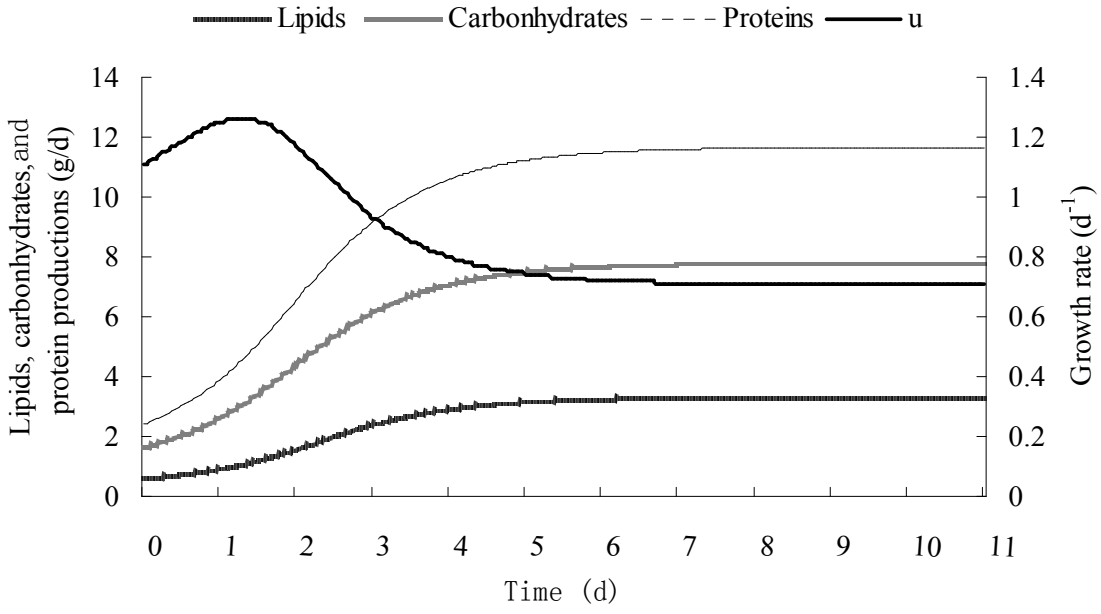

Figure 5.7: A model simulation of the change in growth rate and biomass productions (lipids, carbohydrates, and proteins) over time in the CAB.

Simulations were also run under the actual Ds (D_s = 0.0107 d^{-1}, Q_{in} = 0.0007 m^3/d) to estimate the amount of phosphorus, nitrogen, and CO_2 consumptions during the microalgae growth in the CAB. Nutrients were assumed to be continuously fed into the in-flowing water line or air line to maintain a target of approximately 4 mg nitrate (NO_3^-) L^{-1}, 2.25 mg phosphate PO_4^{3-}, and pH = 6 (Benson, 2003). To determine the optimum loading rates of the nutrients to the reactor, the loading mass of the nutrients, was adjusted until the optimum nutrients concentrations were obtained in the model simulations. The optimum loading rates for an inflow of 0.0007 m^3/d are shown in Table 5.4. The trends of changes in nitrogen, phosphorus, and CO_2 contestations over time were shown in Figure 5.8. When the nutrients are added at a constant input rate, the nutrients concentrations increase in the simulated culture until the biomass population approaches carrying capacity and then the nutrient concentration decrease. Based on mass balance, the total inflow of nutrients were converted into outflow to biomass, outflow from the culture, and settling of nutrients. The nutrient outflows to biomass increase as microalgae consume nutrients in order to produce biomass. The loss of nutrients due to settling of particulate nutrients is dependent on their concentrations and k_{s_n}. At the beginning of the simulations, the nutrient concentrations start at an initial concentrations of optimum and increase with the additional inflows to accommodate the high growth rate during the exponential growth phase. Compared with the trend line of biomass production in Figure 5.5, the highest biomass production was observed at day 4 (entering the stationary growth phase), when nitrogen, phosphorus, and CO_2 reach the maximum concentration. To maintain the culture at this maximum biomass concentration

the nutrients start declining due to consumption by the algae biomass and returns to optimal concentration during the stationary growth phase.

Table 5.4: The nutrients loading parameters and optimum concentrations in the CAB.

Nutrients	*Phosphorus*	*Nitrogen*	*CO_2*
Optimum loading mass rate (g/d)	30	214	4170
Final concentration (mg/L)	2.26	4.07	2.15

(a)

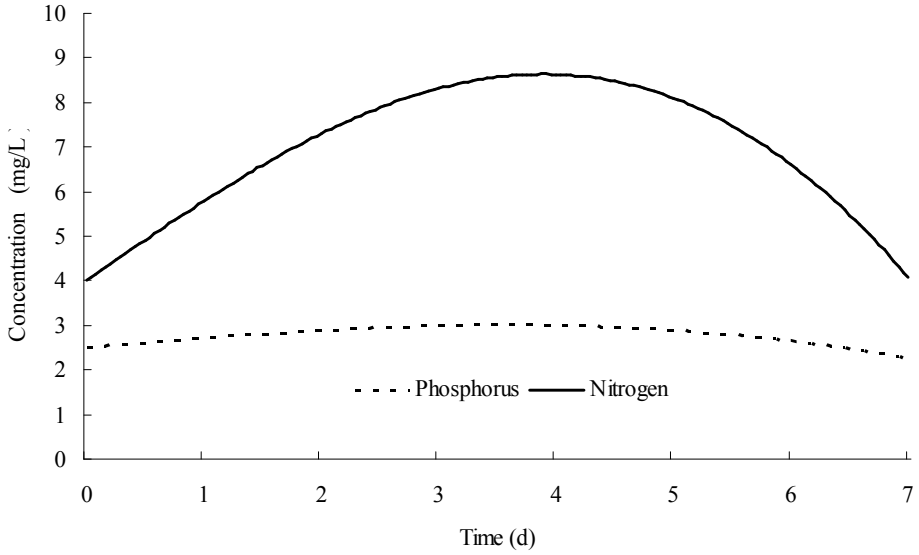

(b)

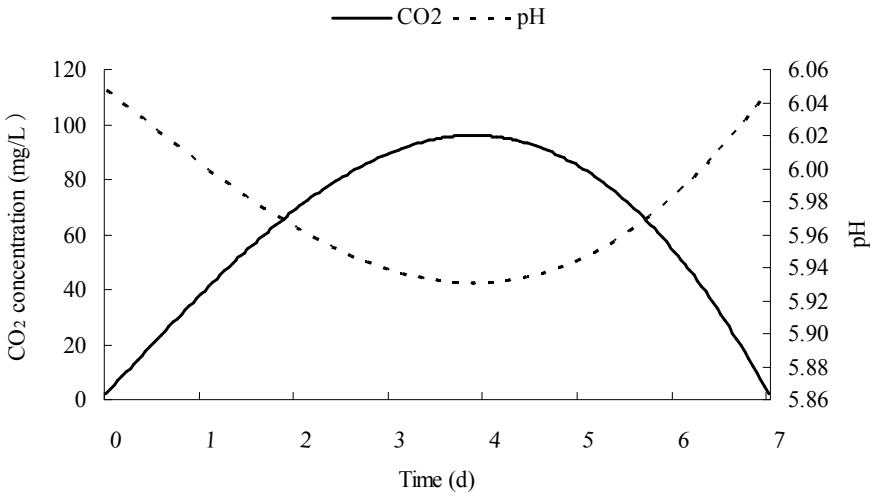

Figure 5.8: A model simulation of the changes in nitrogen, phosphorus, and CO_2 concentration under actual D_s over time in the CAB. (a) Phosphorus and nitrogen concentrations versus time; (b) CO_2 concentration and pH versus time.

Chapter 6: Conclusions and Recommendations

6.1 Summary and Conclusions

In this study, a mechanistic model for lipid production and biomass growth of microalgae in a vertical flat-plate photobioreactor was proposed. The model has been assessed with experimental data of *Nannochloropsis Salina* in the FACE 4 photobioreactors. The presented model suggests that lipid production may be simplified within the framework of fundamental biological and physiological processes with respect to growth and lipid production, ecological stoichiometry, and dominant environmental factors which influence photosynthesis. More experimental data is needed for validation of the model. Based on the results of this study, the following conclusions can be drawn:

1. Numerical relationships of the light dynamics and their impact on growth kinetics of *Nannochloropsis Salina* in the FACE 4 photobioreactors were determined for model development. Mathematical expressions and parameters were developed including these relationships: (1) PPFD emitted by lamp and the PPFD hitting the surface of the reactor (I_o); (2) the average PPFFR at a certain distance of culture penetration (I_z) and the biomass concentration (X); light attenuation coefficient (k_o) and biomass concatenation (X); the average PPFFR in the reactor (I_a) and the biomass (X); average PPFFR (I_a) and the specific growth rate (μ) in the experimental unit.
2. A light diffusion coefficient (k_a) of 0.0256 cm^{-1} and a biomass attenuation coefficient (k_b) of 0.0007 cm^{-1} were estimated for the FACE 4 photobioreactors

system though light diffusion and attenuation studies respectively. Light attenuation coefficient (k_o) was found to yield a linear partition of $k_o = 0.0326 + 0.0007X$, so light attenuation linearly increased with an increase in biomass.

3. The specific growth rate (μ) was found to follow Steele's equation from the growth study, resulting in the maximum growth rate (μ_{max}) of 1.262 d^{-1}.
4. A negative exponential relationship between lipid production and biomass growth rate (μ) was estimated in the microalgae photobioreactors system.
5. The mechanistic model illustrates the trends in light dynamics, growth kinetics, and lipid production in satisfactory agreement with measured data.
6. Simulation produced by the calibrated model were used to predict and optimize lipid production in the FACE 4 photobioreactors.
7. Simulation studying indicated that the lipid production could be optimized to as much as 3.2724 g/day, if the CABs were run at a continuous flow of 0.046 m^3/day or 46 liters/day.

6.2 Recommendations for Future Research

Future research on this mechanistic model development remains to be done in order to optimize lipid yields, gain detailed and better understanding of biological processing strategies, and scale up from the laboratory to the industrial production scale. Based on this study, future work should be carried out on the following topics:

1. Future experiments on carbohydrate and protein production are expected in order

to calibrate that part of the model.

2. More experiments with high lipid production should be done in order to validate the model and optimize lipid production. The high lipid production can be achieved under nitrogen limitation environments. Because the nutrient stress leads not only to the accumulation of lipids, but also to reduction in microalgae growth, resulting in an increase of the lipids production. It will provide information to identify the optimal lipid production conditions.
3. Once partitioning of lipids and nutrients are calibrated, economic component should be incorporate in the model.
4. Efforts should be made to investigate the dominant limiting factors for scaling-up the photobioreacor systems. The availability of nutrients, nitrogen and phosphorus in particular, and CO_2 are considered possible potential show-shoppers to sustained biomass and lipid production on large-scale.
5. Consideration of running the FACE 4 CABs in series in order to improve the biomass and lipid production.

Bibliography

Acien Fernandez, F.G., Garcia Camacho, F., Sanchez Perez, J.A., Fernandez Sevilla, J.M., Molina Grima, E.,1997. A model for light distribution and average solar irradiance inside outdoor tubular photobioreactors for the microalgal mass culture. Biotechnol. Bioeng. 55, 701-714.

Acien Fernandez, F.G., Garcia Camacho, F., Sanchez Perez, J.A., Fernandez Sevilla, J.M., Molina Grima, E., 1998. Modeling of biomass productivity in tubular photobioreactors for microalgal cultures: effects of dilution rate, tube diameter and solar irradiance. Biotechnol. Bioeng. 58, 605-616.

Adams, J. M.; Gallagher, J. A., 2009. Donnison, I. S. Fermentation study on Saccharina latissima for bioethanol production considering variable pre-treatments. J. Appl. Phycol. 21, 569-574.

Azachi, M., Sadka, A., Fisher, M., Goldshlag, P., Gokhman, I., Zamir, 2002. A. Salt induction of fatty acid elongase and membrane lipid modifications in the extreme halotolerant alga *Dunaliella salina*. Plant Physiol. 129, 1320-1329.

Barnabe and Barnabe-Quet, 2000. Ecology and Management of Coastal Waters: The Aquatic Environment. Springer Praxis. Chichester.

Basova, M.M., 2005. Fatty acid composition of lipids in microalgae. Int. J. Algae. 7, 33-57.

Becker E.W., 2007. Micro-algae as a source of protein. Research review paper, Biotechnol. 25, 207-210.

Beiser, A., 1973. Physics. Cummings Publishing Co., California.

Benson, B.C., 2003. Optimization of the Light Dynamics in the Hydraulically Integrated Serial Turbidostat Algal Reactor (HISTAR), PhD Dissertation, The Department of Civil and Environmental Engineering, Louisiana State Univeresity.

Benson B.C., Fernandez C.J., Fox J. M., 2012. Mechanistic Model Development of Fundamental biological and Physiological Processes Governing Lipid Production by Microalgae. SunGrant. 19.

Benson B.C., Gutierrez-Wing M.T., Rusch K.A., 2007. The development of a mechanistic model to investigate the impacts of the light dynamics on algal productivity in a HISTAR, Aquactultural Eng. 36, 198-211.

Benson B.C., Rusch K.A., 2005. Investigation of the light dynamics and their impact on algal growth rate in HISTAR, Aquacultural Eng. 35, 122-134.

Benson, B.C., Rusch, K.A., 2006. Investigation of the light dynamics and their impact on microalgal growth ratge in a Hydraulically Integrated Serial turbidostat Algal Reactor (HISTAR). J. Aqua.Eng. 35(2), 122-134.

Briggs M.W., 2004. Biodiesel Production from Algae; University of New Hampshire Biodiesel Group.

Brown M.R., and Jeffrey S.W., 1992, Biochemical composition of microalgae from the green algal classes *Chlorophyceaea* and *Prasinophyceae*. 1. Amino acids, sugar and pigments, Journal Experimental Marine Biology and Ecology. 161, 91-113.

Brown, M.R., Dunstan, G.A., Norwood, S.J., Miller, K.A., 1996. Effects of harvest stage and light on the biochemical composition of the diatom *Thalassiosira pseudonana*. J.

Phycol. 32, 64-73.

Buehner M.R., Young P.M., Willson B., 2009. Microalgae Growth Modeling and Control for a Vertical Flat Panel Photobioreactor. American Control Conference ThA. 10, 4.

Camacho Rubio F, Acién Fernández F.G., García Camacho F., Sánchez Pérez J.A., Molina Grima E., 1999. Prediction of dissolved oxygen and carbon dioxide concentration profiles in tubular photobioreactors for microalgal culture. Biotechnol Bioeng. 62, 71-86.

Carvalho A.P., Meireles L.A., Malcata F.X., 2006. Microalgal reactors: a review of enclosed system designs and performances. Biotechnol Prog. 22, 1490-506.

Chapra, S.C., 1997. McGraw-Hill series in water resources and environmental engineering; The McGraw-Hill, New York, 612-613.

Chisti Y., and Gavrilescu M., 2005. Biotechnology-a sustainable alternative for chemical industry. Biotechnol Adv. 23, 471-99.

Chisti, Y. 2007.Biodiesel from microalgae. Biotechnol Adv. 25, 294-306.

DOE/ASAP, 2012. Advancements in sustainable algal production (ASAP), DE-FOA-0000615.

Dubinsky, Z., Berman, T., 1979. Seasonal changes in the spectral composition of down-welling irradiance in Lake Kinneret (Israel). Limnol. Oceanogr. 24, 652-663.

Droop, M.R., 1968. Vitamin B12 and marine ecology. IV. the kinetics of uptake growth and inhibition in *Monochrysis lutheri.* J. Mar. Biol. Assoc. 48(3), 689-733.

Epply, R. W., 1972. Temperature and phytoplankton Growth in the Sea. Fishery Bulletin 70

(4), 1063-1085.

Folch J., Lees M., Sloanesttanley G.H., 1957. A simple method for the isolation and purification of total lipides from animal tissues. J.Biol Chem. 226(1), 497-509.

Gallegos C.L., 1996. Seagrass depth limits in the Indian river lagoon: Application of an optical water quality model. Estuarine, coastal and shelf science. 42(2), 267-288.

Geider R., MacIntyre H., Kana T., 1998. A dynamic regulatory model of phytoplanktonic acclimation to light, nutrients, and temperature. Limnology and Oceanography 43, 679-694.

González-Fernández, C., Molinuevo-Salces, B., García-González, M. C., 2011. Nitrogen transformations under different conditions in open ponds by means of icroalgae−bacteria consortium treating pig slurry. Bioresour. Technol. 102, 960−966.

Gouveia L., Oliver A.C., 2009. Microalage as a raw material for biofuels production. J Ind Microbiol Biotechnol. 36(2), 269-274.

Grognard F., Akhmetzhanov A., Masi P., and Bernard O., 2010. Optimization of a photobioreactor biomass production using natural light. IEEE. 4961-4969.

Guckert, J.B.; Cooksey, K.E., 1990. Triglyceride accumulation and fatty acid profile changes in *Chlorella* during high ph-induced cell cycle inhibition. J. Phycol. 26, 72–79.

Guschina, I.A., Harwood, J.L., 2006. Lipids and lipid metabolism in eukaryotic algae. Prog. Lipid Res. 45, 160-186.

Harned H.S. and Davis R., J., 1943. The Ionization Constant of Carbonic Acid in Water and the Solubility of Carbon Dioxide in Water and Aqueous Salt Solutions from 0 to 50℃.

J.Am.Chem.Soc. 65, 2030-2037.

Harwood, J.L., 1998. Membrane Lipids in Algae. In Lipids in Photosynthesis: Structure, Fuction and Genetics; Siegenthaler, P.-A., Murata, N., Eds.; Kluwer Academic Publishers: Kluwer, The Netherlands. 53-64.

Hill J., Nelson, E., Tilman, D., Polasky S., Tiffany, D., 2006. Environmental, economic, and energetic costs and benefits of biodiesel and ethanol biofuels. Proc. Natl. Acad. Sci. USA. 103, 11206-11210.

Hu Q, Kurano N., Kawachi M., Iwasaki I., Miyachi A., 1998. Ultrahigh-cell-density culture of a marine alga Chlorococcum littorale in a flat-plate photobioreactor. Applied Microbiology and Biotech. 46, 655-62.

Hu Q., Sommerfeld M., Jarvis E., Ghirardi M., Posewitz M., Seibert M., Darzins A., 2008. Microalgal triacylglycerols as feedstocks for biofuel production: perspectives and advances. The Plant J. 54, 621-639.

Huisman J.,1999. Population dynamics of light-limited phytoplankton: microcosm experiments. Ecology 80, 202-210.

IEO, 2013. U.S. International energy outlook with projections to 2040. Energy Information Administration, DOE/EIA-0484.

Jon V.W., Miller T.W., Hobbs S., Hook P., Crowe B., Huesemann M., 2012. Effect of light and temperature on fatty acid production in *Nannochloropsis Salina*. Energies. 5(3), 731-740.

Jorgensen, S.E., 1979. Handbook of Environmental Data and Ecological Parameters. Pergamon Press, New York.

Karube I., Takeuchi T., Bares D. J., 1992. Biotechnological Reduction of CO_2 Emissions. Advances in Biochemical Eng./Biotech. 46, 63-79.

Khotimchenko, S.V. and Yakovleva, I.M., 2005. Lipid composition of the red alga *Tichocarpus crinitus* exposed to different levels of photon irradiance. Phytochemistry, 66, 73-79.

Khozin-Goldberg A.E., Cohen, Z., 2007. Effect of nitrogen starvation on optical properties, pigments, and arachidonic acid content of the unicellular green alga Parietochloris incisa (Trebouxiophyceae, Chlorophyta). J. Phycol. 43, 833-843.

Kimball, A.L., 1923. A College Text-book of Physics. Henry Holt and Co., New York, 720.

Kirk, J.T.O., 1994. Light and Photosynthesis in Aquatic Ecosystems, 2nd ed. Cambridge University Press, UK. 509.

Klausmeier C., Litchman E., Daufresne T., Levin S., 2008. Phytoplankton stoichiometry. Ecology Research 23, 479-485.

Lee M., Min B, Chang C., Jin E., 2006. Isolation and Characterization of a xanthophyll aberrant mutant of the green alga Nannochloropsis oculataMarine Biotech. 8 (3), 238-245.

Lester W.W., Adams M.S., Farmer A.M., 1988. Effects of light and temperature on photosynthesis of the nuisance alga Cladophora glomerata (L.) Kutz from Green Bay, Michigan. New Phytol. 109, 53.

Levasseur M., Thompson P.A., Harrison P.J., 1993. Physiological acclimation of marine phytoplankton to different nitrogen sources. J. Phycol. 29, 87-595.

Lopez-Alonso D.L., Belarbi E.H., Fernandez-Sevilla J.M., Rodriguez-Ruiz J., Molina-Grima E.M., 2000. Phytochem. 54, 461-471.

Lubian L.M., Montero O., Moreno-Garrido I., Huertas I.E., Sobrino C., Gonzalez-del Valle M., Pares G., 2000. Nannochloropsis (Eustigmatophyceae) as source of commercially valuable pigments Journal of Applied Phycology 12 (3-5), 249-255.

Mairet F., Bernard O., Lacour T., and Sciandra A., 2011. Modelling microalgae growth in nitrogen limited photobioreactor for estimating biomass, carbohydrate and neutral lipid productivities. IFAC, 10591-10596.

Maksimova L.V., Bratkovskaya L.B., Plekhanov S.E., 2004. Extracellular Carbohydrates and Polysaccharides of the Alga *Chlorella pyrenoidosa* Chick S-39. Biology Bulletin 31(2), 175-181.

Meng, X., Yang, J., Xu, X., Zhang, L., Nie, Q., Xian, M., 2009. Biodiesel production from oleaginous microorganisms. Renew. Energy. 34, 1-5.

Merzlyak M.N., Chivkunova O.B., Gorelova O.A., Reshetnikova I.V., Solovchenko A.E., Khozin-Goldberg I., Cohen Z., 2007. Effect of nitrogen starvation on optical properties, pigments, and arachidonic acid content of the unicellular green alga Parietochloris incisa (Trebouxiophyceae, Chlorophyta). J. Phycol. 43, 833-843.

Mohammady N.G.E., 2011. Characterization of the Fatty Acid Composition of *Nannochloropsis salina* as a Determinant of Biodiesel Properties. Z Naturforsch C.

66(7-8), 328-332.

Molina Grima, E., Fernandez Sevilla, J.M., Sanchez Perez, J.A., Garcia Camacho, F.,1996. A study on simultaneous photolimitation and photoinhibition in dense microalgal cultures taking into account incident and averaged irradiance. J. Biotechnol. 45, 59-69.

Molina Grima E., 1999. Microalgae, mass culture methods. In: Flickinger MC, Drew SW, editors. Encyclopedia of bioprocess technology: fermentation, biocatalysis and bioseparation. 3, 1753-69.

Molina Grima E, Acién Fernández F.G., García Camacho F., Chisti Y., 1999. Photobioreactors: light regime, mass transfer, and scaleup. J Biotechnol. 70(2), 31-47.

Molina E., Fernandez J., Acien F.G., Chisti Y., 2001. Tubular Photobioreactor Design for Algal Cultures 92, 113-131.

Ogbonna, J.C., Yada, H., Tanaka, H., 1995. Light supply coefficient: a new engineering parameter for photobioreactor design. J. Ferm. Bioeng. 80 (4), 369-376.

Ogbonna, J.C., and Tanaka, H., 1997. Industrial-size Photobioreators. Chemtech, 27, 43-49.

Packer A., Li Y., Andersen T., Hu Q., Kuang Y., Sommerfeld M., 2011. Growth and neutral lipid synthesis in green microalgae: A mathematical model. Bioresource Tech., 102, 111-117.

Renaud, S.M., Thinh, L.V., Lambrinidis, G., Parry, D.L., 2002. Effect of temperature on growth, chemical composition and fatty acid composition of tropical Australian microalgae grown in batch cultures. Aquaculture 211, 195-214.

Richardson J.W., Johnson M.D., and Outlaw J.L., 2012. Economic comparison of open pond raceways to photo bio-reactors for profitable production of algae for transportation fuels in the Southwest. Algal Researech. 1(1), 93-100.

Richmond A., Cheng-Wu Z., Zarmi Y., 2003. Efficient use of strong light for high photosynthetic productivity: interrelationships between the optical path, the optimal population density and cell-growth inhibition. Biomolecular Eng. 20(4-6), 229-36.

Richmond A., 2000. Microalgal biotechnology at the turn of the millennium: a personal view. Journal of Applied Phyco. 12(3-5), 441-51.

Richmond A, Cheng-Wu Z, Zarmi Y., 2003. Efficient use of strong light for high photosynthetic productivity: interrelationships between the optical path, the optimal population density and cell-growth inhibition. Biomolecular Eng. 20(4-6), 229-36.

Rossignol N., Lebeau T., Jaouen P., Robert J.M., 2000. Comparsion of Two Membrance-Photobioreactors, with free of immobile cells, for the production of pigments by a marine diatom. Bioproc. Eng. 23(5), 495-502.

Rusch K.A, Malone R.F., 1998. Microalgal production using a hydraulically integrated serial turbidostat algal reactor (HISTAR): a conceptual model. Aquaculture Eng. 18 (4) 251-264.

Rusch K.A., Christensen J.M., 2007. The Hydraulically integrated serial turbidostat algal reactor (HISTAR) for microalgal production, Aquacultural Eng. 27, 249-264.

Sakthivel R., Elumalai S., Mohommad arif M., 2011. Microalgae lipid research, past, present: A critical review for biodiesel production, in the future. Journal of Experimental

Science. 2(10), 29-49.

Samson R, Leduy A., 1985. Multistage continuous cultivation of blue-green alga Spirulina maxima in flat tank photobioreactors. Canadian Journal of Chemical Eng. 63, 105-112.

Sánchez M.A., Cerón M.C., Gómez A.C., García F.C., Molina E.G., Chisti Y., 2003. Shear stress tolerance and biochemical characterization of Phaeodactylum tricornutum in quasi steady-state continuous culture in outdoor photobioreactors. Biochem Eng. J.,16, 287-297.

Sayegh F.A.Q., Montagnes D.J.S., 2010. Temperature shifts induce intraspecific variation in microalgal production and biochemical composition, Bioresources Tech. 102, 3007-3013.

Seambiotic Corporation Webpage, 2010. http://www.seambiotic.com

Sharma K.K., Schuhmann H., Schenk P.M., 2012. High Lipid Induction in Microalgae for Biodiesel Production. Energies. 5, 1532-1553.

Shen, Y.; Pei, Z.; Yuan, W.; Mao, E., 2009. Effect of nitrogen and extraction method on algae lipid yield. Int. J. Agric. Biol. Eng. 2(1), 51-57.

Shibles , 1976. Terminology pertraining to phtosynthesis. Crop. Sci. 16, 438-439.

Shifrin N. S. and Chisholm S. W., 1981. J. Phycol., 17, 374-384.

Sims R., Talyor M., Saddler J., and Mabee W., 2008. From 1st to 2nd generation biofuel technologies: an overview of current industry and R&D activities. IEA Bioenergy, OECD/IEA, 15.

Spolaore P., Joannis-Cassan C., Duran E., Sambert A.I., 2006. Commercial applications of microalgae, J Biosci Bioeng. 101, 87-96.

Steele, J.H., 1965. Notes on some theoretical problem in production ecology. In: Goldman, C.R. (Ed.), Primary Production in Aquatic Environments. University of California Press, Berkeley.

Stumm W. , Morgan J. J., 1981. Aquatic Chemistry. Wiley-Interscience, New York.

Thimijan R.W., Heins R.D., 1983. Photometric, radiometric, and quantum light units of measure: A review of procedures for interconversion. HortScience. 18, 818-822.

Thompson, G.A., 1996. Lipids and membrane function in green algae. Biochemica Biophysica. 1306, 17-45.

Tredici, M., and Zittelli, G., 1998. Efficiency of Sunlight Utilization: Tubular Versus Flat Photobioreactors. Biotech. and Bioeng. 57(2), 187-197.

U.S. DOE., 2010. National Algal Biofuels Technology Roadmap (Technology Roadmap). U.S. Department of Energy, Office of Energy Efficiency and Renewable Energy, Biomass Program.

Venkata Mohan, S., Bhaskar, Y. B., Krishna, T. M., Chandrasekhara Rao, N., Lalit Babu, V., Sarma, P. N., 2007. Biohydrogen production from chemical wastewater as substrate by selectively enriched anaerobic mixed consortia: Influence of fermentation pH and substrate composition. Int. J. Hydrogen Energy. 32, 2286-2295.

Wada, H. and Murata, N., 1998. Membrane lipids in cyanobacteria. In Lipids in Photosynthesis: Structure, Function and Genetics (Siegenthaler, P.A. and Murata, N.,

eds). Dordrecht, The Netherlands, Kluwer Academic Publishers. 65-81.

Watanabe, Y., de la Noue, J., Hall, D.O., 1995. Photosynthetic Performance of a Helical Tubular Photobioreactor Incorporating the Cyanobacterium *Spirulina platensis*. *Biotechn platensis*. Biotech. and Bioeng. 47, 261-269.

Wegeberg s., Felby C., 2010. Algae biomass for bioenegy in Denmark-Biological/Technical challenges and opportunities. Bio. 424.

Williams P.J.B., Laurens L.M.L., 2010. Microalgae as biodiesel & biomass feedstocks: Review & analysis of the biochemistry, energetics & economics. Energy & Environmental Sci. 10939.

Xue S.Z., Su Z.F., Cong W., 2011. Growth of Spirulina Platensis Enhanced Under Intermittent Illumination, Biotech.151, 271-77.

Zhang, Y., Dubé, M.A., McLean, D.D., Kates, M., 2003. Biodiesel production from waste cooking oil. 1. Process design and technological assessment. Bioresour. Technol. 89, 1-16.

Appendix A

Mechanistic Model

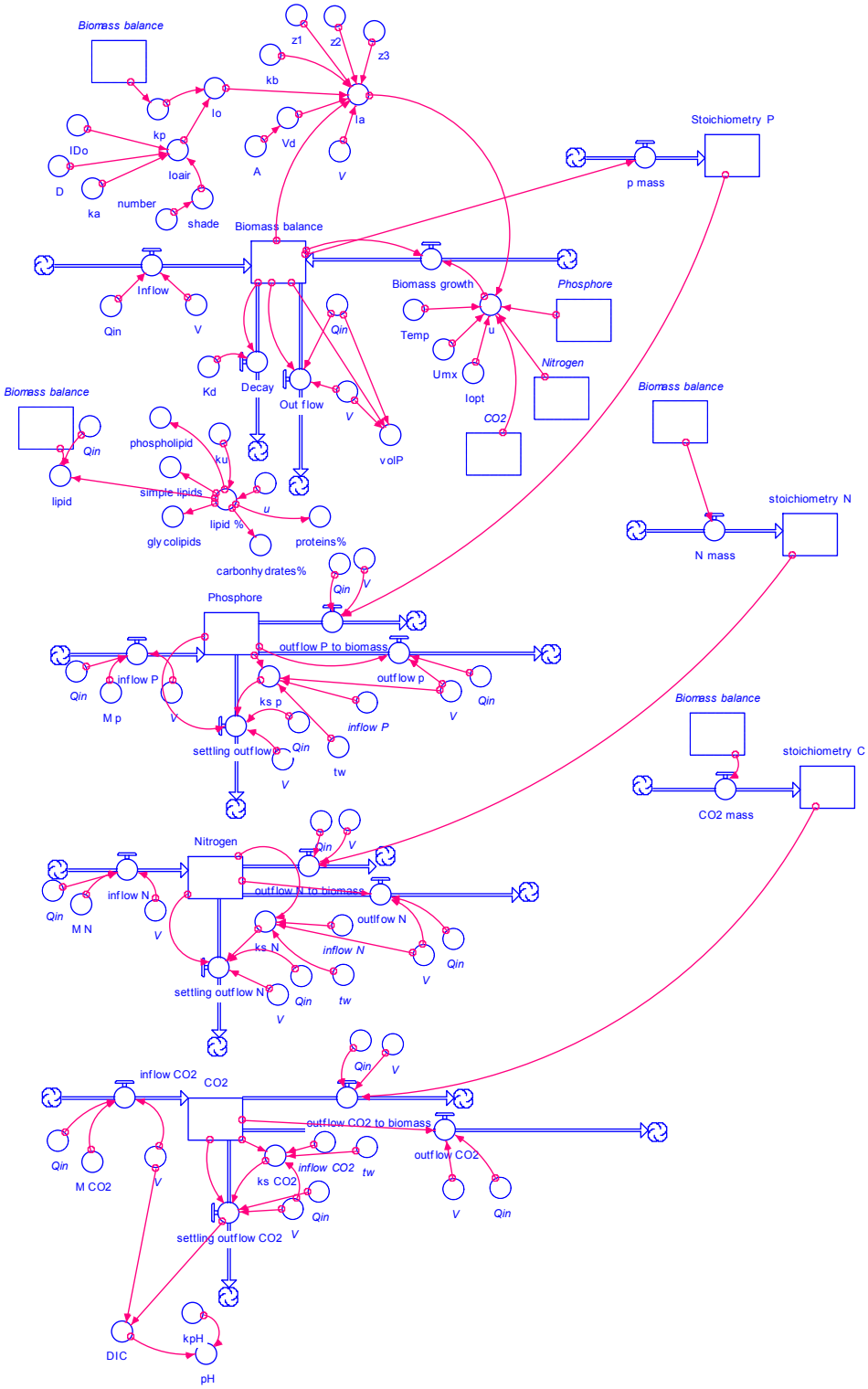

Figure A. 1: Map of the mechanistic model in the FACE 4 photobioreactors in STELLA.

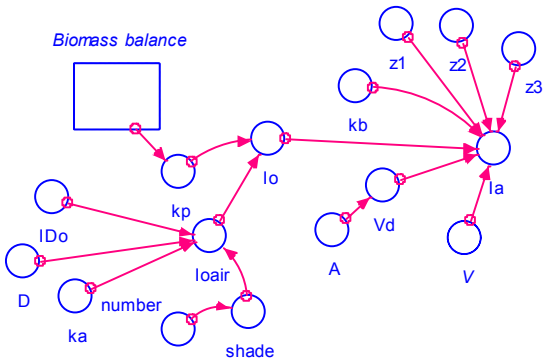

Figure A.2: Light dynamics model in the FACE 4 photobioreactors.

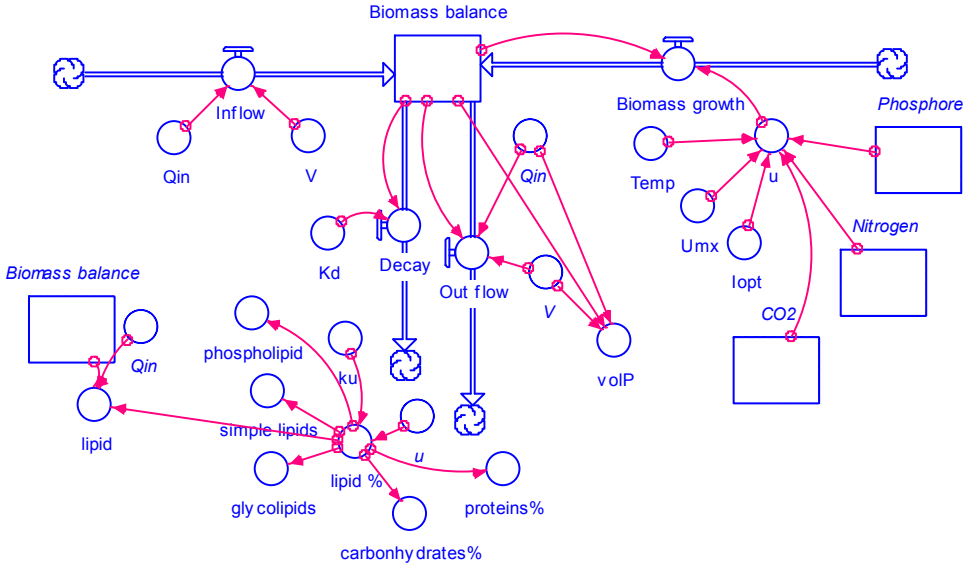

Figure A.3: Lipid production and biomass growth model.

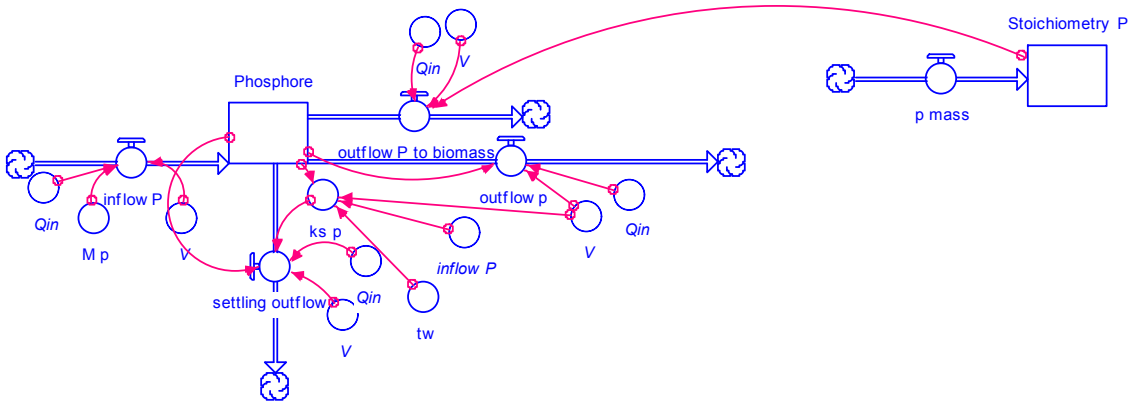

Figure A.4: Conceptual model component of the phosphore flow in the reactor.

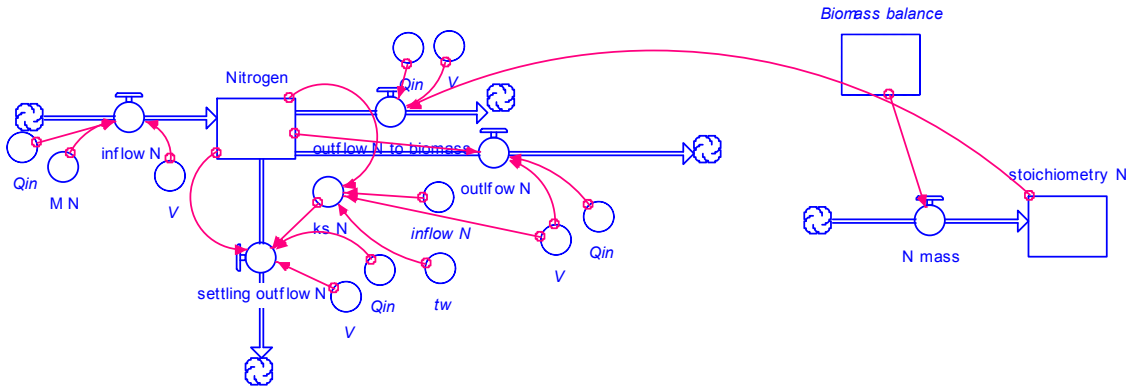

Figure A.4: Conceptual model component of the nitrogen flow in the reactor.

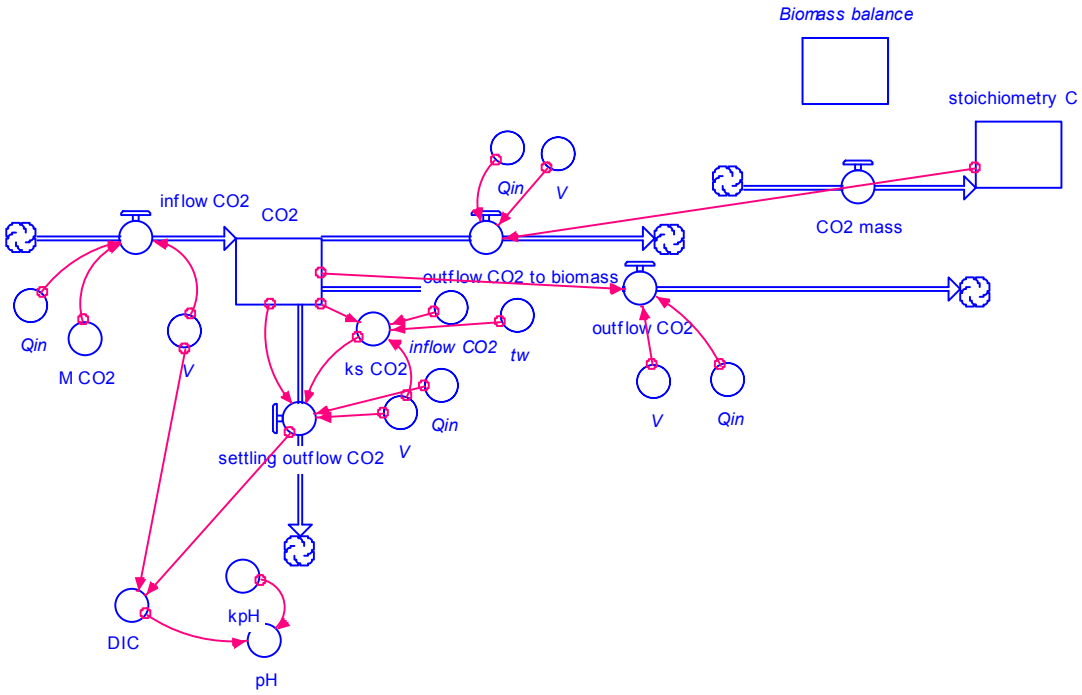

Figure A.5: Conceptual model component of the CO_2 flow in the reactor.

The following is the codes using in this mechanistic model.

Biomass_balance(t) = Biomass_balance(t - dt) + (Inflow + Biomass_growth - Out_flow - Decay) * dt
INIT Biomass_balance = 100
INFLOWS:
Inflow = Qin/V
Biomass_growth = Biomass_balance*u
OUTFLOWS:
Out_flow = (Qin*Biomass_balance)/V

Decay = Kd*Biomass_balance
CO2(t) = CO2(t - dt) + (inflow_CO2 - outflow_CO2 - outflow_CO2_to_biomass - settling_outflow_CO2) * dt
INIT CO2 = 2.1
INFLOWS:
inflow_CO2 = (Qin*M_CO2)/V
OUTFLOWS:
outflow_CO2 = (CO2*Qin)/V
outflow_CO2_to_biomass = Qin*stoichiometry_C/V
settling_outflow_CO2 = CO2*ks_CO2*Qin/V
Nitrogen(t) = Nitrogen(t - dt) + (inflow_N - outflow_N_to_biomass - settling_outflow_N - outlfow_N) * dt
INIT Nitrogen = 4
INFLOWS:
inflow_N = (Qin*M_N)/V
OUTFLOWS:
outflow_N_to_biomass = Qin*stoichiometry_N/V
settling_outflow_N = Nitrogen*ks_N*Qin/V
outlfow_N = (Nitrogen*Qin)/V
pH(t) = pH(t - dt) + (enter_DIC) * dt
INIT pH = 6
INFLOWS:
enter_DIC = GRAPH((pHo+pH*TpH)/kpH)
(0.00, 0.00), (10.0, 0.00), (20.0, 0.00), (30.0, 0.00), (40.0, 0.00), (50.0, 0.00), (60.0, 1.50), (70.0, 0.00), (80.0, 0.00), (90.0, 0.00), (100, 0.00)
pHo(t) = pHo(t - dt) + (enter_DICo) * dt
INIT pHo = 6
INFLOWS:
enter_DICo = settling_outflow_CO2/V
Phosphore(t) = Phosphore(t - dt) + (inflow_P - outflow_P_to_biomass - outflow_p - settling_outflow_p) * dt
INIT Phosphore = 2.5
INFLOWS:
inflow_P = (M_p*Qin)/V
OUTFLOWS:
outflow_P_to_biomass = Stoichiometry_P*Qin/V
outflow_p = (Qin*Phosphore)/V
settling_outflow_p = ks_p*Phosphore*Qin/V
stoichiometry_C(t) = stoichiometry_C(t - dt) + (CO2_mass) * dt
INIT stoichiometry_C = 2.1
INFLOWS:

CO2_mass = Biomass_balance*1.47
stoichiometry_N(t) = stoichiometry_N(t - dt) + (N_mass) * dt
INIT stoichiometry_N = 4
INFLOWS:
N_mass = Biomass_balance*0.072
Stoichiometry_P(t) = Stoichiometry_P(t - dt) + (p_mass) * dt
INIT Stoichiometry_P = 2.5
INFLOWS:
p_mass = Biomass_balance*0.01
A = 0.6387
carbonhydrates% = (1-lipid_%/100)*0.4*100
D = 25.4
glycolipids = lipid_%*0.39
Ia =
(SUM((Vd*(Io*(EXP(kb*Biomass_balance*z1))))+(Vd*(Io*(EXP(kb*Biomass_balance*z2)
)))+(Vd*(Io*(EXP(kb*Biomass_balance*z3)))))/V)
IDo = 903.07
Io = (-kp*0.0127)+Ioair
Ioair = (IDo*EXP(ka*D))*shade
Iopt = 158.3
ka = -0.0257
kb = -0.0007
Kd = 0.0001
Ku = -0.5323
kp =
((360*Biomass_balance)/(430+Biomass_balance+(Biomass_balance*Biomass_balance/2500
)))*100
kpH = 3
ks_CO2 = inflow_CO2/(V*CO2)-1/tw
ks_N = inflow_N/(V*Nitrogen)-1/tw
ks_p = inflow_P/(V*Phosphore)-1/tw
lipid = lipid_%*0.01*Biomass_balance*Qin
lipid_% = 18.543*EXP(kl*u)
M_CO2 = 4170
M_N = 214
M_p = 35
number = 0
phospholipid = lipid_%*0.38
proteins% = (1-lipid_%/100)*0.6*100
Qin = 0.0007
shade = 0.9887*EXP(-0.4988*number)

simple_lipids = lipid_%*0.22
Temp = 25
TpH = 7
tw = 7
u =
Umx*((1.066^(Temp-25))*((Ia/Iopt)*(EXP((-Ia/Iopt)+1)))*(MIN(Nitrogen/(Nitrogen+0.020)
,Phosphore/(Phosphore+0.005),CO2/(CO2+0.020))))
Umx = 1.25
V = 0.06489
Vd = 0.03386667*A
volP = Biomass_balance*Qin/V
z1 = 3
z2 = 6
z3 = 9

Appendix B

Data from the Light Studies

Table B.1: Light attenuation study at selected culture concentrations in a CAB of the FACE 4 photobioreactors.

Culture (%)	*Biomass (mg/L)*	*Average PPFFR ($\mu mols^{-1}m^{-2}$)*	*K_o (cm^{-1})*
100	787.2	47.0378	0.5383
75	565.103125	54.263	0.4526
50	426.74375	77.221	0.3611
25	273.225	128.493	0.2203
0	0	365.7631	0.0098

Table B.2: Light attenuation through culture in the experimental unit.

Distance from light sources side wall (cm)		**2.54**	**5.08**	**7.62**
Culture (%)	Biomass (g/m3)	Average PPFFR ($\mu mols^{-1}m^{-2}$)		
100	787.200	115.733	14.839	91.000
75	565.103	117.884	28.289	62.156
50	426.744	153.267	47.152	44.188
25	273.225	191.500	105.024	24.250
0	0	378.617	369.083	360.306

Table B.3: Light diffusion study at selected distance from the lamp in each CAB of the FACE 4 photobioreactors.

	Surface PPFFR ($\mu mols^{-1}m^{-2}$)			
Distance from light source (cm)	CAB1	CAB 2	CAB 3	CAB 4
10.16	728.998	567.187	823.238	707.402
25.4	482.935	386.727	472.884	476.069
40.64	350.790	261.056	338.423	339.851

Table B.4: Data for relationships between surface PPFFR (I_o) at both front and back sides of CABs and thickness at three selected distances from the light source.

	Average PPFFR ($\mu mols^{-1}m^{-2}$)							
Distance from light source (cm)	CAB1 front	CAB1 back	CAB2 front	CAB 2 back	CAB3 front	CAB 3 back	CAB4 front	CAB 4 back
10.16	728.998	325.785	567.187	265.611	823.238	320.864	707.402	262.114
25.4	482.935	235.985	386.727	179.651	472.884	211.645	476.069	205.396
40.64	350.790	188.175	261.056	129.646	338.423	161.537	339.851	151.632

Table B.5: Data for the relationships between I_o and I_{oair} under selected culture concentrations.

Culture (%)	**0**		**25**		**50**		**75**		**100**	
Biomass (mg/L)	0		273.225		426.74375		565.103125		787.2	
Thickness of the wall =1.27 cm	PPFFR ($\mu mols^{-1}m^{-2}$)									
Sensor locations	Io	Ioair	Io	Ioair	Io	Ioair	Io	Ioair	Io	Ioair
1	379.417	417.9	379.417	158.7	379.4171	149.4	379.417	105.6	379.4171	112.4
2	333.264	420	333.264	197.2	333.2641	154	333.264	65.9	333.2641	121.9
3	292.794	385	292.794	181.3	292.7936	143.1	292.794	83.61	292.7936	92.6
4	335.892	345	335.892	184.7	335.8915	145.2	335.892	124.3	335.8915	111.2
5	393.72	397.15	393.72	209.1	393.72	166.6	393.72	147.55	393.72	132.5
6	374.517	389.7	374.517	209.3	374.5166	156.3	374.517	135	374.5166	120.7
7	354.646	361.9	354.646	202.4	354.646	155.1	354.646	133.3	354.646	106.9
8	378.186	369.6	378.186	201.4	378.1855	165.6	378.186	142.9	378.1855	126.9
9	381.418	321.3	381.418	179.4	381.4175	144.1	381.418	122.8	381.4175	116.5

Appendix C

Data from the Growth Studies

Table C.1: Change in the biomass concentration and average PAR during the growth study.

Date	time	Optical Density(abs)	Biomass(mg/L)	Average PPFFR ($\mu mols^{-1}m^{-2}$)	Total Hours
6/8/2012	0AM	0.078	0.0417	137.7304	0
6/8/2012	6AM	0.1	0.0643	135.6623	6
6/8/2012	12PM	0.106	0.0705	135.1037	12
6/8/2012	6PM	0.107	0.0715	135.0108	18
6/9/2012	0AM	0.128	0.0931	133.0751	24
6/9/2012	6AM	0.138	0.1034	132.1631	30
6/9/2012	12PM	0.169	0.1354	129.3754	36
6/9/2012	6PM	0.152	0.1179	130.8967	42
6/10/2012	0AM	0.245	0.2136	122.7872	48
6/10/2012	6AM	0.284	0.2537	119.5379	54
6/10/2012	12PM	0.289	0.2589	119.1275	60
6/10/2012	6PM	0.311	0.2815	117.3388	66
6/11/2012	0AM	0.349	0.3206	114.3122	72
6/11/2012	6AM	0.394	0.3670	110.8288	78
6/11/2012	12PM	0.428	0.4020	108.2675	84
6/11/2012	6PM	0.443	0.4174	107.1564	90
6/12/2012	0AM	0.483	0.4586	104.249	96
6/12/2012	6AM	0.493	0.4689	103.5345	102
6/12/2012	12PM	0.54	0.5173	100.2416	108
6/12/2012	6PM	0.575	0.5533	97.85768	114
6/13/2012	0AM	0.626	0.6058	94.48506	120
6/13/2012	6AM	0.687	0.6686	90.60346	126
6/13/2012	12PM	0.68	0.6614	91.04067	132
6/13/2012	6PM	0.682	0.6634	90.91554	138
6/14/2012	0AM	0.765	0.7489	85.87153	144
6/14/2012	6AM	0.856	0.8426	80.66237	150
6/14/2012	12PM	0.745	0.7283	87.06075	156
6/14/2012	6PM	0.804	0.7890	83.59906	162
6/15/2012	0AM	0.863	0.8498	80.275	168
6/15/2012	6AM	0.89	0.8776	78.79823	174
6/15/2012	12PM	0.918	0.9064	77.29545	180

6/15/2012	6PM	0.94	0.9290	76.13483	186
6/16/2012	0AM	0.968	0.9578	74.68285	192
6/16/2012	6AM	0.983	0.9733	73.91642	198
6/16/2012	12PM	0.959	0.9486	75.14651	204
6/16/2012	6PM	0.976	0.9661	74.2731	210
6/17/2012	0AM	1.022	1.0134	71.96033	216
6/17/2012	6AM	1.033	1.0248	71.41803	222
6/17/2012	12PM	1.038	1.0299	71.17288	228
6/17/2012	6PM	1.022	1.0134	71.96033	234
6/18/2012	0AM	1.096	1.0896	68.38993	240
6/18/2012	6AM	1.1	1.0937	68.20206	246
6/18/2012	12PM	1.079	1.0721	69.19415	252

Table C.2: Data for the relationship between biomass concentration and optical density.

Biomass (mg Dry wt./L)	*Optical Density*
1055	1.066
823	0.859
706	0.661
302	0.38
0	0.025

Table C.3: Data for the relationship between biomass concentration and average PPFFR during the growth study.

Culture (%)	Average PPFFR ($\mu mols^{-1}m^{-2}$)	Dry weight concentrations(mg Dry wt./L)
100	70.367	1055
75	76.500	823
50	86.950	706
25	112.127	302
0	150.800	0

Bao, Qilin. Bachelor of Science, Wuhan Institute of Technology, Fall 2010; Master of Science, University of Louisiana at Lafayette, Fall 2011; Master of Science, University of Louisiana at Lafayette, Fall 2013
Major: Engineering, Civil Engineering option
Title of Thesis: Microalgae Growth and Lipid Production in a Vertical Flat-Plate Photobioreactor: Mechanistic Model Development
Thesis Director: Dr. Barbara C. Benson and Dr. Daniel Dianchang Gang
Pages in Thesis: 130; Words in Abstract: 210

Abstract

Energy production via extracted lipids from microalgae has emerged as a promising alternative to fossil fuels. To optimize microalgae biomass production in photobioreactors, identification of optimal operating conditions, optimization of the microalgae production processes, and quantification of fundamental biochemical responses to the environmental factors are the most significant challenges. These need to be addressed for microalgae biomass productions to become economically feasible. For that, this study developed a mechanistic model of microalgal lipid production with respect to environmental and growth conditions, such as photosynthetic photon flux density (PPFFD), essential nutrients, temperature, and CO_2 availability. The main objective of this mechanistic model was to identify nutrient and light conditions that optimize the lipid synthesis in flat-plate photobioreactors with metal halide lamps. In this model, mass balance, quantum mechanics, and soichiometry were taken into account to simulate microalgae biomass production and chemical conversion of light energy into lipids. Mathematical expressions of various fundamental biological and physiological processes governing lipid productivity were

determined and integrated into the model to study their complex interactions and to predict biomass, protein, carbohydrate, and lipid productivities. Simulations were compared with actual data for *Nannochloropsis salina* culture grown the four automated and controlled environment photobioreactors (FACE 4) located at Texas Agrilife Research Center for model calibration and validation.

Biographical Sketch

Qilin Bao is currently pursuing a Master of Science degree in Civil Engineering at the University of Louisiana at Lafayette. Her research field is modeling microalgae growth and lipid production in a flat-plate photobioreactor for estimating effects of nutrients and light on growth and lipid accumulation. She received her bachelor's degree in Chemical Engineering with distinction from Wuhan Institute of Technology, China in July 2010. She received her Master of Science degree in Chemical Engineering from University of Louisiana at Lafayette in December 2011. After graduation, she hopes to research the application of biofuels.